Neuron
Article

KCC2 Expression Promotes the Termination of Cortical Interneuron Migration in a Voltage-Sensitive Calcium-Dependent Manner

Dante Bortone[1] and Franck Polleux[2,*]
[1]Neurobiology Curriculum, University of North Carolina, Chapel Hill
[2]University of North Carolina, Chapel Hill
Neuroscience Center, Department of Pharmacology, 115 Mason Farm Road, Chapel Hill, NC 27599-7250, USA
*Correspondence: polleux@med.unc.edu
DOI 10.1016/j.neuron.2009.01.034

SUMMARY

The molecular mechanisms controlling the termination of cortical interneuron migration are unknown. Here, we demonstrate that, prior to synaptogenesis, migrating interneurons change their responsiveness to ambient GABA from a motogenic to a stop signal. We found that, during migration into the cortex, ambient GABA and glutamate initially stimulate the motility of interneurons through both $GABA_A$ and AMPA/NMDA receptor activation. Once in the cortex, upregulation of the potassium-chloride cotransporter KCC2 is both necessary and sufficient to reduce interneuron motility through its ability to reduce membrane potential upon $GABA_A$ receptor activation, which decreases the frequency of spontaneous intracellular calcium transients initiated by L-type voltage-sensitive calcium channel (VSCC) activation. Our results suggest a mechanism whereby migrating interneurons determine the relative density of surrounding interneurons and principal cells through their ability to sense the combined extracellular levels of ambient glutamate and GABA once $GABA_A$ receptor activation becomes hyperpolarizing.

INTRODUCTION

Balance between excitation and inhibition in cortical circuits is dictated in part by the relative number of excitatory glutamatergic pyramidal neurons and inhibitory GABAergic interneurons. This balance is of critical importance for the proper function of the adult neocortex (Rubenstein and Merzenich, 2003). Although the mechanisms stimulating the motility and guiding the migration of cortical interneurons are beginning to be unraveled (Flames et al., 2004; Marin et al., 2001; Polleux et al., 2002; Poluch et al., 2003; Powell et al., 2001), the extracellular cues and signaling pathways instructing when and where cortical interneurons stop migrating are currently unknown.

The mode of migration of pyramidal neurons and interneurons differs greatly, and these differences include the cellular constraints leading to the termination of their migration. Pyramidal neurons are born from asymmetric divisions of radial glial progenitors in the ventricular zone of the dorsal telencephalon (Noctor et al., 2001). They migrate radially toward the pial surface by translocating along radial glial processes (Kriegstein and Noctor, 2004; Rakic, 1972). Upon reaching the top of the cortical plate, radial migration is terminated by the detachment from this substrate (Dulabon et al., 2000; Pinto-Lord et al., 1982), allowing subsequent generations of pyramidal cells to bypass their predecessors, forming the cortex in an "inside-out" manner. On the other hand, interneurons migrate in a saltatory, start-stop fashion from the medial and caudal ganglionic eminences (the MGE and CGE, respectively) to the dorsal telencephalon where these interneurons migrate tangentially through the marginal zone and intermediate zone (Ang et al., 2003; Lavdas et al., 1999; Marin and Rubenstein, 2001; Marin et al., 2001; O'Rourke et al., 1992, 1995; Polleux et al., 2002; Tanaka et al., 2006). Although interneurons can transiently fasciculate with radial glial fibers during their invasion of the cortical plate (Polleux et al., 2002), they are most frequently seen moving tangential to the direction of radial glial processes even within the cortical plate (O'Rourke et al., 1995; Polleux et al., 2002; D.B. and F.P., unpublished data). This suggests that radial glial processes are not a required substrate for cortical interneuron migration. Unlike pyramidal neurons, for which detachment from the radial glial scaffold at the top of the cortical plate is thought to be a determining factor, the absence of a required substrate for interneuron migration obfuscates the spatial and temporal mechanisms that might underlie the termination of their migration.

Some phenotypic features of cortical interneurons are genetically specified by the expression of transcription factors, including *Arx*, *Dlx1/2*, *Nkx2.1*, and *Lhx6* in the medial ganglionic eminence (MGE) (Anderson et al., 1997; Colombo et al., 2007; Kitamura et al., 2002; Lavdas et al., 1999; Sussel et al., 1999; Zhao et al., 2008). Lhx6-expressing interneurons originate from the MGE and primarily differentiate into the parvalbumin-positive subpopulation of cortical interneurons (Cobos et al., 2005, 2006; Liodis et al., 2007; Zhao et al., 2008), mainly comprising large basket cells and chandelier cells that make restricted synaptic contacts on the soma and axon initial segment of pyramidal neurons, respectively. These interneurons present fast-spiking patterns of axon potential firing (Butt et al., 2005; Kawaguchi and Kondo, 2002) and are thought to control oscillatory patterns of neural activities, such as theta and gamma waves (Freund, 2003).

Gamma-aminobutyric acid (GABA), the primary inhibitory neurotransmitter of the central nervous system, has been proposed to play multiple roles in controlling neuronal migration. GABA receptors are typically categorized into three types: $GABA_A$, $GABA_B$, and $GABA_C$. $GABA_A$ and $GABA_C$ are ionotropic receptors composed of five heteromeric subunits and are predominantly permeable to chloride ions. These two ion channels can be distinguished pharmacologically, as $GABA_C$ receptors are not inhibited by bicuculline, a $GABA_A$ antagonist. $GABA_B$ receptors are metabotropic (G protein-coupled receptors) and are therefore not dependent on the electrochemical equilibrium of chloride ions for their function. Tangentially migrating interneurons synthesize GABA and also possess the means to release it through a nonvesicular mechanism (Manent et al., 2005) that might involve reversal of GABA transporters (Conti et al., 2004). Migrating interneurons also have the capacity to respond to GABA in an autocrine/paracrine manner, since they express both ionotropic $GABA_A$ and metabotropic $GABA_B$ receptors during their migration (Cuzon et al., 2006; Lopez-Bendito et al., 2003; Lujan et al., 2005), yet the function of this complete signaling package in migrating interneurons is poorly understood (Represa and Ben-Ari, 2005).

GABA has been suggested to exert many, sometimes conflicting, effects on neuronal proliferation, migration, and differentiation in the developing central nervous system (Andang et al., 2008; Behar et al., 1996, 1998; Bolteus and Bordey, 2004; Cuzon et al., 2006; Lopez-Bendito et al., 2003; LoTurco et al., 1995; Marty et al., 1996). Here, we report that, upon reaching the cortex, depolarization through activation of $GABA_A$ receptors or activation of NMDA/AMPA glutamate receptors induces calcium transients that stimulate interneuron motility. These effects require activation of L-type voltage-sensitive calcium channels (VSCCs). Interestingly, several days after reaching the cortex, migrating interneurons upregulate the potassium/chloride (K^+/Cl^-) exchanger KCC2 (also called Solute Carrier Family 12, Member 5; *SLC12A5*), which controls the reversal potential of chloride (Cl^-) ions and therefore determines the developmental switch from depolarizing to hyperpolarizing following $GABA_A$ receptor activation (Ben-Ari, 2002). We demonstrate that expression of KCC2 is both necessary and sufficient to induce responsiveness to GABA as a stop signal by negatively regulating the frequency of spontaneous intracellular calcium transients in migrating interneurons. Therefore, KCC2 expression acts as a switch to induce a voltage-sensitive, calcium-mediated reduction of interneuron motility. Our results suggest that migrating cortical interneurons are able to sense and integrate the ambient, local extracellular levels of GABA and glutamate as a way to determine when to stop migrating.

RESULTS

The Majority of Cortical Interneurons Terminate Migration during the First Postnatal Week

To first document when interneurons stop migrating in the developing mouse cortex in vivo, we performed real-time confocal imaging of acute cortical slices isolated from a fluorescently labeled BAC-transgenic mouse line provided by the GENSAT consortium (Gong et al., 2003). In this transgenic mouse, enhanced green fluorescent protein (EGFP) is expressed under the control of the regulatory elements of LIM homeobox 6 (Lhx6), a transcription factor expressed specifically in MGE progenitors (Lavdas et al., 1999). These Lhx6-EGFP mice express EGFP in ~65% of cortical interneurons in vivo. Most of these Lhx6-positive interneurons will differentiate into parvalbumin-positive large basket cells and chandelier cells postnatally (Cobos et al., 2006). Time-lapse experiments of these Lhx6-EGFP mice revealed a gradual reduction in interneuron migration from E15 to P7 as shown in Figures 1B–1D (Movies S1–S3). Although some interneurons have terminated their migration in the cortical plate (CP) by E15 (15.1% ± 2.8%; Figure 1E), the vast majority continues to translocate. By P1, 57.8% ± 1.9% of interneurons stopped migrating, whereas almost all cortical interneurons have terminated migration by P7 (91.6% ± 1.4%).

Because of the saltatory nature of their translocation, quantitative assessment of interneuron migration was performed by computing two distinct parameters: (1) we defined the *moving speed* as the rate of translocation (μm/hr) when an interneuron is moving, i.e., not including the time when it pauses, and (2) the *pause time* indicates the proportion of time that the interneuron spent pausing during the time-lapse recording. Most investigations using time-lapse microscopy of neuronal migration report only the average speed as defined by distance traveled over a certain period of time (Cuzon et al., 2006). This measure can be ambiguous due to the saltatory nature of interneuron migration. Changes in *average speed* are caused by a change in either moving speed and/or pause time. By separating these two components, we were able to uncover significant changes that would not be apparent otherwise. Most importantly, the moving speed of cortical interneurons declines modestly from 23.0 ± 1.2 μm/hr at E15 to 18.5 ± 1.3 μm/hr at P1; however, there is no significant decline found from P1 to P7 as one might expect (Figure 1F). Rather, it is the increase in pausing frequency that primarily accounts for the transition to a sedentary state. This percentage increased significantly between all ages, increasing from an average of 75.3% ± 1.6% at E15 to 92.4% ± 1.1% by P7 (Figure 1G). Movie S3 best illustrates this: in this movie, two interneurons in the upper left corner do not move for most of the recording. However, when they do move, they move just as fast as less mature interneurons (see Movie S2). This movie illustrates that interneurons terminate migration primarily by increasing pausing frequency and duration rather than by decreasing their moving speed. Importantly, these parameters are exquisitely sensitive to the length of time-lapse observations, i.e., if shorter (<2–3 hr) time-lapse recordings are used and only moving interneurons are quantified, the significance of increasing pause time as a feature of termination of migration would be significantly underestimated.

GABA Application Induces Pausing Behavior in a Subset of Migrating Interneurons Expressing KCC2

Time lapsing migrating interneurons in slices presents several challenges. (1) the first challenge in time-lapsing acute brain slices for prolonged periods of time (>12 hr) lies in tracking a single interneuron as they move into the three-dimensional (3D) slice and frequently out of the focal plane. This relative freedom of movement in the Z axis compromises not only the number and

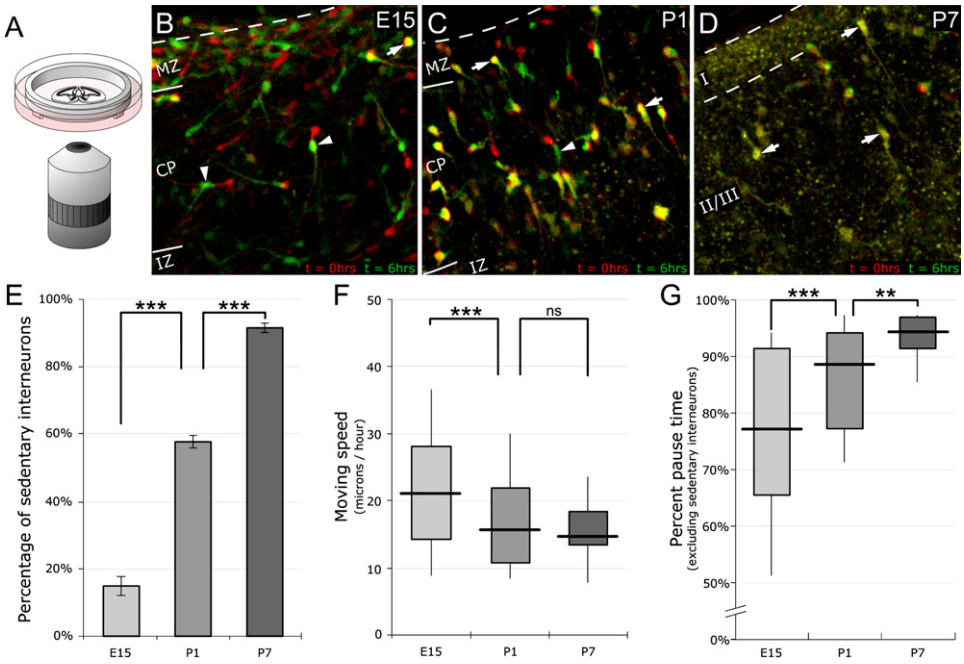

Figure 1. Characterizing the Termination of Cortical Interneuron Migration

(A) Illustration of time-lapse set-up. Cell culture media has access to slice from below, while temperature, humidity, and O_2/CO_2 levels are controlled by the incubation chamber atmosphere.

(B–D) Merged images showing the decrease in motility of Lhx6-EGFP+ interneurons in cortical slices at embryonic day (E)14.5 (B), postnatal day (P)1, and P7 after ex vivo culture for 1–2 days. Frame corresponding to the start of imaging (t = 0) is pseudocolored in red. Image taken 6 hr later is pseudocolored in green. Yellow cell bodies indicate interneurons that did not migrate during these 6 hr. Arrowheads indicate migrating interneurons, while arrows point to sedentary interneurons.

(E) Movements of interneurons in the cortical plate were quantified. By P7, the majority of interneurons show no detectable translocation during 6 hr.

(F and G) Box plots indicate developmental decline in movement over time. Individual box indicates mid-50th percentile range of individual neuron measurements taken. Whiskers extend from 10th to 90th percentiles. Horizontal bold line indicates the mean. The average moving speed showed an initial decrease between E15 and P1, but showed no decline between P1 and P7 (F). The primary mechanism whereby cortical interneurons migration stops is by a steady increase in the proportion of time interneurons spent pausing (G). Nonmoving interneurons have been excluded for quantification in panel (G) since their percentage of pause time is 100% by definition.

See Movies S1–S3 for the corresponding time-lapse animations.

duration of single interneuron observations, but all movements occurring in the Z axis are lost as well. Imaging these stacks in the Z plane at the resolution, depth, and frequency necessary to enable longer and more accurate observations of interneuron migration was not possible without introducing unacceptable levels of phototoxicity. (2) Another strong limitation of using slices is linked to small-molecule diffusion: a drug must diffuse through media, the insert membrane and the slice (300 μm) to reach our interneuron population. Since the spatial and temporal aspects of small-molecule diffusion in slices is difficult to estimate, it would be difficult to know when interneurons were truly exposed to a given pharmacological treatment and at what concentration.

To circumvent these challenges, we developed a two-dimensional (2D) migration assay. As interneurons will not migrate on simple coated substrates such as poly-L-lysine/laminin or fibronectin and their migration on collagen and matrigel is limited (data not shown), we used dissociations of wild-type pyramidal neurons as a 2D substrate for explants of MGE isolated from EGFP-expressing isochronic littermates (Figure S1A). EGFP+ interneurons migrate from the MGE explant and across this wild-type dissociation just as they would normally in the cortex. We found that this assay enabled longer, more accurate observations at higher temporal frequencies and provided immediate pharmacological access to the migrating interneurons.

We initially used this 2D assay to test if interneuron responsiveness to putative stop signals is due to cell-autonomous or cell-non-autonomous changes. First, we performed isochronic and heterochronic cocultures where the age of the cortical substrate for migration varies from 2 DIV to 7 DIV (see Figure S1). Our results demonstrate that after 2 DIV, most interneurons migrate robustly (equivalent to E16.5; Figure S1A; Movie S4) but when both interneurons and their cortical substrate have matured for 7 DIV (equivalent to P1), a significant proportion (~55%) of MGE-derived interneurons have stopped migrating (Figure S1B; Movie S5). These results suggest that (1) interneurons do terminate their migration in vitro according to a tempo that is comparable to ex vivo and that (2) the fine structure of the cortex is not necessary for the termination of interneuron migration, as this structure is lost in the dissociation process. Furthermore, heterochronic experiments revealed that when "immature" interneurons (E14.5 + 2 DIV) were plated on "mature" cortical substrate (E14.5 + 7 DIV), the interneurons migrated at the same rate as in isochronic conditions (E14.5 + 2 DIV MGE-derived interneurons migrating on 2 DIV

cortical substrate) (Figure S1C; Movie S6, quantified in Figures S1D and S1E). This strongly suggests that migratory responsiveness to putative extracellular stop signals requires some intrinsic maturation of these interneurons, such as the upregulation of an intracellular "gating" factor.

Interneurons possess both the capacity to release and to respond to GABA and yet, in spite of much evidence that GABA can modulate the migration of cortical and hippocampal neurons (Manent et al., 2005; Represa and Ben-Ari, 2005), the exact nature of GABA's effect on cortical interneuron migration, specifically through ionotropic receptors, remains unclear (Behar et al., 1996, 1998; Cuzon et al., 2006). Interneurons from EGFP-expressing MGE explants were allowed to migrate on a substrate of dissociated isochronic wild-type cortical neurons for 4.5 DIV and were time lapsed for 6 hr prior and 6 hr after the addition of vehicle only (Figure S2B) or GABA (20 μM) (Figure S2C). This method allowed us to quantify the migration properties of individual interneurons before and after drug addition (Figures S2D–S2G). Interneurons that were not present for the entirety of the 12 hr imaging sessions were excluded from the analysis. Interestingly, the moving speed did not decline significantly after addition of GABA, while their pausing frequency increased slightly but significantly (7.0% ± 1.5%; data not shown). The increase in the pausing frequency of interneurons receiving GABA was significantly higher ($p = 0.0183$) than the developmentally related increase in pausing frequency observed in interneurons receiving only media. This modest yet significant increase, specifically in pausing frequency, while maintaining stable moving speeds upon GABA addition strikingly resembles the attributes of the age-related termination of migration observed in situ (Figure 1). In other words, a significant increase in stalling was not only observed during the maturation of cortical interneurons (in vivo and in vitro), but increased stalling was also seen upon exogenous addition of GABA.

Although a significant trend was observed at the population level, i.e., slightly more interneurons show increased pausing frequency rather than decreased pausing upon GABA addition, this preliminary analysis exposed a very significant degree of variability in the response of individual interneurons to GABA addition. Strikingly, some interneurons within this group responded by increasing their pause times (cell 1 in Figures S2D–S2G), while others showed no change or a decrease in pause times upon GABA addition (cell 2 in Figures S2D–S2G). What could account for this significant degree of variability in the migratory response of interneurons to GABA?

KCC2 Upregulation Is Highly Variable among Migrating Interneurons In Vivo

There are at least two intrinsic factors that could contribute to this differential response of migrating interneurons toward GABA: (1) the heterogeneous expression of GABA receptors subunits and (2) the nature of the chloride (Cl^-) gradient across the membrane dictating the direction of chloride ion flow upon opening of ionotropic $GABA_A$ receptors. Differential expression of ionotrophic GABA receptor subunits could alter the cell's responsiveness to GABA (Cuzon et al., 2006) by conferring distinctive properties, including cellular localization, agonist affinity, rates of ion permeability, and desensitization. However, $GABA_A$ receptors are the most diverse ligand-gated ion channel composed of a staggering 21 subunits (Fritschy and Brunig, 2003). Single-cell RT-PCR analysis on migrating interneurons revealed that the majority of cortical interneurons express combinations of α(3-5), β(1-3), and γ1 subunits as they are migrating (Cuzon et al., 2006). However, the functional relevance of this potential diversity of $GABA_A$ receptor subunit composition for neuronal migration is unclear at this point.

Another critical modulator of ionotropic GABA function, the reversal of Cl^- electrochemical potential in neurons, is predominantly controlled by the expression of one protein, the K^+/Cl^- cotransporter, KCC2 (Rivera et al., 1999). Early in development, the expression of this chloride extruder is low relative to other chloride transporters, such as NKCC1, resulting in a high intracellular concentration of chloride. The driving force of this gradient causes a depolarizing efflux of chloride upon the binding of GABA to ionotropic $GABA_A$ receptors. As a neuron matures, the upregulation of KCC2 extrudes chloride, which leads to a reversal of its chloride electrochemical driving force (Ben-Ari, 2002; Payne et al., 1996; Rivera et al., 1999) and therefore to a hyperpolarizing influx of chloride ions upon ionotropic GABA receptor activation, which underlies the inhibitory function of GABA in the mature CNS.

We tested if KCC2 expression is heterogeneous among migrating cortical interneurons by performing immunofluorescent staining in vitro and in vivo. Our in vitro analysis reveals drastically different KCC2 expression levels between interneurons from MGE explants (Figures S3A–S3D). Also of note, pyramidal neurons, which composed the dissociated substrate, show very little KCC2 expression at the same age (Figure S3D). To confirm the physiological relevance of this variability of KCC2 expression observed in vitro, we performed immunofluorescent staining for KCC2 on Lhx6-EGFP cortical interneurons in vivo (Figures S3E–S3H). These results were consistent with the variability observed in vitro. Surprisingly, variability in KCC2 expression was observed in every layer of the neocortex at P0, including the cortical plate (Figures S3E–S3H). In order to compare the time course of KCC2 expression in interneurons and pyramidal neurons, we labeled the latter population using dorsal telencephalic electroporation at E14.5. This electroporation technique specifically labels radially migrating pyramidal neurons with no cross labeling of tangentially migrating interneurons (Figures S4A–S4C). After 4 days, allowing both subpopulations of neurons to migrate, these slices were fixed and immunostained for KCC2, which revealed little to no KCC2 expression in pyramidal neurons in situ (Figures S3L–S3N) at an age when a large proportion of interneurons already express this cotransporter (Figures S3I–S3K).

The 2D in vitro assay was adapted to more directly isolate and quantify KCC2 expression in these two distinct neuronal subpopulations. Cortical pyramidal cells were electroporated with monomeric red fluorescent protein (mRFP) at E14.5, dissociated, and cultured in vitro with MGE-EGFP explants (Figures S4F–S4I). Upon fixation, immunostaining for KCC2 at 4 DIV (Figures S3O–S3T) and 8 DIV (Figure S3U–S3Z) confirmed that KCC2 is upregulated in interneurons significantly earlier than pyramidal cells (Figure S3AA). By 8 DIV, KCC2 protein expression observed in interneurons was still twice that of pyramidal cells ($p < 0.0001$; Figure S3AA). In addition, there is significantly less variability in

the level of KCC2 expression among pyramidal neurons than among migrating interneurons (Figure S3AA).

A time course of KCC2 expression in the developing neocortex of Lhx6-EGFP was performed in vivo to see if interneurons upregulated KCC2 before or after entering the cortex (Figure S5). Upon the initial entry of interneurons into the cortex at E14.5, little to no KCC2 expression was observed in any cortical layer. By E16.5 some staining is detected almost exclusively in Lhx6-EGFP+ interneurons in the cortical plate. By birth (P0), KCC2 expression is observed in cortical interneurons present in all layers, primarily associated with Lhx6-EGFP+ interneurons, with the most intense staining occurring in the cortical plate. Taken altogether, these results demonstrate that migrating interneurons upregulate KCC2 expression (1) nonsynchronously ~1 week after reaching the cortex and (2) do so at least 1 week before pyramidal neurons.

KCC2 Expression Is Correlated with Responsiveness to GABA as a Stop Signal in Migrating Interneurons

To test the hypothesis that heterogeneous KCC2 expression underlies the differential responses to extracellular GABA application in migrating cortical interneurons, we combined the quantification of an individual interneuron's migratory responses to GABA addition (Figure S2) with post hoc immunofluorescent staining of KCC2 in the same interneurons (Figures 2A–2J; Movie S7). Cocultures were time lapsed for 12 hr (6 hr before and 6 hr after addition of GABA or other drug treatments). Immediately after the acquisition of the last frame, these time-lapsed cultures were fixed and stained for KCC2, MAP2, and EGFP (Figures 2G–2J). Each interneuron tracked during time lapse and pharmacological treatment was relocated and imaged, enabling the fluorescence of KCC2 to be correlated to the migratory response of individual interneurons following GABA addition (Figures 2B–2J).

This analysis revealed two different subpopulations of interneurons with markedly different response to GABA application. We binned our migration data according to the KCC2 fluorescence of the individual interneurons. Interneurons with KCC2 fluorescence lower than the average value for that imaging session were binned into the low-KCC2 group while those higher than the average were binned into the high-KCC2 group. Interneurons expressing low levels of KCC2 showed no significant changes in moving speed (Figure 2L) or percentage of time moving following GABA application (green dots in Figure 2K and see also left box plot in Figure 2M). Strikingly, migrating interneurons expressing high levels of KCC2 responded to GABA addition by significantly increasing the time they spent pausing (upward shift in box plot in Figures 2L and 2M; Figures 2K and 2M). As observed when characterizing the termination of migration in situ, this GABA-induced increase in percentage of pausing time occurs without a significant decrease in moving speed (Figure 2L).

Is this response to GABA as a stop signal in migrating interneurons expressing KCC2 mediated by activation of $GABA_A$ receptors? Coapplication of 20 μM GABA with 10 μM bicuculline methiodide (BMI), a competitive $GABA_A$ receptor antagonist, abolished the effect of GABA application on the percentage of time pausing in interneurons expressing high levels of KCC2 (Figure 2M). Interestingly, coapplication of GABA + BMI significantly *increased* the percentage of pause time in interneurons expressing low levels of KCC2 (third box plot from the left in Figure 2M). These results are also evident when viewing the averaged, frame-by-frame data for interneurons subdivided into high- and low-KCC2-expressing interneurons (Figure S5E). Our results show that (1) expression of KCC2 is correlated with the ability of interneurons to respond to GABA as a stop signal and (2) that in migrating cortical interneurons expressing low levels of KCC2, ambient GABA exerts a tonic, motogenic function stimulating interneuron migration as shown by bicuculline-induced reduction of motility in low-KCC2-expressing cells. Therefore, these data suggest that KCC2 might act as a "switch" transforming GABA from a motogenic to a stop signal in migrating interneurons.

KCC2 Expression Alone Can Account for Increased Pausing in Response to $GABA_A$ Receptor Activation

So far, our results provide a strong correlation between KCC2 upregulation in migrating interneurons and their ability to stop migrating in response to GABA; however, these results raise three important questions. (1) Is premature, forced KCC2 expression in migrating interneurons sufficient to induce responsiveness to GABA as a stop signal? (2) Does the early, motogenic function mediated by $GABA_A$ receptor activation require low KCC2 expression? And (3) is the transport activity of KCC2 required to confer the responsiveness to GABA as a stop signal?

Although binning interneurons into high and low levels of KCC2 expression did reveal statistically significant results, the threshold we chose for binning the two groups (based on the average KCC2 fluorescence) was rather arbitrary. To test the sufficiency of KCC2 in this GABA-induced pausing response, E14.5 wild-type MGEs were electroporated with human KCC2-IRES-EGFP expression plasmids (KCC2*; Figure 3A). This construct successfully upregulates KCC2 expression compared to endogenous expression (Figures 3B–3D; 8-fold increase over endogenous expression, data not shown). Expression of exogenous KCC2 has been shown in the past to successfully extrude chloride and convert the effect of GABA from depolarizing to hyperpolarizing (Cancedda et al., 2007; Fiumelli et al., 2005). To knock down endogenous KCC2 expression, we designed a short-hairpin (sh)RNA targeting mouse KCC2 mRNA (shKCC2) but not human KCC2, which allowed us to perform rescue of the knockdown using human KCC2*. We confirmed the knockdown of endogenous KCC2 in migrating interneurons by electroporating E14.5 MGE explants with either a control construct expressing a nonspecific shRNA or shKCC2 (Figure 3A) and immunostaining for KCC2 after 7 DIV, i.e., when the vast majority of interneurons have normally upregulated KCC2 (Figure 3). Our shRNA approach is very effective at knocking down endogenous KCC2 protein expression below detectable levels in interneurons (Figures 3E–3K) but fails to knock down KCC2* (data not shown). None of these treatments decreased interneuron viability as measured by expression of activated caspase-3 (Figure S7).

After confirming our capacity to control the level of KCC2 expression in migrating interneurons, we then determined the responsiveness of these interneurons to $GABA_A$ receptor activation or inhibition. Knocking down endogenous expression of KCC2 (shKCC2) or premature expression of KCC2 (shKCC2 + KCC2*) reproduced the responses found with endogenously low and high KCC2 expression, respectively (Figures 2 and 3). Again,

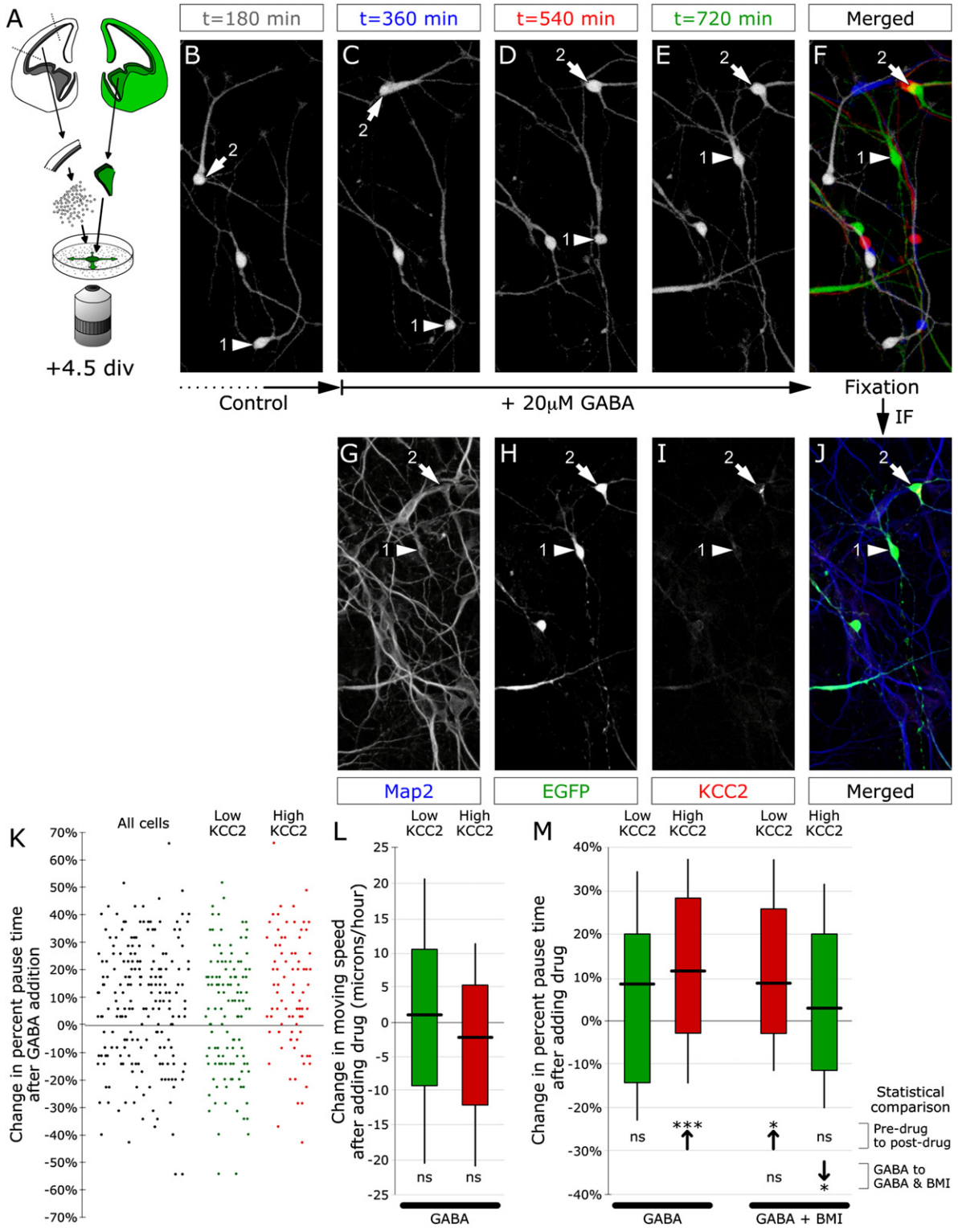

Figure 2. GABA Decreases Motility of Interneurons Expressing High Levels of KCC2 via $GABA_A$ Receptor Activation

(A) E14.5 wild-type neocortex was dissociated, providing a 2D substrate for the migration of MGE-derived EGFP-expressing interneurons.

(B–F) Time series of migrating interneurons pseudocolored at equally spaced time frames before extracellular application of 20 μM GABA ([B], white, 180 min after start of imaging, i.e., 180 min before application of GABA; [C], blue, 360 min after start of imaging corresponding to time of GABA application) and after application

$GABA_A$ receptor activation using $GABA_A$ agonist muscimol (10 μM) caused no significant change in the pausing frequency in interneurons expressing low levels of KCC2 (shKCC2), while interneurons expressing KCC2* paused significantly more than control isochronic interneurons expressing only EGFP (Figure 3L). Conversely, antagonizing $GABA_A$ receptors with BMI (10 μM) caused low-KCC2-expressing shKCC2 interneurons to pause more frequently and decreased the pausing frequency of KCC2*-expressing interneurons (Figure 3L). The recapitulation of Figure 2's results using forced knock down or overexpression of KCC2 confirms the causality of KCC2 expression in increasing pausing frequency upon $GABA_A$ receptor activation.

The Effects of KCC2 on Interneuron Motility Require Its N-Terminal-Dependent Transporter Properties

KCC2 has recently been shown to mediate some of its function by interacting with the actin cytoskeleton through the ability of its intracellular C terminus to bind the actin-binding protein 4.1B (Li et al., 2007). To test the hypothesis that the effects of KCC2 expression are due to these cytoskeletal interactions, we attempted to rescue the effects of knocking down KCC2 (shKCC2) with an N-terminal deletion (KCC2*-NTD). This deletion was previously shown to ablate the transport activity of KCC2 without affecting its cytoskeletal interactions. A C-terminal deletion could not be used to cleanly eliminate the cytoskeletal interactions of KCC2 (Li et al., 2007) since the C terminus has also been shown to affect the transport activity of KCC2 in iso-osmotic conditions (Mercado et al., 2006). KCC2*-NTD expresses at levels identical to full-length KCC2 (Figures 3B–3D and S8A–S8C). Interneurons expressing NTD-KCC2* (and shKCC2 to knock down endogenous expression) were unaffected by muscimol and showed a significant increase in pausing frequency upon BMI application (Figure S8D). This demonstrates that the transport properties of KCC2 are required for its effect on inducing responsiveness to GABA as a stop signal in migrating interneurons.

Forced Hyperpolarization Reduces Interneuron Motility

Our results so far (and some others presented below) strongly suggest that depolarizing signals such as GABA acting through $GABA_A$ receptors prior to KCC2 upregulation stimulate interneuron migration. Conversely, upon KCC2 upregulation, $GABA_A$ receptor activation, which should hyperpolarize interneurons, caused a significant increase in pausing frequency. One possibility is that interneurons integrate hyperpolarizing and depolarizing signals to determine when to stop migrating. To test this hypothesis, we electroporated an inward-rectifying potassium channel (K_{ir} 2.1) along with shKCC2 (in order to make sure that we are restricting our analysis to interneurons expressing low levels of KCC2). K_{ir} 2.1 has been previously shown to significantly and constitutively reduce membrane potential by inducing potassium efflux (Cancedda et al., 2007). Our results show that expression of K_{ir} 2.1 significantly increases pausing frequency in migrating interneurons compared to expression of shKCC2 alone or control EGFP expression (Figure 3L). These results indicate that forced hyperpolarization is sufficient to promote pausing in interneurons.

KCC2 Expression Regulates the Termination of Interneuron Migration

To further reinforce the relevance of increased KCC2 expression with the *termination* of interneuron migration rather than simply decreasing their motility, KCC2 expression was measured in older cultures and correlated with migration properties. E14.5 EGFP+ MGE-derived interneurons were cultured for 7 DIV on isochronic wild-type dissociated cortical substrate, time lapsed for 6 hr, fixed, and immunostained for KCC2 (Figure 4; Movie S8). At this later time point, we observed a perfect correlation between KCC2 expression and the absence of cell body translocation in cortical interneurons, strongly suggesting that KCC2 upregulation is tightly coupled with the *termination* of interneuron migration and not only with decreased motility.

If this model is correct, precocious KCC2 expression should be sufficient to induce premature termination of interneuron migration. E14.5 wild-type slices were electroporated specifically in the MGE with control (EGFP only) or KCC2-IRES-EGFP constructs at E14.5 and cultured for 4 days ex vivo (Figure 5A). Control electroporations show robust migration from the MGE into the cortex (Figure 5B), while KCC2-overexpressing interneurons display limited migration mostly restricted within the ventral telencephalon (Figure 5C). The quantification demonstrates a 2-fold reduction in the percentage of MGE-derived interneurons reaching the dorsal telencephalon in KCC2-expressing compared to control slices (29.0% ± 5.3% versus 54.4% ± 5.0%, respectively; Figure 5D). These results demonstrate that premature expression of KCC2 is sufficient to reduce interneuron migration to the cortex in the presence of endogenous levels of GABA.

To test if KCC2 expression is required to stop interneuron migration, E14.5 MGE explants were electroporated with control shRNA, shKCC2, or shKCC2 rescued with human KCC2*. These

of GABA ([D], red, 540 min after start of imaging, i.e., 180 min after GABA application; [E], green, 720 min after start of imaging, i.e., 360 min after GABA application). See Movie S7 for the animated version of this panel.

(G–J) Interneuron cultures that were time lapsed where fixed immediately after the last frame and immunostained for MAP2, EGFP, and KCC2. The same cells that were time lapsed were then reimaged to assess their level of KCC2 expression.

(K) This technique allows the matching of individual interneuron responses to pharmacological treatments with KCC2 expression in individual interneurons. Interneuron responses to GABA application were binned into low and high KCC2 populations (green and red, respectively), which demonstrate a significant shift in pausing frequency for the high-KCC2-expressing subpopulation of interneurons but not for the low-KCC2-expressing interneurons.

(L and M) Box-whisker plot representation of interneuron responses to drug application binned according to KCC2 expression levels. Throughout the paper, box plots in red represent putative responses to "hyperpolarizing" $GABA_A$ receptor activation (high-KCC2-expressing interneurons), whereas green box plots indicate responses to putative "depolarizing" $GABA_A$ receptor activation. No significant changes in moving speed were detected in either subpopulation following 20 μM GABA (L) or GABA with concurrent application of $GABA_A$ receptor antagonist bicuculline methiodide (BMI; 10 μM; data not shown). (M) Low KCC2 interneurons showed no significant increase in pause time upon GABA application, while high KCC2 interneurons showed a significant ($p = 0.0004$) increase in pausing after GABA application. Coapplication of BMI with GABA abolished the effect of GABA alone ($p = 0.0308$), leading to no significant difference between pre- and post-drug pausing frequency. Conversely, BMI coapplication did cause any significant increase in pausing frequency for interneurons expressing low level of KCC2.

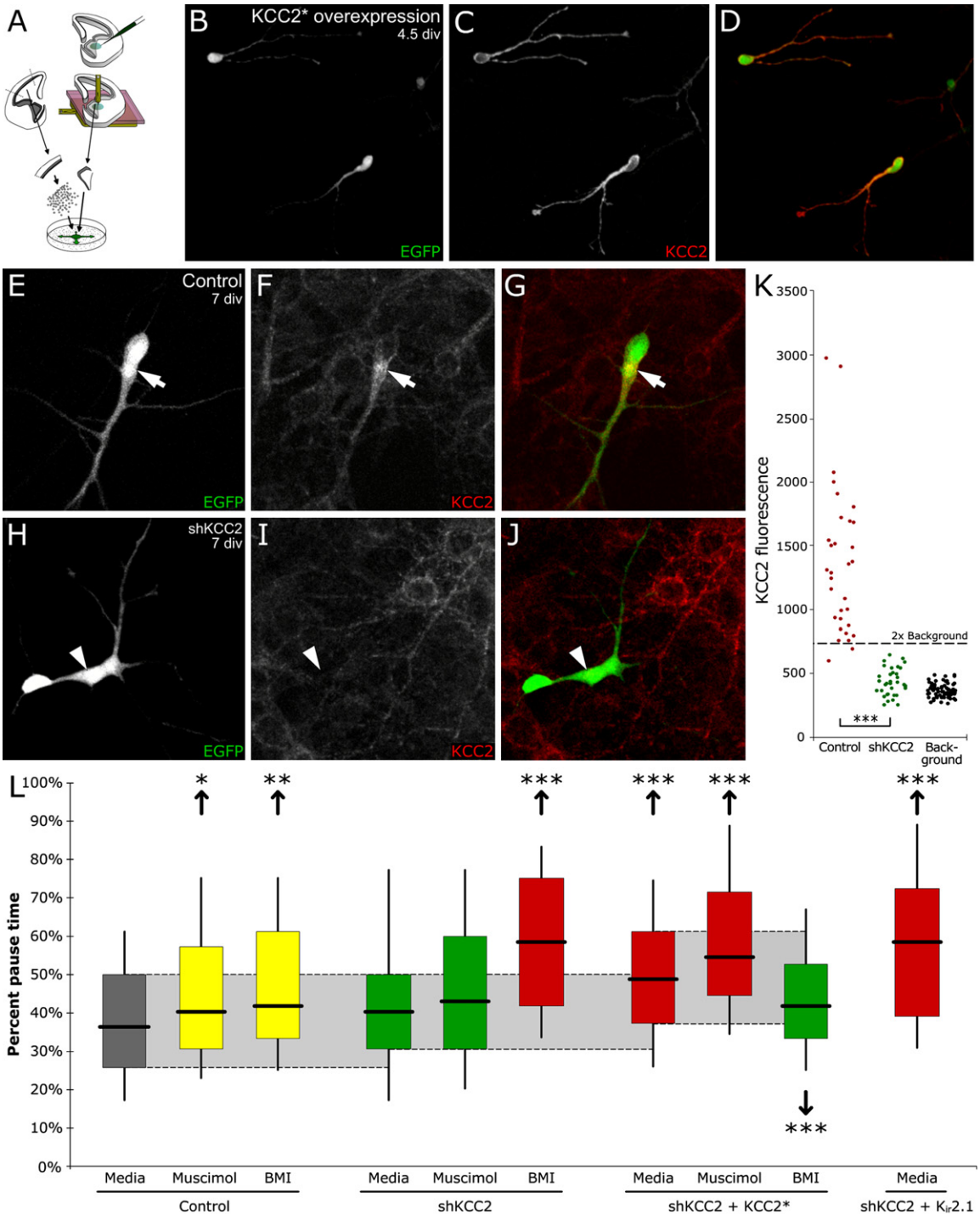

Figure 3. KCC2 Expression Is Necessary and Sufficient to Reduce Cortical Interneuron Motility

(A–D) KCC2 was overexpressed in E14.5 wild-type MGE explants by electroporation of EGFP-IRES human KCC2 construct (KCC2*). (B–D) Expression was verified by high immunofluorescence after 4.5 DIV.

(E–J) Short-hairpin RNAi targeted against mouse KCC2 (shKCC2) is very effective to knock down endogenous KCC2 expression in interneurons. (E–G) Interneuron electroporated with a construct encoding EGFP at E14.5 was immunostained for KCC2 (red) at 7 DIV. (H–J) Interneuron electroporated with a control EGFP and a construct encoding shKCC2 at E14.5 shows no KCC2 expression at 7 DIV.

(K) Quantification shows a significant reduction in KCC2 with use of shKCC2. Measurements of background KCC2 immunoreactivity show that KCC2 is approaching undetectable background levels with introduction of shKCC2. Fluorescence was measured in 12 bits (value range of 0–4095).

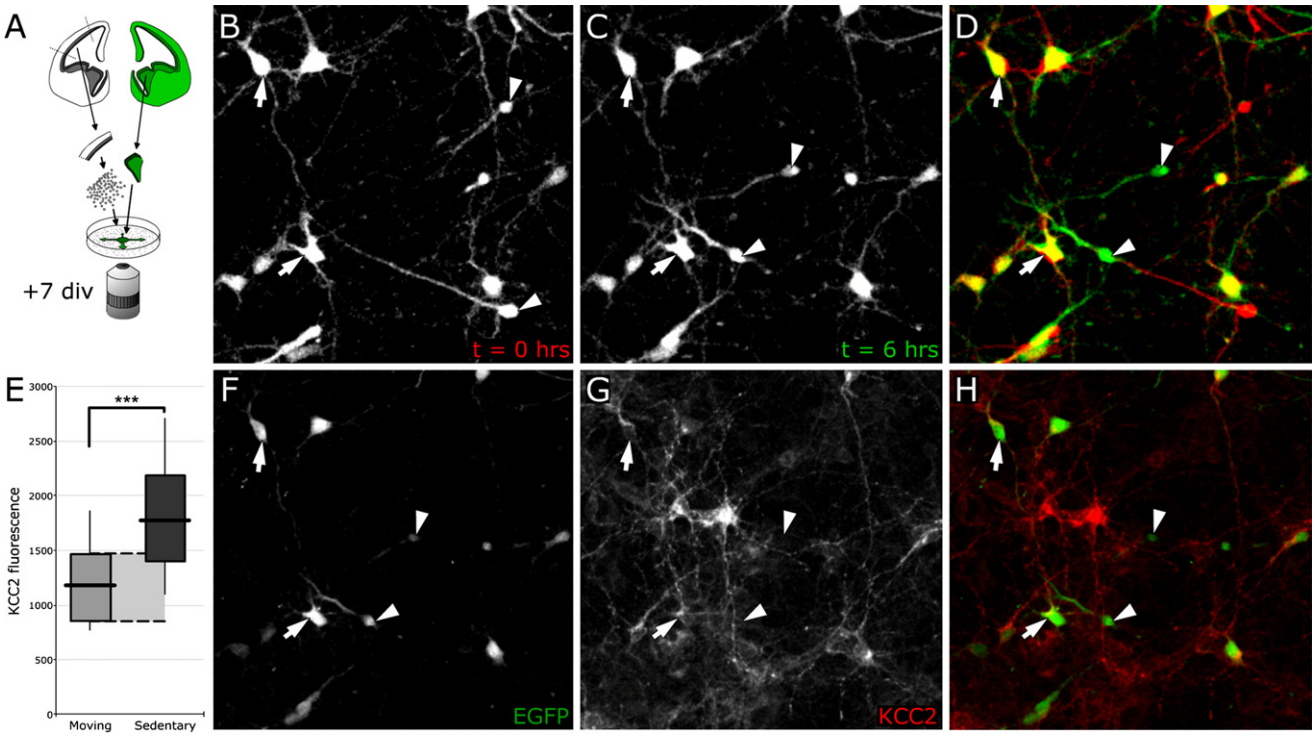

Figure 4. KCC2 Is Strongly Correlated with the Termination of Interneuron Migration

(A) E14.5 EGFP-MGE explants were placed on E14.5 wild-type dissociations and cultured for 7 DIV. These interneurons were then time lapsed for 6 hr (B–D), fixed, and immunostained for KCC2 (F–H). (E) Box plots show 10th, 25th, 50th, 75th, and 90th percentiles of KCC2 fluorescence in moving versus sedentary interneurons. Light-gray shading shows the 25th–75th percentile range of KCC2 expression in the motile population of interneurons. Binning interneurons into moving and nonmoving populations reveals significantly higher KCC2 expression in the sedentary population ($p < 0.0001$). Note that yellow "colabeling" in time-lapse representation (D) corresponds with yellow colabeling of KCC2 with interneurons (H). Movie S8 provides an example of the raw time-lapse data.

interneurons were time lapsed at 7 DIV, i.e., when most interneurons have already upregulated KCC2 and stopped migrating in vitro and in vivo (see Figure 1 and Figures S1 and S3). By 7 DIV, only a few interneurons are still migrating in control electroporations (30.5% ± 3%; Figures 5E and 5H; Movie S9) corresponding approximately to the percentage of interneurons migrating in vivo at P1 (E14.5 + 7 days; see Figure 1). Importantly, knocking down KCC2 almost doubles the proportion of migrating cortical neurons to 55.5% ± 3.5% (Figures 5F and 5H; Movie S10). KCC2* expression successfully rescued the termination of interneuron migration, leaving 93.2% ± 2.1% in a sedentary state (Figures 5G and 5H; Movie S11). Therefore, expression of KCC2 is necessary and sufficient for proper termination of interneuron migration.

KCC2 Expression in Migrating Interneurons Negatively Regulates the Frequency of Intracellular Calcium Transients

The frequency of intracellular calcium dynamics has been shown to control positively the rate of migration of cerebellar granule cells (Komuro and Kumada, 2005) and to negatively regulate the rate of extension of axonal growth cones (Gomez and Spitzer, 1999). We hypothesized that regulating the outcome of $GABA_A$ receptor activation from depolarizing to hyperpolarizing could alter the intracellular calcium dynamics of migrating interneurons through differential activation of voltage sensitive calcium channels (VSCCs) coupled or not to the release of calcium from internal stores. Calcium responses have been observed in migrating cortical interneurons, but only upon pharmacological manipulations such as the application of muscimol, NMDA, and kainate (Soria and Valdeolmillos, 2002). Therefore, at this point, the spatial and temporal features of *endogenous* intracellular calcium dynamics in migrating cortical interneurons have not been reported.

In order to first document intracellular calcium dynamics in migrating interneurons, we electroporated mRFP in E14.5 MGE progenitors and cultured these explants on isochronic dissociated cortical neurons as a 2D substrate for 4 DIV. These cocultures were then loaded with the cell-permeant calcium-sensitive dye, Oregon green BAPTA-AM. Spontaneous calcium transients could clearly be monitored in these migrating interneurons at

(L) Similar to interneurons expressing low levels of KCC2, interneurons expressing shKCC2 (KCC2 knockdown) respond to BMI application (10 μM) by pausing significantly more frequently ($p < 0.0001$). KCC2* rescues the knockdown by pausing them more with $GABA_A$ receptor activation (10 μM muscimol; $p < 0.0001$) and less with blocking the receptors ($p < 0.0001$). Box plots are color coded to represent putative depolarized (green), hyperpolarized (red), or mixed (yellow) interneuron population with respect to appropriate control, depending on the treatment. Light-gray shading shows the 25th–75th percentile range of appropriate control.

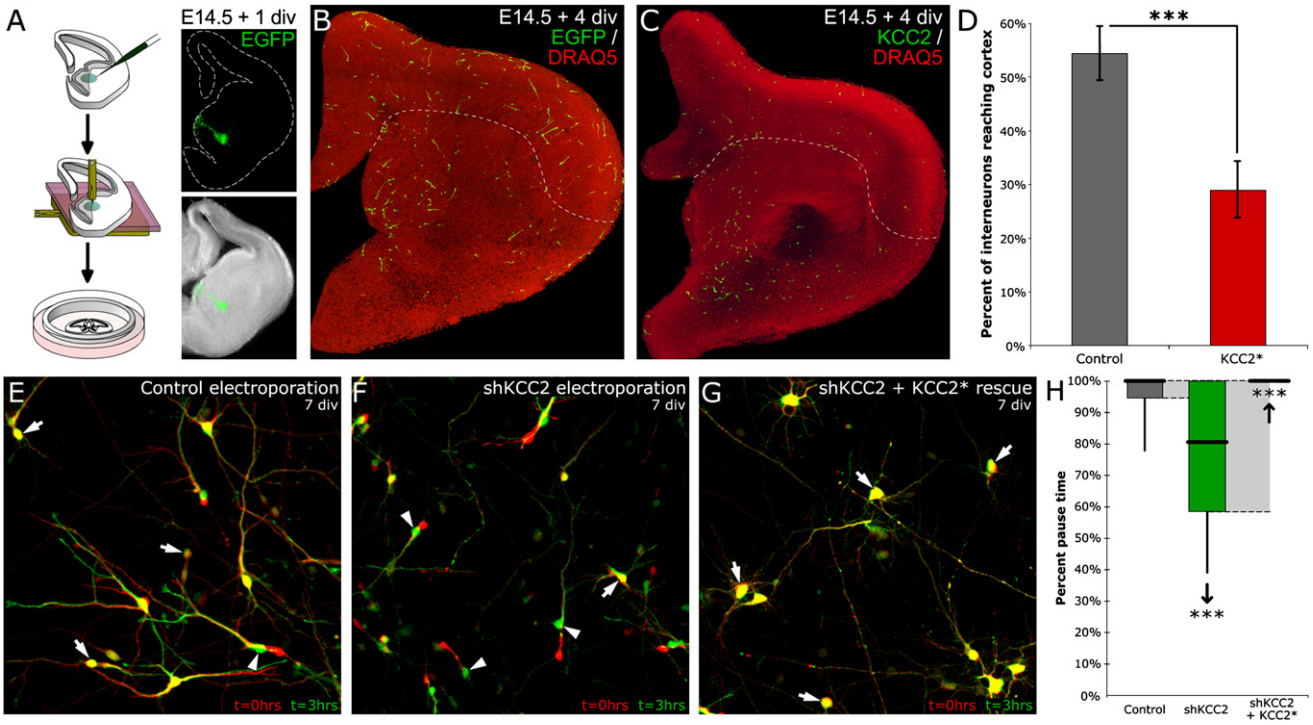

Figure 5. KCC2 Expression Is Necessary and Sufficient for the Inhibition of Cortical Interneuron Migration

(A) Wild-type embryonic cortical slices (300 μm thick) were injected in the MGE with either control EGFP constructs or EGFP-IRES-KCC2*-expressing constructs and subsequently electroporated. Slice pictures show early EGFP expression in MGE after 1 DIV.

(B and C) While EGFP controls (B) show robust migration of interneurons from the striatum into the dorsal telencephalon, precocious expression of KCC2* in slices reduces migration to the cortex by ~2-fold.

(D) Quantification shows a significant decrease ($p < 0.0001$) in the percentage of interneurons migrating into the cortex from the ventral telencephalon in KCC2-overexpressing interneurons. KCC2* box plot is red to indicate putative "hyperpolarizing" effect of $GABA_A$ receptor activation.

(E–G) MGEs electroporated with either (E) control plasmid, (F) shKCC2, or (G) shKCC2+KCC2* were explanted on wild-type cortical dissociated cultures for 7 DIV and time lapsed for 6 hr. Pictures show initial frame (t = 0) shown in red and 3 hr later shown in green. Decrease of "yellow overlap" in labeled interneurons after knocking down KCC2 indicates fewer sedentary interneurons as well as the fact that rescue using KCC2* expression is sufficient to stop interneuron migration.

(H) Box plots show percent pause times of cortical interneuron population. Green box plot indicates treatment that would result in depolarizing effect of $GABA_A$ receptor activation. KCC2* rescue would hyperpolarize population, but could not be colored due to 93% termination rate and complete compression of the box. Light-gray shading shows middle 50th percent range of appropriate control population. Quantification shows a significant decrease in the pause times of interneurons expressing the shKCC2 ($p < 0.0001$) and a significant rescue with KCC2*($p < 0.0001$). See Movies S9–S11 for representative examples of the time lapse shown in this figure.

E14.5 + 4 DIV without the addition of any drugs (Figures 6A–6E). Movie S12 shows three migrating interneurons; only one of these interneurons (far right) shows an obvious spike following a calcium wave through the surrounding cells and its own somal translocation. Although the occurrence of these calcium transients was not observed in all interneurons (Figure 6E), which might be, at least in part, due to variability of KCC2 expression, we nevertheless confirmed the existence of calcium signaling during the course of interneuron migration without pharmacological intervention.

To determine if KCC2 expression was directly responsible for the diverse range of calcium dynamics observed in migrating interneurons, we compared the calcium dynamics of migrating interneurons where we knocked down KCC2 expression using shRNA (shKCC2) to interneurons where we overexpressed KCC2*. Movie S13 shows calcium dynamics of KCC2 knockdown interneurons in a montage of four fields. Most interneurons (9 of 16 cells) with knocked down KCC2 expression display several calcium transients per hour (Figure 6F).

The high number of calcium transients observed in shKCC2 interneurons is in stark contrast to the absence of similar transients when KCC2 is overexpressed in isochronic migrating interneurons (E14.5 + 4 DIV). A montage of the types of calcium dynamics displayed by KCC2-overexpressing interneurons can be seen in Movie S14. In these interneurons, no calcium transients were observed (0 of 14 cells). Three representative traces of intracellular calcium dynamics observed in KCC2-expressing interneurons are shown in Figure 6G, illustrating the complete absence of these calcium transients.

To test the hypothesis that these calcium transients were due to the depolarizing effects of $GABA_A$ receptor activation in interneurons expressing low levels of KCC2, we knocked down KCC2 and performed calcium imaging in the presence of BMI (10 μM). As observed for KCC2-overexpressing interneurons, the removal of the GABA depolarizing effect eliminated the calcium transients typically observed in migrating interneurons (Figure 6H and Movie S15).

The quantification of the frequency of calcium transient can be rather arbitrary since it depends heavily on the threshold used to define these "transients." To quantify the frequency of these calcium transients in an unbiased and objective way, we performed relative power spectral density (RPSD) analysis on the recorded calcium traces. This analysis separates time from the frequency component of the raw calcium traces, providing a quantitative representation of what specific frequencies dominate the recorded calcium signals. This analysis revealed a significantly higher occurrence of "slow" (0.003–0.03 Hz) intracellular calcium transients in shKCC2 interneurons compared to KCC2*-expressing interneurons (Figure 6I). When these values were binned into 0.003–0.03 Hz versus >0.03 mHz, RPSD of shKCC2 interneurons was significantly higher than that of KCC2-overexpressing cells (Figure 6J). Interneurons electroporated with shRNA against KCC2 also showed a significantly higher RPSD at 0.003–0.03 Hz frequencies compared to >0.03 Hz frequencies, while KCC2-overexpressing interneurons showed no statistical difference in RPSD binned for 0.003–0.03 Hz or >0.03 Hz categories. Application of BMI was similarly effective in eliminating the calcium transients observed in KCC2 knockdown interneurons (Figure 6H), demonstrating that, in migrating interneurons expressing low or no KCC2, these spontaneous calcium transients are mediated by $GABA_A$ receptor-mediated depolarization. These data show that KCC2 upregulation negatively regulates the frequency of intracellular calcium transients occurring in migrating interneurons by reducing depolarization induced by GABA-mediated activation of $GABA_A$ receptors.

If there is a causal relationship between the frequency of intracellular calcium transients and the termination of interneuron migration upon KCC2 upregulation, we hypothesized that prevention of intracellular calcium transients would be sufficient to prematurely stop interneuron migration as previously shown for cerebellar granule cells (Komuro and Kumada, 2005). To chelate intracellular calcium in situ, we incubated acute telencephalic slices isolated from E14.5 Lhx6-EGFP transgenic embryos with 25 μM BAPTA-AM for 2 hr before imaging. We then performed confocal time-lapse microscopy and compared the dynamics of Lhx6-EGFP interneuron migration in situ to isochronic control slices. When comparing a control time lapse (Figure 6H; Movie S1) to a calcium-chelated slice (Figure 6L; Movie S16), it is apparent that intracellular calcium chelation is sufficient to inhibit or frequently stop the migration in cortical interneurons (visualized by white pseudocolor in Figure 6). The quantification of these movies shows that most (84.9% ± 2.8%) interneurons are migrating in control conditions at E14.5 + 1 DIV while only 51.4% ± 0.3% of interneurons migrate when intracellular calcium is sequestered (Figure 6M). This result strongly suggests that intracellular calcium transients observed in interneurons are required for their migration and that KCC2 upregulation is sufficient to ablate these intracellular calcium dynamics leading to termination of interneuron migration.

The Effect of GABA-Mediated Calcium Transients on Interneuron Motility Are Mediated by Activation of Voltage-Sensitive Calcium Channels

We hypothesized that the activation of $GABA_A$ channels in interneurons expressing no or low KCC2 leads to depolarization through efflux of chloride leading to opening of voltage-sensitive calcium channels and therefore to calcium entry. After confirming the expression of L-type VSCC subunits $Ca_V1.2$ and -1.3 in migrating cortical interneurons at this developmental stage (Figure S9), we tested this hypothesis by utilizing our 2D assay at E14.5 + 4.5 DIV in order to test the acute effect of blocking different types of VSCCs in interneuron migration. Antagonists for N-type and L-type VSCC (5 μM GVIA omega-conotoxin and 10 μM nifedipine, respectively) were tested for effects on pausing frequency in migrating interneurons. While both antagonists significantly increased the pause times of interneurons, the effect of blocking L-type calcium channels using nifedipine was significantly more potent (Figures 7A–7C; Movies S17 and S18), leading to interneurons spending on average 85%–90% of their time not moving. The acute blockade of L-type VSCCs caused a complete and immediate termination of migration of ~40% of interneurons observed (22 of 60) and a significant increase in pausing time in the other interneurons (Figures 7A–7C). Interestingly, applying bayK8644 (an agonist of VSCCs, which increases the duration of the "open" state of L-type Ca^{2+} channels) was sufficient to decrease the number of sedentary interneurons at 7 DIV from 70% to 40% (Figure S10; Movies S9 and S21) and extend the window of cortical interneuron migration.

GABA- or Glutamate-Mediated Depolarization Stimulates the Migration of Cortical Interneurons

Although Figure 5 showed that KCC2 overexpression does cause a large increase in the proportion of sedentary interneurons at 7 DIV, Figure 3 indicated that KCC2 expression coupled to GABA application does not cause a complete termination of migration. If GABA-mediated hyperpolarization is responsible for terminating migration, why is the effect of KCC2 upregulation only partial? These results, combined with the more dramatic effect of antagonizing L-type VSCCs, led us to hypothesize that other depolarizing cues were contributing to the stimulation of interneuron migration even in the absence of GABA-mediated depolarization. An obvious candidate was glutamate-mediated activation of AMPA/NMDA receptors, which are expressed by migrating interneurons (Metin et al., 2000; Soria and Valdeolmillos, 2002). To test this, we performed experiments where $GABA_A$ receptors are activated by muscimol in interneurons expressing KCC2 at E14.5 + 4.5 DIV, only this time in the presence of AMPA and NMDA antagonists (NBQX 10 μM and APV 100 μM, respectively; Figures 7D–7F; Movies S19 and S20). Blocking AMPA/NMDA receptors induced a significant increase (+30%) in the percentage of interneurons terminating migration. This result demonstrates that migrating interneurons are under tonic AMPA/NMDA receptor-mediated depolarization, which significantly stimulates their motility. Interestingly, decreasing the level of KCC2 expression in interneurons (shKCC2) rescues the loss of AMPA/NMDA receptor signaling in the presence of muscimol (Figures 7E and 7F).

Conversely, we wanted to confirm that $GABA_A$ receptor activation in interneuron expressing low or no KCC2 acted as a motogenic cue. In previous experiments, this effect may have been partially obscured by the tonic effect of AMPA/NMDA receptor activation. It is well established that L-type subunits $Ca_V1.2$ and -1.3 desensitize rapidly not only to high levels of depolarization, but also to high intracellular calcium concentrations (Lacinova

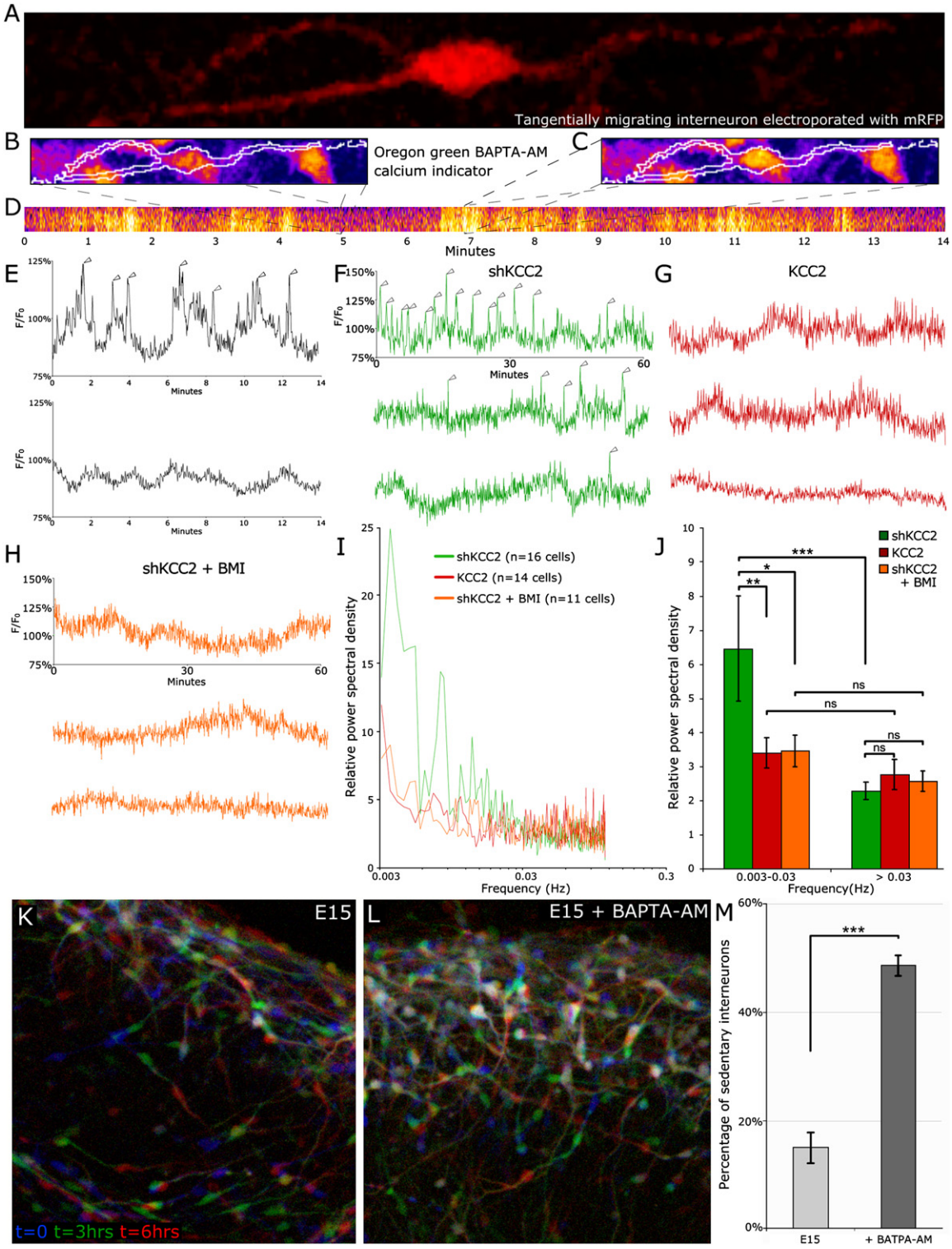

Figure 6. Calcium Signals in Tangentially Migrating Interneurons Are Reduced with KCC2 Upregulation

(A–D) Migrating cortical interneurons show spontaneous calcium transients to a varying degree. (A) An mRFP-electroporated E14.5 MGE interneuron was loaded with Oregon green BAPTA-AM and time lapsed. Pseudocolored images show calcium signal at low (B) and high (C) periods of activity, with white outlining the interneuron. (D) Pseudocolored strip across bottom shows an orthogonal resection through the cell body during the course of the time lapse. Note that no pharmacological treatments were required to elicit these spontaneous calcium signals.

(E) Calcium signals observed in control conditions show wide range of dynamics.

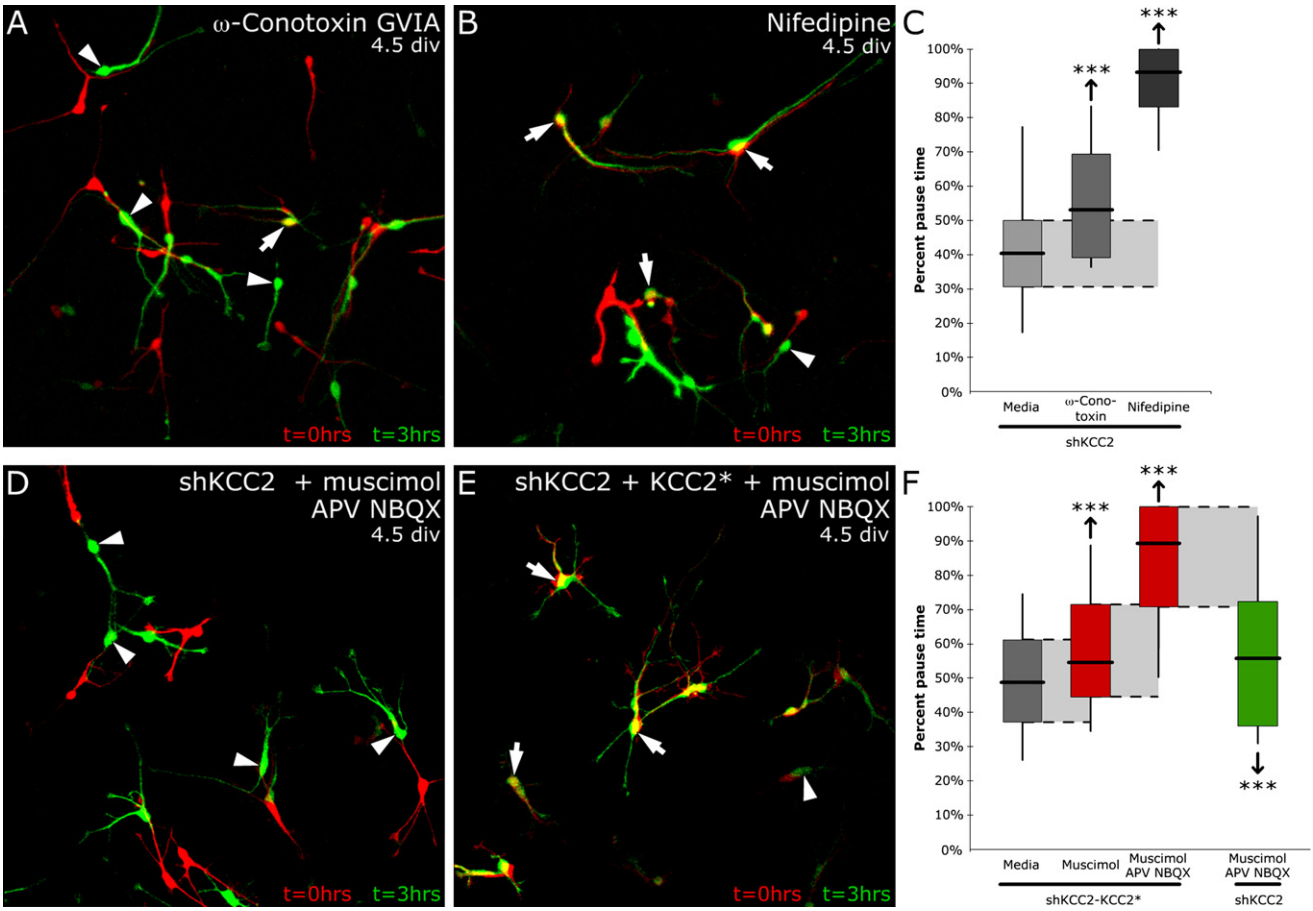

Figure 7. Reduced Activation of VSCCs by Direct Antagonism or Indirectly by Blocking Glutamate Signaling Further Increases Pause Times in Interneurons

(A–C) E14.5 interneurons electroporated with shKCC2 and plated on wild-type dissociated cortex increased in pausing with addition of (A) the N-type VSCC antagonist ω-conotoxin GVIA (5 μM) at 4.5 DIV ($p < 0.0001$) and an even greater effect with the addition of (B) L-type VSCC antagonist, nifedipine (10 μM; $p < 0.0001$). (C) Box plots showing percentage of time pausing for migrating cortical interneurons in conditions shown in (A) and (B). Light-gray shading indicates the 25th–75th range of percentiles of control values. See Movies S17 and S18.

(D–F) KCC2 knockdown interneurons show little effect on pausing when eliminating depolarization due to glutamate signaling (100 μM APV and 10 μM NBQX) as long as depolarization due to muscimol (10 μM) are still present (D and F). Box plots are color coded to indicate whether drug treatment and KCC2 modification would be depolarizing (green) or hyperpolarizing (red) with respect to appropriate control. Note that when KCC2 is upregulated and muscimol is hyperpolarizing, the effect of eliminating AMPA/NMDA-mediated depolarization is highly significant (E and F). See Movies S19 and S20 for corresponding time lapse.

and Hofmann, 2005; Lipscombe, 2002). It is possible that low-KCC2-expressing interneurons have already reached their "maximal level" of VSCC activation prior to additional stimulation of $GABA_A$ receptors with pharmacological treatment. Therefore, we repeated our experiments using muscimol to activate $GABA_A$ receptors on migrating interneurons with shKCC2 and in the

(F–J) KCC2 expression ablates 0.003–0.03 Hz calcium transients. Calcium signals from Oregon green BAPTA-loaded interneurons electroporated with either mRFP and a plasmid encoding shKCC2 (F), mRFP-IRES-KCC2 (G), or shKCC2 + 10 μM BMI (H) are shown. Interneurons with knocked down KCC2 show several calcium spikes (indicated by arrowheads) on top of a larger wave. Neither KCC2-overexpressing nor shKCC2 + BMI interneurons show these types of calcium transient. See Movies S12–S15 for corresponding time-lapse movies. (I) A spectral analysis was done on individual interneurons and averaged for each group, indicating a decrease in calcium signaling in the 0.003–0.03 Hz frequency range upon either KCC2 overexpression or $GABA_A$ receptor blockage. (J) The relative power spectral densities were binned into 0.003–0.03 Hz and >0.03 Hz categories. KCC2 knockdown and BMI-treated interneurons showed significantly higher signaling activity in the range of 0.003–0.03 Hz. At higher frequencies, this difference disappears. KCC2-overexpressing and BMI-treated cells show no significant difference between higher and lower frequencies, indicating that the loss of $GABA_A$ receptor-induced depolarization decreases spontaneous calcium activity in this frequency range.

(K–M) Time-lapsed Lhx6-EGFP interneurons at E15 are shown with initial image (t = 0) in blue, 3 hr in green, and 6 hr in red. Nonmoving cells appear white. Note that chelation of intracellular calcium with 25 μM BAPTA-AM significantly increases the number of stationary interneurons (L) relative to control (K). (M) Quantification shows a decrease (χ^2 analysis, $p < 0.0001$) in the proportion of migrating interneurons following intracellular calcium chelation. See Movies S1 and S16 for corresponding time lapse.

presence of APV/NBQX to block the NMDA/AMPA receptor-mediated VSCC activation (Figures S11A–S11C; Movies S19 and S22). Our results demonstrate that muscimol application alone on shKCC2-expressing interneurons has limited effect on motility compared to control shKCC2 alone, most likely because of a "ceiling effect" on the rate of interneuron motility due to the motogenic effect of tonic activation of AMPA/NMDA receptors. Indeed, blocking AMPA/NMDA receptors in shKCC2-expressing interneurons increases the percentage of pausing time, but, most interestingly, activation of $GABA_A$ receptors in the same shKCC2-expressing interneurons in the presence of NBQX and APV strongly stimulates their motility by reducing their pausing frequency (Figure S11C). This final result demonstrates that, in migrating interneurons expressing low or no KCC2, depolarization through both $GABA_A$ or AMPA/NMDA receptors plays a cumulative, complementary motogenic effect.

DISCUSSION

Our results demonstrates that (1) depolarization through activation of $GABA_A$ receptors (low KCC2) and AMPA/NMDA receptors exerts a complementary motogenic activity on migrating interneurons and (2) that upregulation of KCC2 is necessary and sufficient to reduce interneuron migration by rendering $GABA_A$ receptor activation hyperpolarizing. Interestingly, these effects are largely mediated through the regulation of intracellular calcium dynamics. $GABA_A$ receptor activation in migrating interneurons expressing low levels of KCC2 induces calcium transients, which disappear upon KCC2 upregulation. Furthermore, blocking L-type voltage-sensitive calcium channels is sufficient to stop interneuron migration.

GABA and the Migration of Cortical Interneurons

GABA has been previously proposed to modulate neuronal migration, although the direction of this modulation often varies depending on experimental approaches (reviewed by Owens and Kriegstein, 2002). The opening of ionotropic $GABA_A$ receptors enhances both chemotaxis and chemokinesis in cortical dissociated neurons, although $GABA_A$ receptor activation largely hinders migration of GAD+ cells in the cortical plate (Behar et al., 1996, 1998). In spite of GABA's possible hampering effect on migration, other studies have revealed a positive effect of $GABA_A$ receptor activation on radial (Manent et al., 2005) and tangential migration (Cuzon et al., 2006). By monitoring the response of individual interneurons to GABA and correlating it to KCC2 expression, we uncovered the fact that GABA acts as a motogen for immature low-KCC2-expressing interneurons but acts as a stop signal for interneurons expressing high levels of KCC2 once they reach the cortex. This mechanism might ensure that the paracrine level of ambient GABA (measured as ~0.5 μM in vivo) (Cuzon et al., 2006) does not prematurely stop interneuron migration before they reach the cortex.

Upregulation of KCC2 in Development

Interestingly, premature upregulation of KCC2 in radially migrating pyramidal neurons does not affect their migration but significantly dampens their level of dendritic growth and branching (Cancedda et al., 2007). These results suggest that, in pyramidal neurons, ambient level of GABA is not sufficient to act as a stop signal even if KCC2 is prematurely upregulated. In fact, this is compatible with our results suggesting that pyramidal neurons naturally upregulate KCC2 4–8 days after interneurons at a time when they have already stopped migrating in vivo.

A recent article by Batista-Brito and colleagues revealed an enrichment of KCC2 mRNA in a gene expression microarray analysis of embryonic interneurons (Batista-Brito et al., 2008). However, our results document a strong difference in the timing of KCC2 expression between interneurons. Interestingly, outside the developing cortex, large differences have been found between brain regions during development (Belenky et al., 2008; Belmonte et al., 2004; Gilbert et al., 2007). Furthermore, the chloride gradient has even been found to vary greatly between adjacent neurons within the same structure (Gilbert et al., 2007). Our results add further complexity to this regulation by showing a temporally heterogeneous upregulation even within tangentially migrating cortical interneurons.

Determining what factors regulate KCC2 expression in cortical interneurons would greatly improve the understanding of the mechanisms regulating the termination of interneuron migration. Several experimental manipulations, such as the induction of long-term potentiation, magnesium removal, neuronal stress, seizure kindling, and subplate ablation, have been shown to decrease KCC2 expression (Galanopoulou, 2007; Kanold and Shatz, 2006; Rivera et al., 2004; Wake et al., 2007; Wang et al., 2006). Several conflicting lines of evidence have suggested that BDNF (Rivera et al., 2002, 2004) or GABA itself (Ganguly et al., 2001; Kriegstein and Owens, 2001; Leitch et al., 2005; Ludwig et al., 2003; Rivera et al., 2004; Titz et al., 2003; Toyoda et al., 2003) can regulate KCC2 expression. This may indicate multiple regulatory pathways and/or cell-type and region-specific mechanisms underlying KCC2 transcription and translation. In addition, KCC2 activity can also be modulated by localization, oligomerization, and phosphorylation (Adragna et al., 2004; Blaesse et al., 2006; Lee et al., 2007; Wake et al., 2007). Future experiments will need to determine what factors control KCC2 expression in migrating interneurons once they reach the cortex.

Previous studies have suggested a role for KCC2 upregulation in synaptogenesis and cortical plasticity. Overexpression of KCC2 in rat hippocampal cultures has been found to increase the amount of GABAergic synapses (Chudotvorova et al., 2005). This effect might be due at least partially to a precocious termination of interneuron migration, thereby accelerating the rate at which interneurons make and receive synaptic contacts. GABA signaling plays a critical role in determining the critical period for neuronal plasticity in the visual cortex (Hensch, 2005). Future experiments should test if interference with the termination of interneuron migration leads to the precocious development of GABAergic synapses and may therefore prevent the optimal timing of cortical plasticity.

Integration of GABA and Glutamate Signaling in the Migration of Cortical Interneurons

Our results indicate that depolarization through ionotropic glutamate receptor activation stimulates interneuron migration as potently as $GABA_A$ receptor activation in interneurons expressing low or no KCC2. Therefore, our model (see Figure 8) suggests

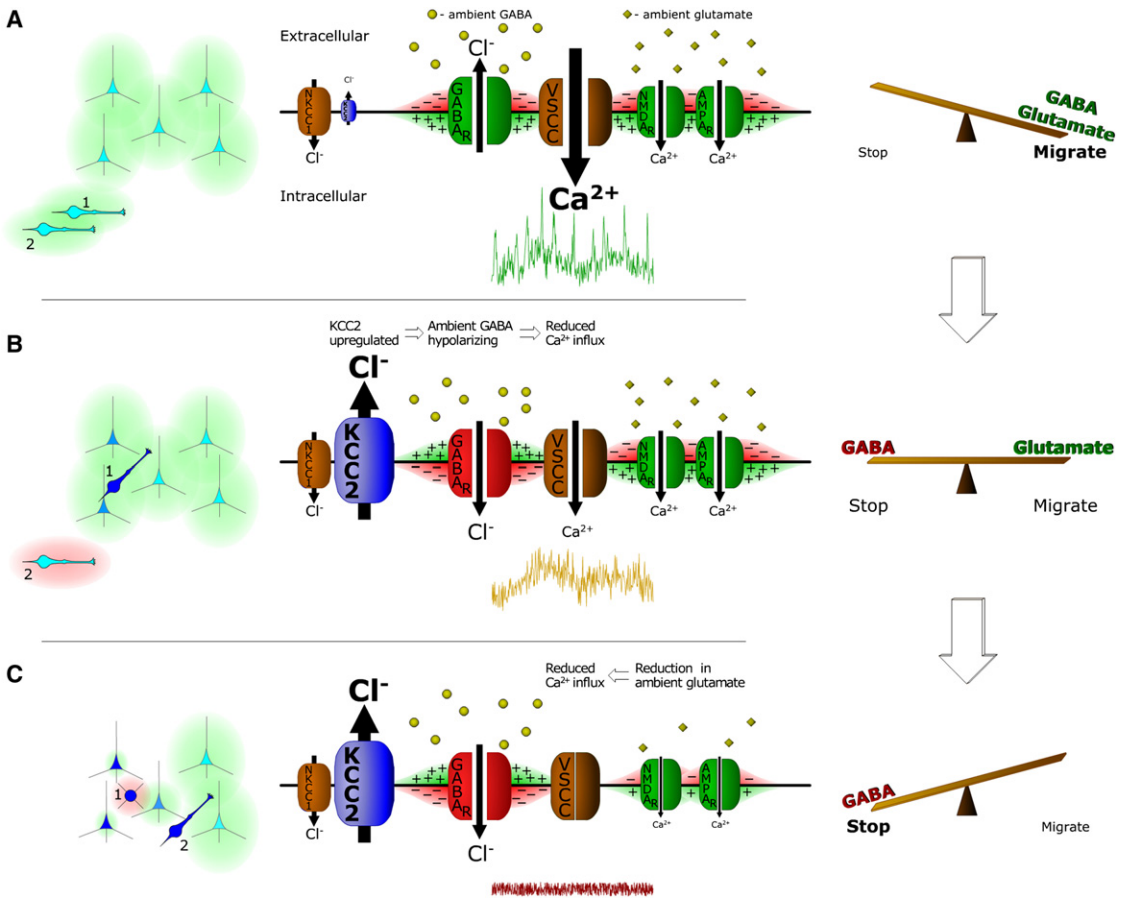

Figure 8. Model—KCC2 Expression Facilitates the Termination of Cortical Interneuron Migration

(A) Initial migration state. Green "halo" represents motogenic effect of glutamate and GABA. Blue shade of interneurons and pyramidal neurons represents degree of KCC2 expression. Membrane magnification illustrates transporter and channel composition of interneurons throughout the figure. Initially, ambient GABA and glutamate stimulate the migration of interneurons by inducing membrane depolarization and activation of VSCCs.

(B) KCC2 upregulation act as a switch rendering ambient GABA hyperpolarizing, reducing Ca^{2+} influx through VSCCs, which significantly reduces interneuron motility. We hypothesize that GABA, when hyperpolarizing, may also have a chemorepulsive effect, which might participate in tiling of interneurons.

(C) Developmental decrease in ambient glutamate mostly due to astrocytic reuptake and confinement to synaptic release further reduces Ca^{2+} influx and contributes to the termination of interneuron migration by reducing global AMPA/NMDA receptor activation on interneurons.

that interneurons integrate ambient levels of GABA and glutamate to determine when to stop migrating. Our results support a model whereby, in order to completely stop migrating, $GABA_A$ receptor-mediated hyperpolarization following KCC2 upregulation must be accompanied by a reduction of tonic AMPA/NMDA receptor activation. This decline might be at least partially due to the upregulation of glutamate transporters by astrocytes or neurons during this period during early postnatal development (Cavelier et al., 2005; Danbolt, 2001).

Glutamate has been previously shown to evoke responses in migrating interneurons (Metin et al., 2000; Poluch et al., 2001, 2003). AMPA receptor activation has been shown to induce the influx of cobalt into tangentially migrating interneurons, indicating the presence of AMPA receptors (Metin et al., 2000). Several studies have also shown that migrating cortical interneurons exhibit transient increase in intracellular calcium upon application of AMPA, kainate, and, in some cases, NMDA receptor agonists (Metin et al., 2000; Soria and Valdeolmillos, 2002), although the function of these calcium transients has remained unclear. Furthermore, NMDA receptor activation has been shown to stimulate neuronal migration by controlling calcium dynamics (Komuro and Rakic, 1993). Our results show that, upon KCC2 upregulation but before synaptogenesis during the first week of postnatal development, cortical interneurons sense and integrate ambient levels of GABA and glutamate, which might reflect the local density of pyramidal neurons versus interneurons (Figure 8). Therefore, we propose that, in migrating interneurons expressing KCC2, the balance between hyperpolarizing ambient GABA and depolarizing ambient glutamate is integrated by the frequency of calcium transients evoked by activation of voltage-sensitive calcium channels. Indeed, chelating intracellular calcium or blocking L-type VSCCs is sufficient to stop interneuron migration (Figure 8).

The ability of immature neurons during migration or during axon pathfinding to use changes of membrane potential as a meaningful signaling event might be a general property. An interesting

study has recently shown that responses to extracellular axon guidance cues elicit changes in membrane potential at the level of individual axonal growth cones and that conversely modifying membrane potential changes growth cone response properties to these axon guidance cues (Nishiyama et al., 2008). Finally, changes in the frequency of calcium spikes in immature *Xenopus* spinal cord neurons alters their neurotransmitter expression, suggesting that specific patterns of calcium dynamics play a role in neurotransmitter homeostasis (Borodinsky et al., 2004). Our results add a new dimension to these findings by showing that migrating interneurons can sense ambient levels of local hyperpolarization and depolarization as a way to determine when to stop migrating through the ability of GABA and glutamate signaling to modify membrane potential and activate VSCCs (see below).

Calcium Signaling and Neuronal Migration

Our data suggest that the mechanism underlying the function of KCC2 upregulation in stopping interneuron migration is the modulation of the frequency of intracellular calcium transients through $GABA_A$ receptor activation (Figure 8). Calcium has often been tied to the process of cellular migration (Komuro and Kumada, 2005; Zheng and Poo, 2007). The GABA-induced changes in neuronal chemotaxis mentioned previously were shown to be calcium dependent (Behar et al., 1996). Counterintuitively, axonal growth cones of *Xenopus* spinal cord neurons move at a rate inversely proportional to the frequency of calcium transients. Altering the calcium signal frequency of these axons was sufficient to induce the corresponding change in axon extension rate (Gomez et al., 1995; Gomez and Spitzer, 1999; Kater and Mills, 1991). Inversely, the rate of migration of cerebellar granule cells is directly proportional to their rate of movement. In this case, a loss of calcium transients was correlated with and sufficient to induce termination of cerebellar granule cell migration (Komuro and Rakic, 1996; Kumada and Komuro, 2004). Alternatively, a recent study showed that migrating olfactory bulb interneurons possessed active L-type calcium channels, yet found that blocking these channels produced no change in their migration rate (Darcy and Isaacson, 2009).

Consequence of Altered Interneuron Migration on Development

The long-term consequences of altering the window of interneuron migration are unknown at the present time but could be quite drastic for cortical circuit assembly. Improper distribution of interneurons may result in cell death in areas where local densities of interneurons are too high (Fuerst et al., 2008) and epileptic activity where interneurons density is too low (Cobos et al., 2005; Li et al., 2008). Not surprisingly, several neurodevelopmental pathologies such as ASD and schizophrenia have been associated with alterations in interneuron number, placement, or maturation. Timothy syndrome, a disorder encompassing multiple dysfunctions, including autistic phenotypes, is caused by a mutation in $Ca_V1.2$ (*CACNA1C*), which increases the open times of voltage-sensitive calcium channels (Splawski et al., 2004). One would expect this mutation to have the same effect on extending interneuron migration as our bayK8644 treatment. A similar investigation uncovered a correlation between autism spectrum disorders and mutations in a T-type calcium channel, $Ca_V3.2$ (*CACNA1H*) (Splawski et al., 2006). Future investigations will determine if deficiency in voltage-sensitive calcium signaling and/or interference with GABA or glutamate signaling during migration leads to improper placement of cortical interneurons. Interestingly, during early postnatal development, acute stress can alter the release of the GABAergic neurosteroid allopregnanolone, which acts as a strong endogenous agonist of $GABA_A$ receptors, and this has been shown to alter the final positioning of GABAergic interneurons in the rat prefrontal cortex (Grobin et al., 2003). We hypothesize that genetic or environmental perturbation of the signaling mechanisms described in the present study might delay the window of cortical interneuron migration and might impact on the onset of inhibitory synaptogenesis in the developing cortex. Future experiments will address how interference with the termination of interneuron migration might affect the maturation and function of the cortical microcircuits.

EXPERIMENTAL PROCEDURES

Animals

All procedures involving animals were approved by the IACUC at UNC-Chapel Hill and were in accordance with NIH guidelines. Transgenic mice expressing EGFP ubiquitously under the control of CMV-enhancer and chicken β-actin promoter (Okabe et al., 1997) were obtained from Jackson Laboratories. Heterozygous Lhx6-EGFP BAC transgenic mice were kindly provided by Drs M-.B. Hatten and N. Heintz (Rockefeller University - GENSAT Consortium; Heintz, 2004), were bred on a Balb/C background for at least ten generations, and maintained in a 12/12 hr light:dark cycle. Timed pregnant mice were obtained by breeding overnight and the following morning is considered as E0.5.

Immunostaining for Slices and Dissociations

Made blocking solution (1 g BSA [A7906, Sigma-Aldrich, St. Louis, MO]/10 ml PBS; 0.3% Triton X-100 [X-100, Sigma-Aldrich, St. Louis, MO] and stored at 4°C). After rinsing in PBS three times for 15 min to remove 4% PFA, incubated overnight in blocking solution at 4°C on shaker. Incubated overnight in blocking solution with 1:1000 primary (chicken polyclonal anti-GFP [A10262; Invitrogen - Molecular Probes, Eugene, OR]; rabbit polyclonal anti-KCC2 [07-432; Upstate, Temecula, CA] against residues 932–1043 of rat KCC2; mouse monoclonal anti-Map2 [clone HM-2; Sigma-Aldrich, St. Louis, MO]; rabbit polyclonal anti-alpha 1C, $Ca_V1.2$ [C1603; Sigma-Aldrich, St. Louis MO]; rabbit polyclonal anti-alpha 1D, CaV1.3 [C1728, Sigma-Aldrich, St. Louis, MO]) at 4°C on shaker. Washed seven times for 15 min in PBS. Washed one time for 15 min blocking solution with 5% goat serum. Incubated overnight in blocking solution, 5% goat serum with 1:1000 secondary (488 goat polyclonal anti-chicken, A11039; 546 goat polyclonal anti-rabbit, A11035; 647 goat polyclonal anti-rabbit, A21245; 647 goat polyclonal anti-mouse, A21236; Invitrogen - Molecular Probes, Eugene, OR) at 4°C on shaker. Washed five times for 15 min in PBS and mounted with GelMount (Biomeda Corp, Foster City, CA).

Pharmacology

After control time-lapse session, 20 μM GABA, made from 20 mM stock in ddH2O (A-5835; Sigma-Aldrich, St. Louis, MO) was added to cultures before time lapsing for a second session. Bicuculline methiodide (2503; Tocris, Ellisville, MO; 10 μM) was added from 10 mM stock in ddH2O. BAPTA-AM (B1205; Invitrogen - Molecular Probes, Eugene, OR; 25 μM) made from 10 mM stock in desiccated DMSO (D2650; Sigma-Aldrich, St. Louis, MO) was added to media underneath slice insert and allowed to load for 2 hr before imaging. Muscimol (M1523; Sigma-Aldrich, St. Louis, MO; 10 μM) was prepared from 10 mM ddH_2O stock solution. BayK8644 (B112, Sigma-Aldrich, St. Louis, MO; 10 μM) was prepared from 500 mM DMSO solution. Nifedipine (N7634; Sigma-Aldrich, St. Louis, MO; 10 μM) was prepared from 5 mM DMSO solution. GVIA ω-conotoxin (C9915; Sigma-Aldrich, St. Louis, MO; 5 μM) was prepared from 1 mM solution in double-distilled (dd)H_2O. DL-2-amino-5-phosphopentanoic acid (AVP; A5282; Sigma-Aldrich, St. Louis, MO; 100 μM) was prepared

from 10 mM solution in media. NBQX (N171; Sigma-Aldrich, St. Louis, MO; 10 μM) was prepared from 10 mM DMSO solution.

Calcium Imaging/Quantification

A stock solution of calcium indicator was made by adding 10 μl DMSO (D2650; Sigma-Aldrich, St. Louis, MO) to 50 μg of Oregon green 488 BAPTA-1, AM (OGB-1; O6807; Invitrogen - Molecular Probes, Eugene, OR). After vortexing for 1 min 5 × 2 μl aliquots were frozen at –80°C. Warm 9.12 μl Pluronic F-127 in 20% DMSO (P3000MP; Invitrogen - Molecular Probes, Eugene, OR) was then added to one aliquot of stock solution. After vortexing for 1 min, a 5 μM working solution was made by adding 5 μl of pluronic-stock solution to 715 μl HBSS and vortexing for another minute.

Ex Vivo Electroporation and Organotypic Slice Culture

As previously described in Hand et al. (2005). See Supplemental Data for detailed procedure.

Confocal Microscopy

Confocal microscopy on fixed tissue was done as described previously (Hand et al., 2005) using a Leica TCS SL inverted confocal microscope equipped with a Marzhauser X-Y motorized stage and a PeCon CO_2- and temperature-controlled stage incubation chamber. Time-lapse microscopy was done as described previously (Hand et al., 2005) with an imaging frequency of a stack captured every 10 min for migration studies. These movies are played back at a rate of 7 frames/s (sped up 4200× real time). Calcium imaging movies were obtained by imaging every 4 s (see calcium imaging section for details).

Detailed Experimental Procedures are available in the Supplemental Data.

SUPPLEMENTAL DATA

The Supplemental Data include Supplemental Experimental Procedures, Statistical Analysis, eleven figures, and 22 movie files and can be found with this article online at http://www.neuron.org/supplemental/S0896-6273(09)00203-7.

ACKNOWLEDGMENTS

We thank members of the Polleux lab for stimulating discussions and comments on the manuscript. We thank Dr. Yu-Qiang Ding (Chinese Academy of Sciences, Shanghai, China), Dr David Mount (Harvard University), Dr. Karl Kandler (University of Pittsburgh), Dr. Catherine E. Krull (University of Missouri, Columbia, MO), Dr. Tom Maynard (University of North Carolina, Chapel Hill) for expression plasmids. Marie Rougié provided outstanding technical help. This work was supported by NARSAD Young Investigator Award (F.P.), a Pew Scholar Award (F.P.), and the NINDS Institutional Center Core Grant to Support Neuroscience Research (P30 NS45892-01).

Accepted: January 30, 2009
Published: April 15, 2009

REFERENCES

Adragna, N.C., Di Fulvio, M., and Lauf, P.K. (2004). Regulation of K-Cl cotransport: from function to genes. J. Membr. Biol. *201*, 109–137.

Andang, M., Hjerling-Leffler, J., Moliner, A., Lundgren, T.K., Castelo-Branco, G., Nanou, E., Pozas, E., Bryja, V., Halliez, S., Nishimaru, H., et al. (2008). Histone H2AX-dependent GABA(A) receptor regulation of stem cell proliferation. Nature *451*, 460–464.

Anderson, S.A., Eisenstat, D.D., Shi, L., and Rubenstein, J.L. (1997). Interneuron migration from basal forebrain to neocortex: dependence on Dlx genes. Science *278*, 474–476.

Ang, E.S., Jr., Haydar, T.F., Gluncic, V., and Rakic, P. (2003). Four-dimensional migratory coordinates of GABAergic interneurons in the developing mouse cortex. J. Neurosci. *23*, 5805–5815.

Batista-Brito, R., Machold, R., Klein, C., and Fishell, G. (2008). Gene expression in cortical interneuron precursors is prescient of their mature function. Cereb. Cortex *18*, 2306–2317.

Behar, T.N., Li, Y.X., Tran, H.T., Ma, W., Dunlap, V., Scott, C., and Barker, J.L. (1996). GABA stimulates chemotaxis and chemokinesis of embryonic cortical neurons via calcium-dependent mechanisms. J. Neurosci. *16*, 1808–1818.

Behar, T.N., Schaffner, A.E., Scott, C.A., O'Connell, C., and Barker, J.L. (1998). Differential response of cortical plate and ventricular zone cells to GABA as a migration stimulus. J. Neurosci. *18*, 6378–6387.

Belenky, M.A., Yarom, Y., and Pickard, G.E. (2008). Heterogeneous expression of gamma-aminobutyric acid and gamma-aminobutyric acid-associated receptors and transporters in the rat suprachiasmatic nucleus. J. Comp. Neurol. *506*, 708–732.

Belmonte, M.K., Cook, E.H., Jr., Anderson, G.M., Rubenstein, J.L., Greenough, W.T., Beckel-Mitchener, A., Courchesne, E., Boulanger, L.M., Powell, S.B., Levitt, P.R., et al. (2004). Autism as a disorder of neural information processing: directions for research and targets for therapy. Mol. Psychiatry *9*, 646–663.

Ben-Ari, Y. (2002). Excitatory actions of gaba during development: the nature of the nurture. Nat. Rev. Neurosci. *3*, 728–739.

Blaesse, P., Guillemin, I., Schindler, J., Schweizer, M., Delpire, E., Khiroug, L., Friauf, E., and Nothwang, H.G. (2006). Oligomerization of KCC2 correlates with development of inhibitory neurotransmission. J. Neurosci. *26*, 10407–10419.

Bolteus, A.J., and Bordey, A. (2004). GABA release and uptake regulate neuronal precursor migration in the postnatal subventricular zone. J. Neurosci. *24*, 7623–7631.

Borodinsky, L.N., Root, C.M., Cronin, J.A., Sann, S.B., Gu, X., and Spitzer, N.C. (2004). Activity-dependent homeostatic specification of transmitter expression in embryonic neurons. Nature *429*, 523–530.

Butt, S.J., Fuccillo, M., Nery, S., Noctor, S., Kriegstein, A., Corbin, J.G., and Fishell, G. (2005). The temporal and spatial origins of cortical interneurons predict their physiological subtype. Neuron *48*, 591–604.

Cancedda, L., Fiumelli, H., Chen, K., and Poo, M.M. (2007). Excitatory GABA action is essential for morphological maturation of cortical neurons in vivo. J. Neurosci. *27*, 5224–5235.

Cavelier, P., Hamann, M., Rossi, D., Mobbs, P., and Attwell, D. (2005). Tonic excitation and inhibition of neurons: ambient transmitter sources and computational consequences. Prog. Biophys. Mol. Biol. *87*, 3–16.

Chudotvorova, I., Ivanov, A., Rama, S., Hubner, C.A., Pellegrino, C., Ben-Ari, Y., and Medina, I. (2005). Early expression of KCC2 in rat hippocampal cultures augments expression of functional GABA synapses. J. Physiol. *566*, 671–679.

Cobos, I., Calcagnotto, M.E., Vilaythong, A.J., Thwin, M.T., Noebels, J.L., Baraban, S.C., and Rubenstein, J.L. (2005). Mice lacking Dlx1 show subtype-specific loss of interneurons, reduced inhibition and epilepsy. Nat. Neurosci. *8*, 1059–1068.

Cobos, I., Long, J.E., Thwin, M.T., and Rubenstein, J.L. (2006). Cellular patterns of transcription factor expression in developing cortical interneurons. Cereb. Cortex *16* (*Suppl 1*), i82–i88.

Colombo, E., Collombat, P., Colasante, G., Bianchi, M., Long, J., Mansouri, A., Rubenstein, J.L., and Broccoli, V. (2007). Inactivation of Arx, the murine ortholog of the X-linked lissencephaly with ambiguous genitalia gene, leads to severe disorganization of the ventral telencephalon with impaired neuronal migration and differentiation. J. Neurosci. *27*, 4786–4798.

Conti, F., Minelli, A., and Melone, M. (2004). GABA transporters in the mammalian cerebral cortex: localization, development and pathological implications. Brain Res. Brain Res. Rev. *45*, 196–212.

Cuzon, V.C., Yeh, P.W., Cheng, Q., and Yeh, H.H. (2006). Ambient GABA promotes cortical entry of tangentially migrating cells derived from the medial ganglionic eminence. Cereb. Cortex *16*, 1377–1388.

Danbolt, N.C. (2001). Glutamate uptake. Prog. Neurobiol. *65*, 1–105.

Darcy, D.P., and Isaacson, J.S. (2009). L-type calcium channels govern calcium signaling in the migrating newborn neurons in the postnatal olfactory bulb. J. Neurosci. *29*, 2510–2518.

Dulabon, L., Olson, E.C., Taglienti, M.G., Eisenhuth, S., McGrath, B., Walsh, C.A., Kreidberg, J.A., and Anton, E.S. (2000). Reelin binds alpha3beta1 integrin and inhibits neuronal migration. Neuron *27*, 33–44.

Fiumelli, H., Cancedda, L., and Poo, M.M. (2005). Modulation of GABAergic transmission by activity via postsynaptic Ca2+-dependent regulation of KCC2 function. Neuron *48*, 773–786.

Flames, N., Long, J.E., Garratt, A.N., Fischer, T.M., Gassmann, M., Birchmeier, C., Lai, C., Rubenstein, J.L., and Marin, O. (2004). Short- and long-range attraction of cortical GABAergic interneurons by neuregulin-1. Neuron *44*, 251–261.

Freund, T.F. (2003). Interneuron Diversity series: Rhythm and mood in perisomatic inhibition. Trends Neurosci. *26*, 489–495.

Fritschy, J.M., and Brunig, I. (2003). Formation and plasticity of GABAergic synapses: physiological mechanisms and pathophysiological implications. Pharmacol. Ther. *98*, 299–323.

Fuerst, P.G., Koizumi, A., Masland, R.H., and Burgess, R.W. (2008). Neurite arborization and mosaic spacing in the mouse retina require DSCAM. Nature *451*, 470–474.

Galanopoulou, A.S. (2007). Developmental patterns in the regulation of chloride homeostasis and GABA(A) receptor signaling by seizures. Epilepsia *48* (*Suppl 5*), 14–18.

Ganguly, K., Schinder, A.F., Wong, S.T., and Poo, M. (2001). GABA itself promotes the developmental switch of neuronal GABAergic responses from excitation to inhibition. Cell *105*, 521–532.

Gilbert, D., Franjic-Wurtz, C., Funk, K., Gensch, T., Frings, S., and Mohrlen, F. (2007). Differential maturation of chloride homeostasis in primary afferent neurons of the somatosensory system. Int. J. Dev. Neurosci. *25*, 479–489.

Gomez, T.M., and Spitzer, N.C. (1999). In vivo regulation of axon extension and pathfinding by growth-cone calcium transients. Nature *397*, 350–355.

Gomez, T.M., Snow, D.M., and Letourneau, P.C. (1995). Characterization of spontaneous calcium transients in nerve growth cones and their effect on growth cone migration. Neuron *14*, 1233–1246.

Gong, S., Zheng, C., Doughty, M.L., Losos, K., Didkovsky, N., Schambra, U.B., Nowak, N.J., Joyner, A., Leblanc, G., Hatten, M.E., and Heintz, N. (2003). A gene expression atlas of the central nervous system based on bacterial artificial chromosomes. Nature *425*, 917–925.

Grobin, A.C., Heenan, E.J., Lieberman, J.A., and Morrow, A.L. (2003). Perinatal neurosteroid levels influence GABAergic interneuron localization in adult rat prefrontal cortex. J. Neurosci. *23*, 1832–1839.

Hand, R., Bortone, D., Mattar, P., Nguyen, L., Heng, J.I., Guerrier, S., Boutt, E., Peters, E., Barnes, A.P., Parras, C., et al. (2005). Phosphorylation of Neurogenin2 specifies the migration properties and the dendritic morphology of pyramidal neurons in the neocortex. Neuron *48*, 45–62.

Heintz, N. (2004). Gene expression nervous system atlas (GENSAT). Nat. Neurosci. *7*, 483.

Hensch, T.K. (2005). Critical period plasticity in local cortical circuits. Nat. Rev. Neurosci. *6*, 877–888.

Kanold, P.O., and Shatz, C.J. (2006). Subplate neurons regulate maturation of cortical inhibition and outcome of ocular dominance plasticity. Neuron *51*, 627–638.

Kater, S.B., and Mills, L.R. (1991). Regulation of growth cone behavior by calcium. J. Neurosci. *11*, 891–899.

Kawaguchi, Y., and Kondo, S. (2002). Parvalbumin, somatostatin and cholecystokinin as chemical markers for specific GABAergic interneuron types in the rat frontal cortex. J. Neurocytol. *31*, 277–287.

Kitamura, K., Yanazawa, M., Sugiyama, N., Miura, H., Iizuka-Kogo, A., Kusaka, M., Omichi, K., Suzuki, R., Kato-Fukui, Y., Kamiirisa, K., et al. (2002). Mutation of ARX causes abnormal development of forebrain and testes in mice and X-linked lissencephaly with abnormal genitalia in humans. Nat. Genet. *32*, 359–369.

Komuro, H., and Rakic, P. (1993). Modulation of neuronal migration by NMDA receptors. Science *260*, 95–97.

Komuro, H., and Rakic, P. (1996). Intracellular Ca2+ fluctuations modulate the rate of neuronal migration. Neuron *17*, 275–285.

Komuro, H., and Kumada, T. (2005). Ca2+ transients control CNS neuronal migration. Cell Calcium *37*, 387–393.

Kriegstein, A.R., and Owens, D.F. (2001). GABA may act as a self-limiting trophic factor at developing synapses. Sci. STKE *2001*, PE1.

Kriegstein, A.R., and Noctor, S.C. (2004). Patterns of neuronal migration in the embryonic cortex. Trends Neurosci. *27*, 392–399.

Kumada, T., and Komuro, H. (2004). Completion of neuronal migration regulated by loss of Ca(2+) transients. Proc. Natl. Acad. Sci. USA *101*, 8479–8484.

Lacinova, L., and Hofmann, F. (2005). Ca2+- and voltage-dependent inactivation of the expressed L-type Ca(v)1.2 calcium channel. Arch. Biochem. Biophys. *437*, 42–50.

Lavdas, A.A., Grigoriou, M., Pachnis, V., and Parnavelas, J.G. (1999). The medial ganglionic eminence gives rise to a population of early neurons in the developing cerebral cortex. J. Neurosci. *19*, 7881–7888.

Lee, H.H., Walker, J.A., Williams, J.R., Goodier, R.J., Payne, J.A., and Moss, S.J. (2007). Direct protein kinase C-dependent phosphorylation regulates the cell surface stability and activity of the potassium chloride cotransporter KCC2. J. Biol. Chem. *282*, 29777–29784.

Leitch, E., Coaker, J., Young, C., Mehta, V., and Sernagor, E. (2005). GABA type-A activity controls its own developmental polarity switch in the maturing retina. J. Neurosci. *25*, 4801–4805.

Li, H., Khirug, S., Cai, C., Ludwig, A., Blaesse, P., Kolikova, J., Afzalov, R., Coleman, S.K., Lauri, S., Airaksinen, M.S., et al. (2007). KCC2 interacts with the dendritic cytoskeleton to promote spine development. Neuron *56*, 1019–1033.

Li, G., Adesnik, H., Li, J., Long, J., Nicoll, R.A., Rubenstein, J.L., and Pleasure, S.J. (2008). Regional distribution of cortical interneurons and development of inhibitory tone are regulated by Cxcl12/Cxcr4 signaling. J. Neurosci. *28*, 1085–1098.

Liodis, P., Denaxa, M., Grigoriou, M., Akufo-Addo, C., Yanagawa, Y., and Pachnis, V. (2007). Lhx6 activity is required for the normal migration and specification of cortical interneuron subtypes. J. Neurosci. *27*, 3078–3089.

Lipscombe, D. (2002). L-type calcium channels: highs and new lows. Circ. Res. *90*, 933–935.

Lopez-Bendito, G., Lujan, R., Shigemoto, R., Ganter, P., Paulsen, O., and Molnar, Z. (2003). Blockade of GABA(B) receptors alters the tangential migration of cortical neurons. Cereb. Cortex *13*, 932–942.

LoTurco, J.J., Owens, D.F., Heath, M.J., Davis, M.B., and Kriegstein, A.R. (1995). GABA and glutamate depolarize cortical progenitor cells and inhibit DNA synthesis. Neuron *15*, 1287–1298.

Ludwig, A., Li, H., Saarma, M., Kaila, K., and Rivera, C. (2003). Developmental up-regulation of KCC2 in the absence of GABAergic and glutamatergic transmission. Eur. J. Neurosci. *18*, 3199–3206.

Lujan, R., Shigemoto, R., and Lopez-Bendito, G. (2005). Glutamate and GABA receptor signalling in the developing brain. Neuroscience *130*, 567–580.

Manent, J.B., Demarque, M., Jorquera, I., Pellegrino, C., Ben-Ari, Y., Aniksztejn, L., and Represa, A. (2005). A noncanonical release of GABA and glutamate modulates neuronal migration. J. Neurosci. *25*, 4755–4765.

Marin, O., and Rubenstein, J.L. (2001). A long, remarkable journey: tangential migration in the telencephalon. Nat. Rev. Neurosci. *2*, 780–790.

Marin, O., Yaron, A., Bagri, A., Tessier-Lavigne, M., and Rubenstein, J.L. (2001). Sorting of striatal and cortical interneurons regulated by semaphorin-neuropilin interactions. Science *293*, 872–875.

Marty, S., Berninger, B., Carroll, P., and Thoenen, H. (1996). GABAergic stimulation regulates the phenotype of hippocampal interneurons through the regulation of brain-derived neurotrophic factor. Neuron *16*, 565–570.

Mercado, A., Broumand, V., Zandi-Nejad, K., Enck, A.H., and Mount, D.B. (2006). A C-terminal domain in KCC2 confers constitutive K+-Cl- cotransport. J. Biol. Chem. *281*, 1016–1026.

Metin, C., Denizot, J.P., and Ropert, N. (2000). Intermediate zone cells express calcium-permeable AMPA receptors and establish close contact with growing axons. J. Neurosci. *20*, 696–708.

Nishiyama, M., von Schimmelmann, M.J., Togashi, K., Findley, W.M., and Hong, K. (2008). Membrane potential shifts caused by diffusible guidance signals direct growth-cone turning. Nat. Neurosci. *11*, 762–771.

Noctor, S.C., Flint, A.C., Weissman, T.A., Dammerman, R.S., and Kriegstein, A.R. (2001). Neurons derived from radial glial cells establish radial units in neocortex. Nature *409*, 714–720.

O'Rourke, N.A., Dailey, M.E., Smith, S.J., and McConnell, S.K. (1992). Diverse migratory pathways in the developing cerebral cortex. Science *258*, 299–302.

O'Rourke, N.A., Sullivan, D.P., Kaznowski, C.E., Jacobs, A.A., and McConnell, S.K. (1995). Tangential migration of neurons in the developing cerebral cortex. Development *121*, 2165–2176.

Okabe, M., Ikawa, M., Kominami, K., Nakanishi, T., and Nishimune, Y. (1997). 'Green mice' as a source of ubiquitous green cells. FEBS Lett. *407*, 313–319.

Owens, D.F., and Kriegstein, A.R. (2002). Is there more to GABA than synaptic inhibition? Nat. Rev. Neurosci. *3*, 715–727.

Payne, J.A., Stevenson, T.J., and Donaldson, L.F. (1996). Molecular characterization of a putative K-Cl cotransporter in rat brain. A neuronal-specific isoform. J. Biol. Chem. *271*, 16245–16252.

Pinto-Lord, M.C., Evrard, P., and Caviness, V.S., Jr. (1982). Obstructed neuronal migration along radial glial fibers in the neocortex of the reeler mouse: a Golgi-EM analysis. Brain Res. *256*, 379–393.

Polleux, F., Whitford, K.L., Dijkhuizen, P.A., Vitalis, T., and Ghosh, A. (2002). Control of cortical interneuron migration by neurotrophins and PI3-kinase signaling. Development *129*, 3147–3160.

Poluch, S., Drian, M.J., Durand, M., Astier, C., Benyamin, Y., and Konig, N. (2001). AMPA receptor activation leads to neurite retraction in tangentially migrating neurons in the intermediate zone of the embryonic rat neocortex. J. Neurosci. Res. *63*, 35–44.

Poluch, S., Rossel, M., and Konig, N. (2003). AMPA-evoked ion influx is strongest in tangential neurons of the rat neocortical intermediate zone close to the front of the migratory stream. Dev. Dyn. *227*, 416–421.

Powell, E.M., Mars, W.M., and Levitt, P. (2001). Hepatocyte growth factor/scatter factor is a motogen for interneurons migrating from the ventral to dorsal telencephalon. Neuron *30*, 79–89.

Rakic, P. (1972). Mode of cell migration to the superficial layers of fetal monkey neocortex. J. Comp. Neurol. *145*, 61–83.

Represa, A., and Ben-Ari, Y. (2005). Trophic actions of GABA on neuronal development. Trends Neurosci. *28*, 278–283.

Rivera, C., Voipio, J., Payne, J.A., Ruusuvuori, E., Lahtinen, H., Lamsa, K., Pirvola, U., Saarma, M., and Kaila, K. (1999). The K+/Cl- co-transporter KCC2 renders GABA hyperpolarizing during neuronal maturation. Nature *397*, 251–255.

Rivera, C., Li, H., Thomas-Crusells, J., Lahtinen, H., Viitanen, T., Nanobashvili, A., Kokaia, Z., Airaksinen, M.S., Voipio, J., Kaila, K., and Saarma, M. (2002). BDNF-induced TrkB activation down-regulates the K+-Cl- cotransporter KCC2 and impairs neuronal Cl- extrusion. J. Cell Biol. *159*, 747–752.

Rivera, C., Voipio, J., Thomas-Crusells, J., Li, H., Emri, Z., Sipila, S., Payne, J.A., Minichiello, L., Saarma, M., and Kaila, K. (2004). Mechanism of activity-dependent downregulation of the neuron-specific K-Cl cotransporter KCC2. J. Neurosci. *24*, 4683–4691.

Rubenstein, J.L., and Merzenich, M.M. (2003). Model of autism: increased ratio of excitation/inhibition in key neural systems. Genes Brain Behav. *2*, 255–267.

Soria, J.M., and Valdeolmillos, M. (2002). Receptor-activated calcium signals in tangentially migrating cortical cells. Cereb. Cortex *12*, 831–839.

Splawski, I., Timothy, K.W., Sharpe, L.M., Decher, N., Kumar, P., Bloise, R., Napolitano, C., Schwartz, P.J., Joseph, R.M., Condouris, K., et al. (2004). Ca(V)1.2 calcium channel dysfunction causes a multisystem disorder including arrhythmia and autism. Cell *119*, 19–31.

Splawski, I., Yoo, D.S., Stotz, S.C., Cherry, A., Clapham, D.E., and Keating, M.T. (2006). CACNA1H mutations in autism spectrum disorders. J. Biol. Chem. *281*, 22085–22091.

Sussel, L., Marin, O., Kimura, S., and Rubenstein, J.L. (1999). Loss of Nkx2.1 homeobox gene function results in a ventral to dorsal molecular respecification within the basal telencephalon: evidence for a transformation of the pallidum into the striatum. Development *126*, 3359–3370.

Tanaka, D.H., Maekawa, K., Yanagawa, Y., Obata, K., and Murakami, F. (2006). Multidirectional and multizonal tangential migration of GABAergic interneurons in the developing cerebral cortex. Development *133*, 2167–2176.

Titz, S., Hans, M., Kelsch, W., Lewen, A., Swandulla, D., and Misgeld, U. (2003). Hyperpolarizing inhibition develops without trophic support by GABA in cultured rat midbrain neurons. J. Physiol. *550*, 719–730.

Toyoda, H., Ohno, K., Yamada, J., Ikeda, M., Okabe, A., Sato, K., Hashimoto, K., and Fukuda, A. (2003). Induction of NMDA and GABAA receptor-mediated Ca2+ oscillations with KCC2 mRNA downregulation in injured facial motoneurons. J. Neurophysiol. *89*, 1353–1362.

Wake, H., Watanabe, M., Moorhouse, A.J., Kanematsu, T., Horibe, S., Matsukawa, N., Asai, K., Ojika, K., Hirata, M., and Nabekura, J. (2007). Early changes in KCC2 phosphorylation in response to neuronal stress result in functional downregulation. J. Neurosci. *27*, 1642–1650.

Wang, W., Gong, N., and Xu, T.L. (2006). Downregulation of KCC2 following LTP contributes to EPSP-spike potentiation in rat hippocampus. Biochem. Biophys. Res. Commun. *343*, 1209–1215.

Zhao, Y., Flandin, P., Long, J.E., Cuesta, M.D., Westphal, H., and Rubenstein, J.L. (2008). Distinct molecular pathways for development of telencephalic interneuron subtypes revealed through analysis of Lhx6 mutants. J. Comp. Neurol. *510*, 79–99.

Zheng, J.Q., and Poo, M.M. (2007). Calcium signaling in neuronal motility. Annu. Rev. Cell Dev. Biol. *23*, 375–404.

Neuron, Volume 62

Supplementary Figures and Supplementary Experimental Procedures and Statistics

KCC2 expression promotes the termination of cortical interneuron migration in a voltage-sensitive calcium-dependent manner

Bortone D. and Polleux F.

Supplementary Figures

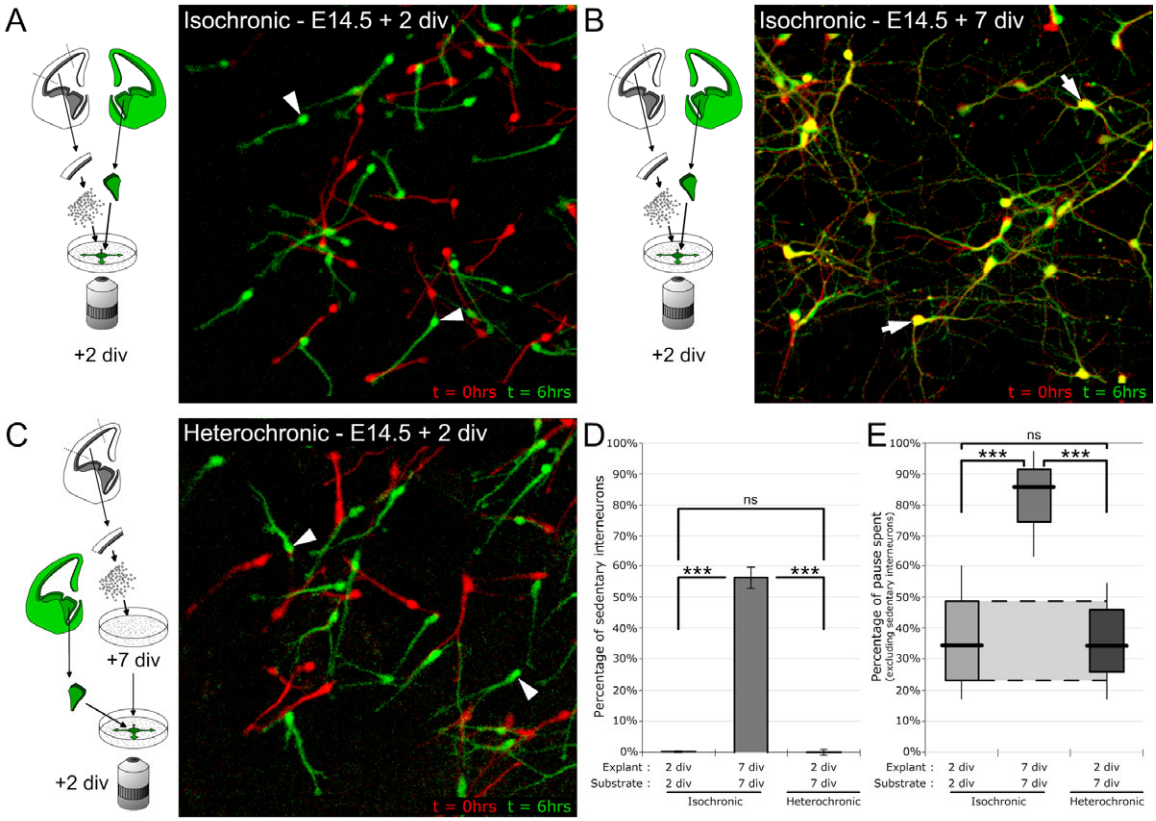

Supplementary Figure 1. Termination of migration has a cell autonomous component
E14.5 wild-type cortical cells were dissociated, plated and co-cultured with EGFP-expressing MGE explants. Frame corresponding to the start of imaging (t=0) is pseudo-colored in red. Image taken six hours later is pseudo-colored in green. Yellow cell bodies indicate interneurons did not migrate between beginning and end of imaging session. Arrowheads indicate migrating interneurons while arrows point to sedentary interneurons. Note isochronic cultures of interneurons phenocopy increase in pause times from 2div (**A**) to 7div (**B**) as observed *in situ*. In heterochronic cultures (**C**), the dissociated E14.5 wild-type substrate was aged 7-9 days before placing E14.5 EGFP-MGE explants. (**D,E**) Quantification shows no significant difference in percentage of sedentary interneurons (E) or pause time (D) on an aged substrate indicating interneurons require a cell autonomous maturation to slow and terminate migration. Since including the pause times of the steadily increasing proportion of sedentary interneurons would have doubtlessly caused our measurements to increase with age, these non-moving cells have been excluded for panel E.

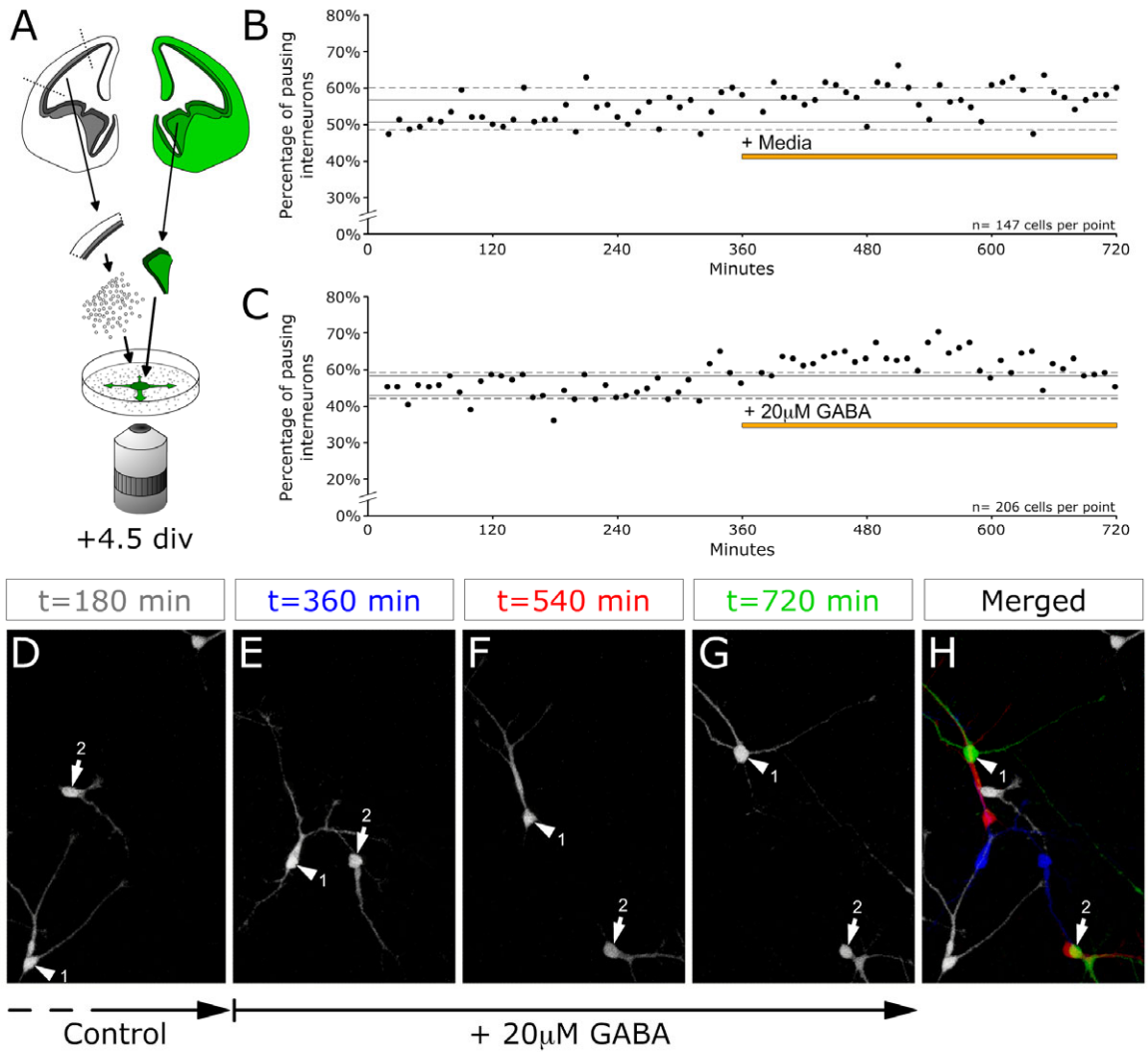

Supplementary figure 2. MGE-derived interneurons have heterogeneous response to GABA application.

(**A**) Illustration of experimental design. Wild-type cortices were dissociated to provide a substrate for explants of EGFP-MGE. After 4.5div interneurons were time-lapsed for a control period of 6 hours. The same interneurons were then time-lapsed for another 6 hours to note individual changes in pausing following drug application (20microM GABA or media). (**B-C**) Percentage of pausing interneurons is shown for each frame for control media (B) and GABA addition (C). Solid lines indicate 50th percentile range of first 6 hours of imaging, while dashed lines indicate 90th an 10th percentile range. Control experiment (B) shows a slight but steady increase in pausing during course of 12 hours time-lapse with no response to media application. GABA-treated interneurons (C) show an increase in pausing in response to GABA application ($p=0.0183$ compared to post-media addition). (**D-G**) Montage of GABA addition time-lapse is shown before and after drug application at 360 minutes. Cell 1 (arrowhead) shows no response to GABA application while cell 2 (arrow) stops migrating. (**H**) Merged image shows time points before GABA addition in white and blue (180 and 360 minutes respectively) and those after GABA addition in red and green (540 and 720 minutes respectively). Yellow 'colocalization' indicates little movement in cell 2 after GABA application.

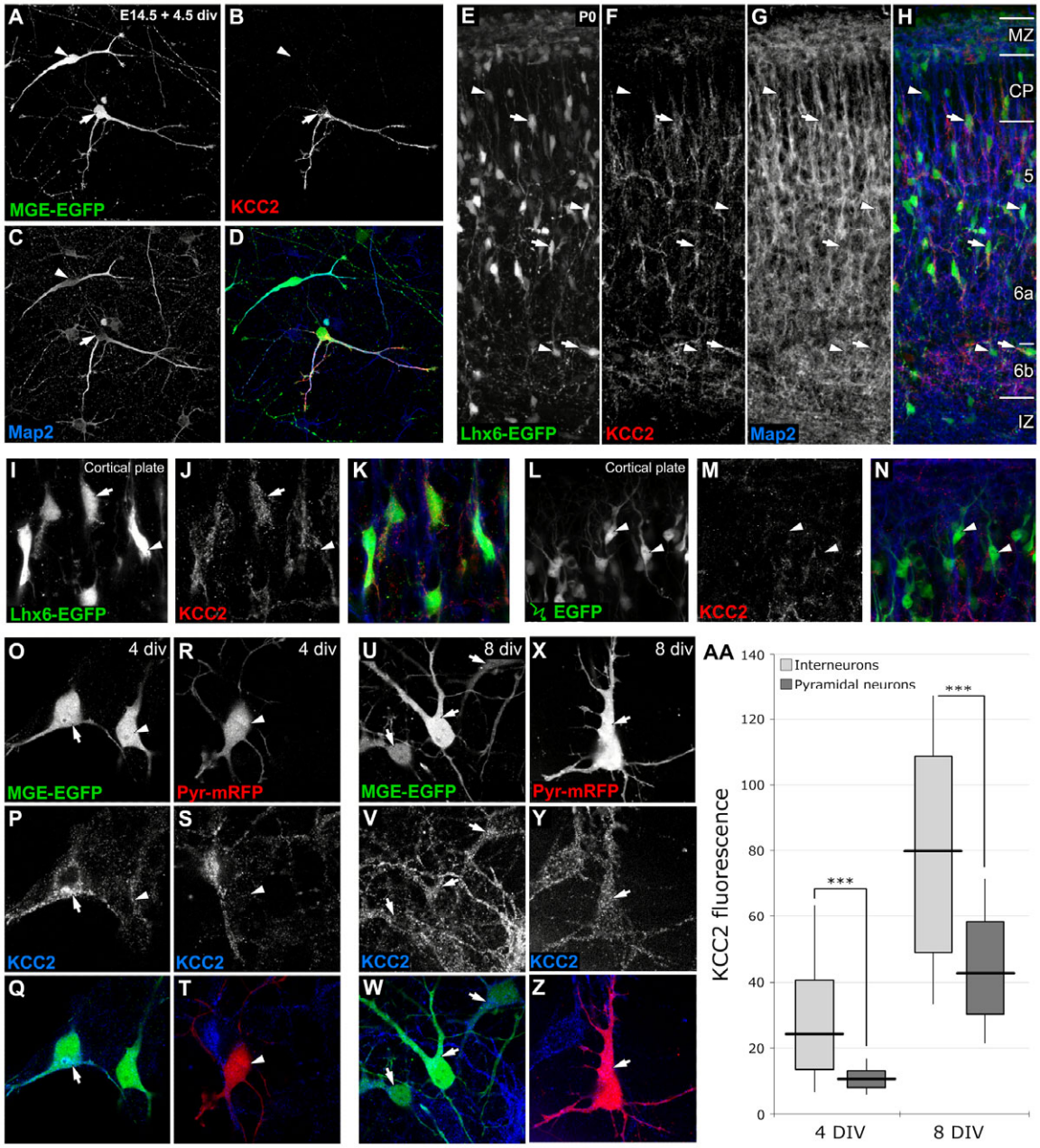

Supplementary figure 3. KCC2 expression is highly variable among cortical interneurons. **(A-D)** Explanted E14.5 EGFP-MGE interneurons show drastically different KCC2 expression after 4.5div in culture. Throughout the figure, arrowheads identify cells expressing low levels of KCC2, while arrows indicate cells expressing high levels of KCC2. **(E-K)** Immunostained sections from a P0 Lhx6-EGFP mouse reveal heterogeneous KCC2 expression in cortical interneurons *in vivo*. **(L-M)** E14.5 dorsal telencephalic progenitors were electroporated with EGFP and slices containing radially migrating pyramidal neurons in the cortical plate (CP) stained for KCC2 after 4.5div. No KCC2 expression is detected. **(O-Z)** Isochronic co-cultures of MGE-EGFP-derived interneurons with mRFP-electroporated dorsal telencephalic progenitors reveals that interneurons up-regulate KCC2 earlier than pyramidal cells *in vitro*. (**AA**) Quantification of KCC2 fluorescence in cortical pyramidal cells was significantly lower than interneurons at 4 and 8div ($p<0.0001$ for both). This box plots reveals also that the variability of KCC2 expression among interneurons was more significant than in pyramidal neurons at early ages.

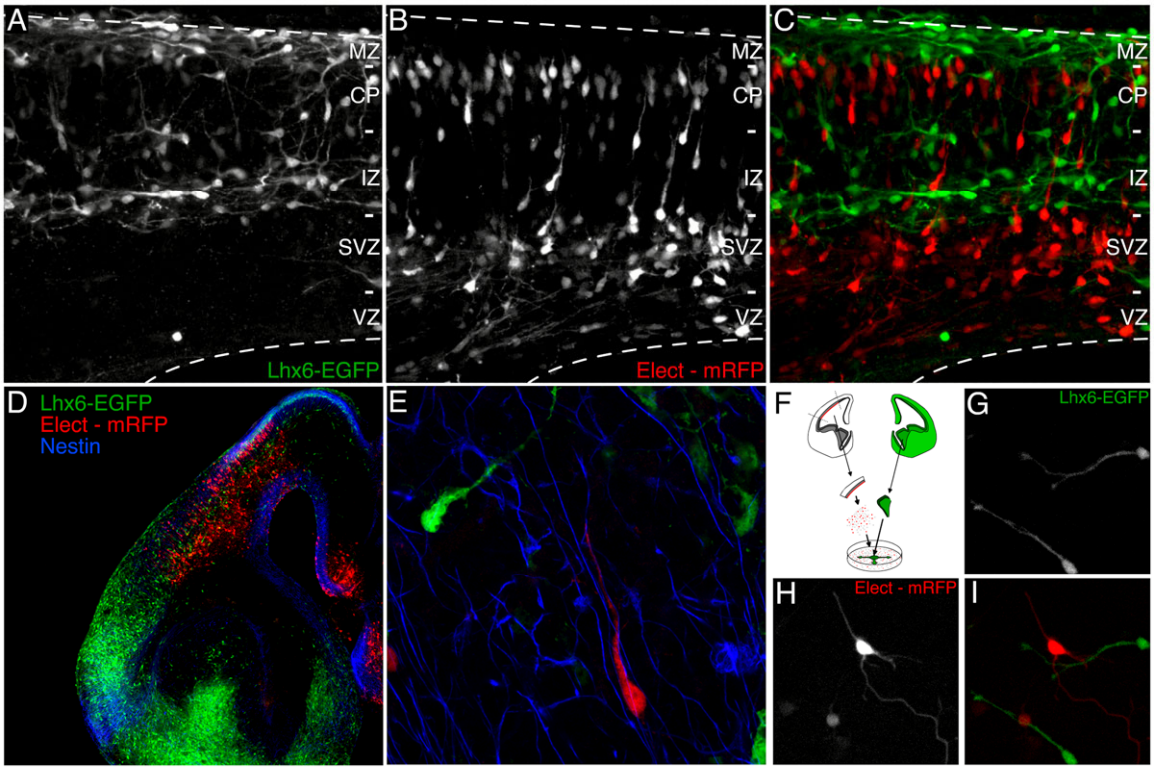

Supplementary figure 4. Dorsal telencephalic electroporation specifically labels radially migrating pyramidal neurons and not tangentially migrating interneurons.
(**A-E**) E14 Lhx6-EGFP embryos underwent dorsal electroporation with monomeric red fluorescent protein (mRFP) and cultured 4 days revealing no co-transfection which indicates this is an effective method to specifically label pyramidal cells. At higher magnification (E) radially migrating neurons (red) but not tangentially migrating interneurons (green) are found closely fasciculated with radial glial fibers labeled with Nestin (blue). (**F-I**) Dissociating dorsally electroporated wild-type pyramidal cells and applying an EGFP-MGE explant enables concurrent culturing and imaging of labeled interneurons and pyramidal cells in 2D.

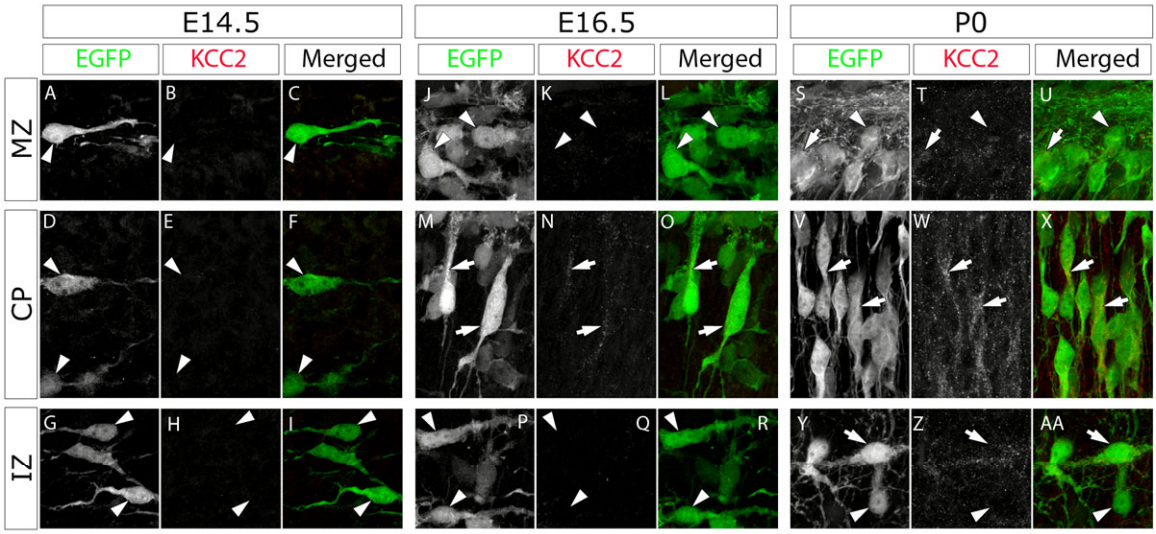

Supplementary figure 5. Migrating cortical interneurons up-regulate KCC2 after reaching the cortex.
Lhx6-EGFP embryos were perfused at E14.5 (A-I), E16.5 (J-R) or P0 (S-AA) and immunostained for EGFP and KCC2. Note that when migrating interneurons reach the cortex at E14.5 and E16.5 they express very little, if any, KCC2 and start up-regulating KCC2 only at P0 i.e. several days after they reach the cortical plate.
Abbreviations: CP - cortical plate; IZ - intermediate zone; MZ - marginal zone; E14.5 - Embryonic day 14.5.

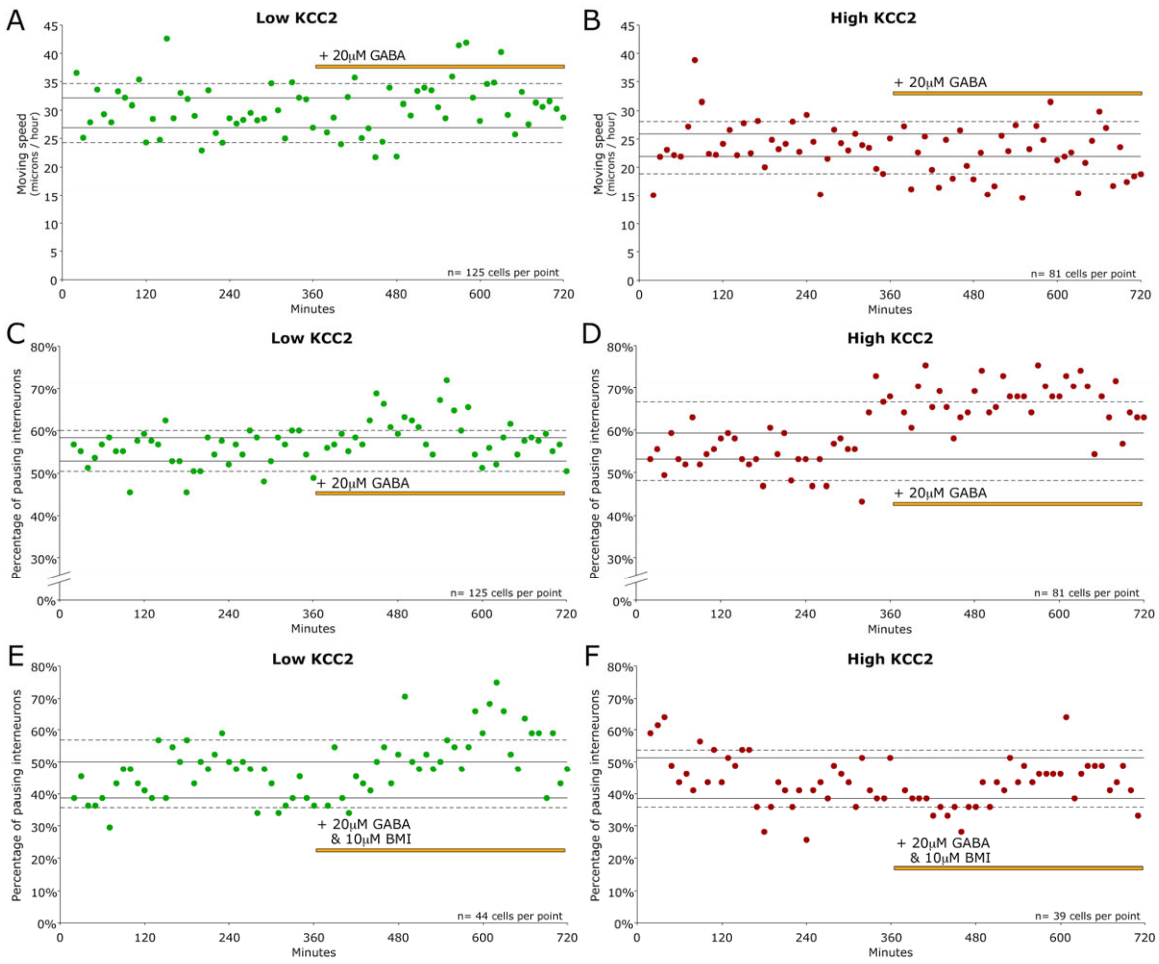

Supplementary figure 6. Frame-by-frame responses to GABA addition

(A-F) Data shown in Figure 4K-M is shown here as frame-by-frame average values of interneurons binned into low and high KCC2 sub-populations. Yellow lines indicate the time of addition of 20microM GABA (A-D) or 20microM GABA plus 10microM BMI (E,F). Solid black lines indicate 25th and 75th percentiles before drug addition. Dotted black lines indicate 10th and 90th percentiles before drug addition. Note the increase in frequency of pausing after GABA addition for high KCC2 expressing interneurons (D), but not upon co-application of GABA and $GABA_A$ antagonist BMI (F). Also note that the frequency of pausing increases in low KCC2-expressing interneurons when GABA is co-applied with BMI.

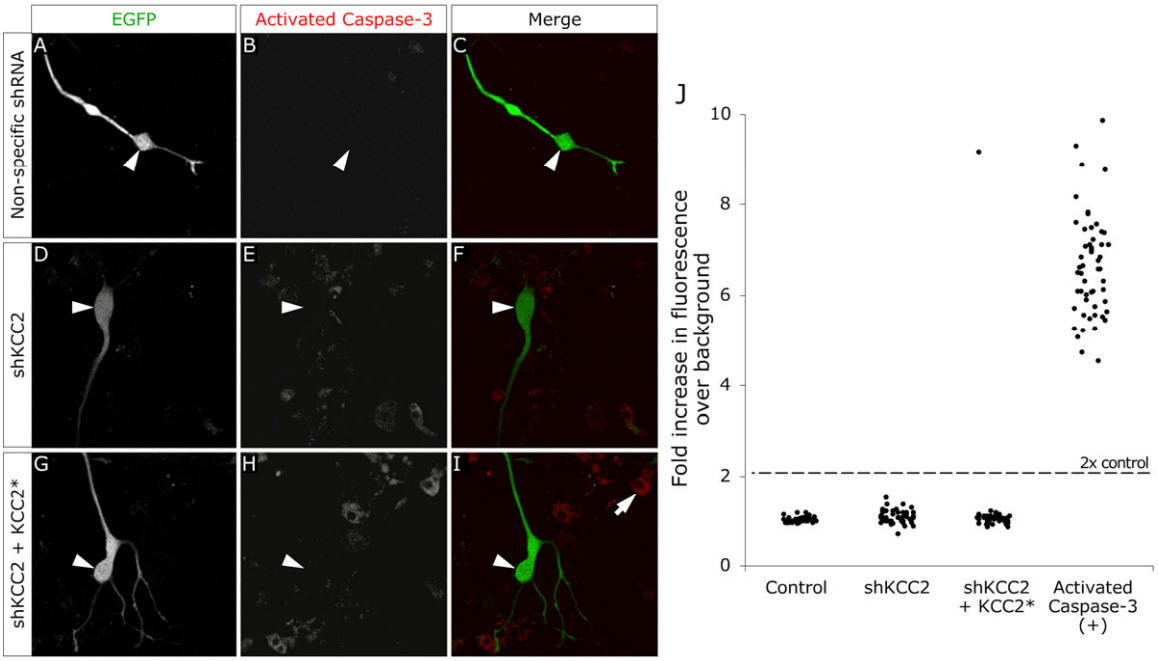

Supplementary figure 7. Manipulating KCC2 expression in migrating interneurons does not induce apoptosis.

(**A-I**) E14.5 MGE explants electroporated with either non-specific shRNA, shKCC2 or shKCC2 rescued with KCC2* were cultured on wild-type cortical dissociations for 4.5div, fixed and immunostained for activated caspase-3. (I) Arrow indicates activated caspase-3 expression in an apoptotic neuron from the substrate wild-type cortical culture. (**J**) Quantifications show the measured fluorescence of KCC2 with respect to background fluorescence in individual interneurons expressing the indicated plasmids. No significant difference in activated caspase-3 expression was found between the 3 conditions (B,E,H arrowheads) using 2 times the average control value as a threshold.

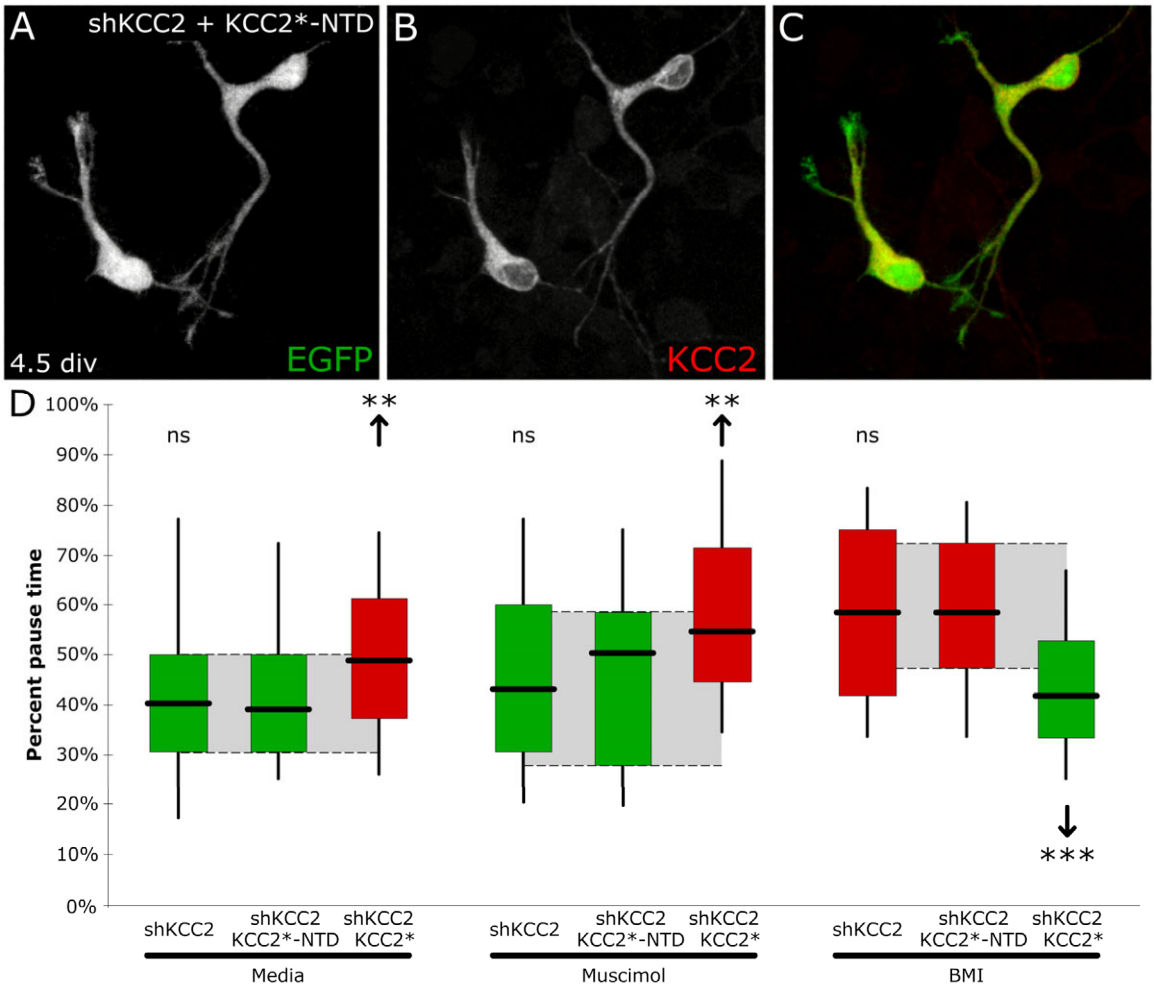

Supplementary figure 8. Effects associated with KCC2 are due to its transport activity
(**A-C**) E14.5 MGE explants were electroporated with constructs expressing shKCC2 and EGFP transport-dead N-terminal deleted human KCC2 (NTD-KCC2*) at 4.5div. Immunostaining for KCC2 (B) shows NTD-KCC2* does not affect expression or localization of the protein. **(D)** Box plots are color-coded to represent whether treatment would result in more depolarized (green) or hyperpolarized (red) cells with respect to non-electroporated cells. Light-grey shading shows middle 50th percent range of appropriate control population. NTD-KCC2* fails to rescue KCC2 knockdown in contrast with full-length human KCC2 (KCC2*). The shKCC2 and full-length KCC2* data is the same as shown in Figure 3.

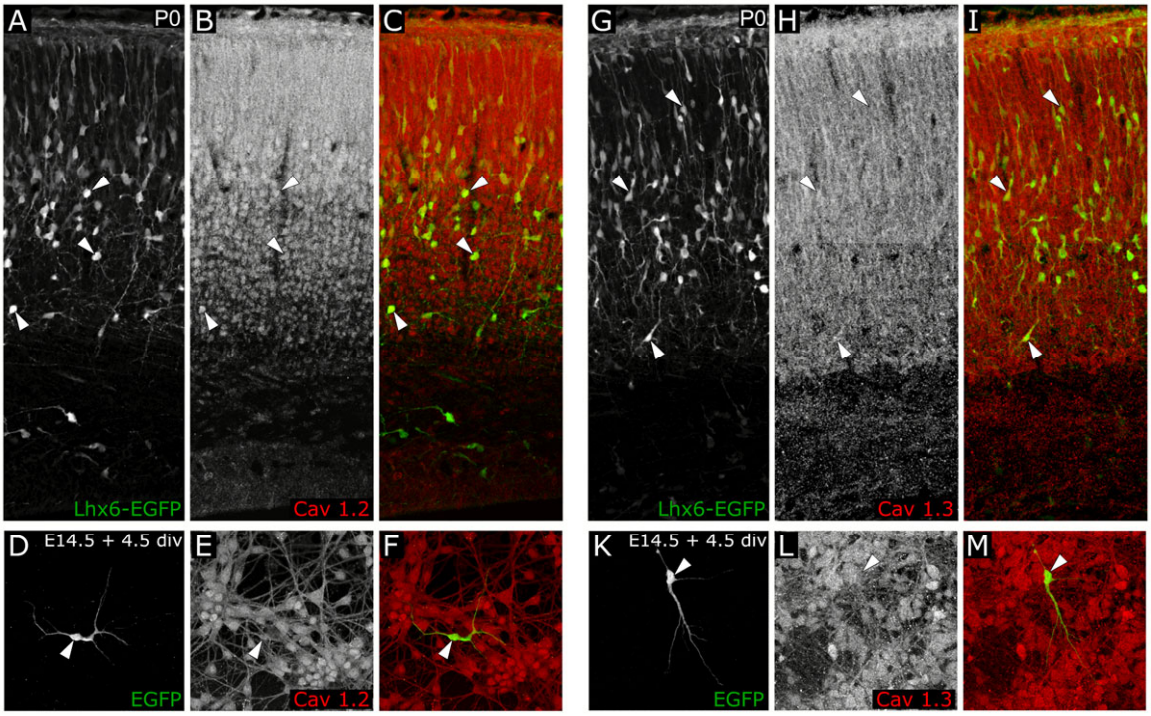

Supplementary figure 9. L-type calcium channel subunits $Ca_V1.2$ and $Ca_V1.3$ are expressed in developing cortical interneurons

(**A-C, G-I**) Sections of P0 Lhx6-EGFP mice brains were sectioned and immunostained for subunits 1.2 and 1.3 of L-type voltage sensitive calcium channels. (**D-F, K-M**) The expression of these subunits is maintained after culturing E14.5 MGE explants for 4.5div. Arrowheads indicate co-labeled cells.

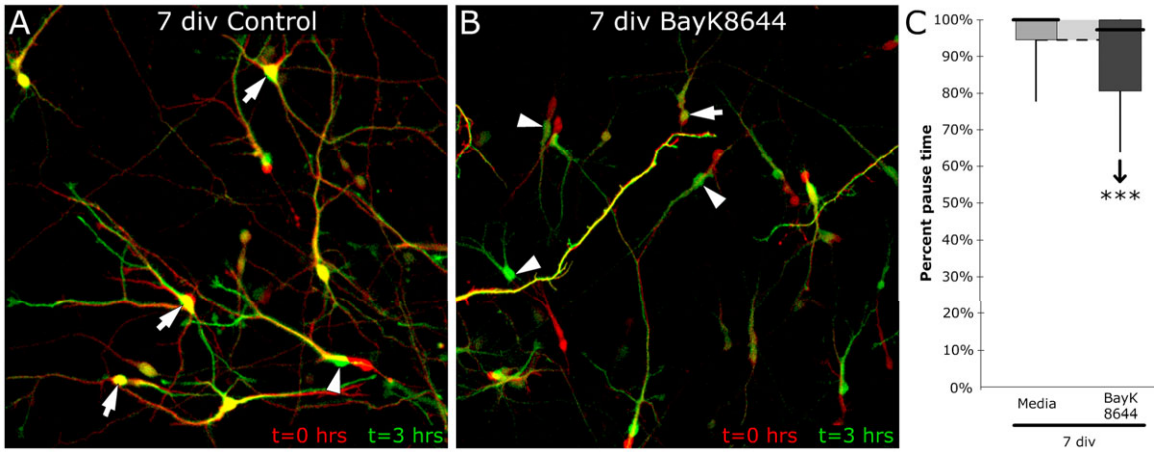

Supplementary figure 10. L-type calcium channel agonist bayK8644 prolongs migration of cortical interneurons

E14.5 explants were electroporated with control constructs, plated on wild-type dissociations, incubated with the L-type VSCC agonist bayK8644 from 4-7div and time-lapsed. Box plots show percent pause times of the cortical interneuron population. Light-grey shading shows the 25th-75th percentiles range of control values. Increasing open-channel frequency of L-type calcium channels delays the termination of migration for the majority of cortical interneurons ($p<0.0001$). Data shown in A and C were previously shown in figure 5. See Suppl. Movies 9 and 21 for corresponding time-lapse.

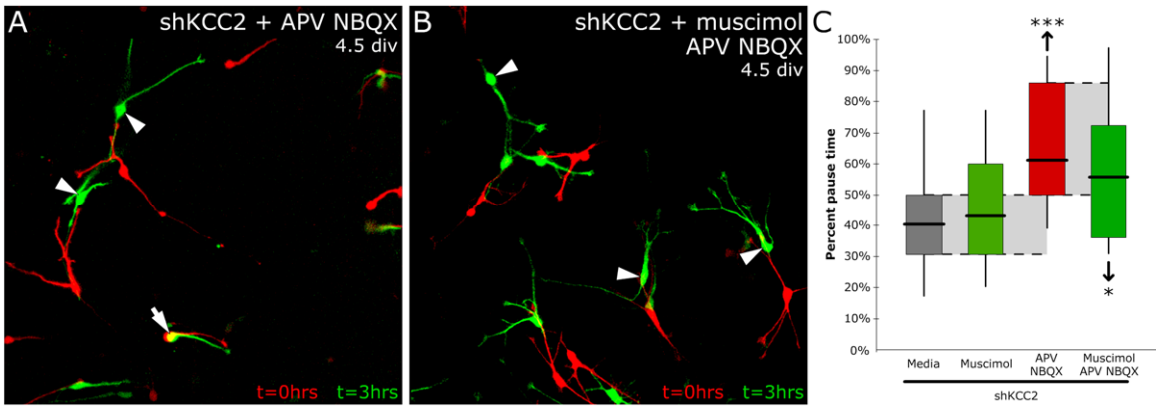

Supplementary figure 11. Muscimol-induced depolarization reduce cortical interneuron pausing frequency in the absence of glutamatergic signaling.
E14.5 MGEs were electroporated with shKCC2 and cultured for 4.5div before time-lapsing in the presence of either (**A**) 100μM APV and 10μM NBQX to block NMDA/AMPA receptors-mediated depolarization or (**B**) APV, NBQX and 10μM muscimol in order to block NMDA/AMPA receptors-mediated depolarization and activate $GABA_A$ receptor-mediated depolarization (shKCC2 cells). (**C**) Box plots are color-coded to represent whether treatment would result in more depolarized (**green**) or hyperpolarized (**red**) cell with respect to control cells. Light-grey shading shows middle 50th percent range of appropriate control population. While antagonizing glutamate signaling significantly decreases motility (i.e. increases pause times ($p<0.0001$)) compared to control, depolarizing shKCC2 interneurons with muscimol significantly rescues this effect ($p=0.0375$). Data shown in B and C were previously shown in figures 7 and 3, respectively. See Suppl. Movies 19 and 22 for corresponding time-lapse.

ww

Supplementary Material and Methods

Tissue preparation and sectioning

Time-pregnant mice are euthanized by rapid cervical dislocation before embryo collection. To prepare avertin 40x stock solution, 1g of 2,2,2-tribromoethanol (99%) (840-2; Sigma-Aldrich, St. Louis MO) was dissolved with 1mL of Tert-amyl alcohol (99%) (246-3; Sigma-Aldrich, St. Louis MO) in a glass container and stored at 4^{o}C protected from light for no more than 6 months before use. Working solution was made adding 40x stock solution to 37^{o} C PBS dropwise. Intraperitioneal injections of Avertin were made of 250-300uL per 10 grams of mouse body weight to achieve deep anesthesia. After the pups failed to respond to a toe prick the mice were perfused with 4% PFA in PBS made from 16% Paraformaldehyde solution (Cat. # 15710, Electron Microscopy Sciences, Hatfield PA). Brains were then dissected and fixed overnight in 4% PFA before rinsing 3x 30 minutes with PBS, orbital shaking at room temperature, sectioning at 80 microns with a vibratome (VT1000S; Leica; Wetzlar, Germany) and immunostained.

Calcium imaging/quantification

A stock solution of calcium indicator was made by adding 10microL DMSO (D2650; Sigma-Aldrich, St. Louis MO) to 50 μg of Oregon Green 488 BAPTA-1, AM (OGB-1; O6807; Invitrogen - Molecular Probes, Eugene OR). After vortexing for 1 min 5x 2microL aliquots were frozen at –80^{o}C. Warm 9.12 microL Pluronic F-127 in 20% DMSO (P3000MP; Invitrogen - Molecular Probes, Eugene OR) was then added to one aliquot of stock solution. After vortexing for 1 min, a 5μM working solution was made by adding 5microL of pluronic - stock solution to 715microL HBSS and vortexing for another minute.

Interneurons electroporated with pCIG4-Tomato (gift from Dr. Tom Maynard, University of North Carolina - Chapel Hill) or pCIG4-Tomato-IRES-hKCC2 were loaded with working solution at 4div by removing media from dissociation (saving it at 37^{o}C) and washing 3x in 37^{o}C HBSS. Working solution was applied to the dish and incubated for 30min at room temperature, while protected from light. Cells were then washed once with HBSS, once with 37^{o}C serum free media, and then the old conditioned media was added back to the dish.

Imaging sessions were done by sequentially scanning the red (plasmid) and green (OGB-1) channels with an open pinhole to allow faster scanning (once every 4 seconds). Data were extracted from these movies by creating a macro for ImageJ (NIH, Bethesda MD). This macro divides the green by the red channel to correct for changes in cell thickness as the interneuron migrates. The macro also masks out all data not corresponding to the cell bodies of interneurons as they migrate. The average intensity values of these cell bodies were measured and used to calculate a Fluorescence/Fluorescence at t=0 (F/F_0) for every frame.

The spectral analysis was done using the protocol and SpectralAnalysis tool designed for MatLab (The Mathworks, Natick MA) by Per Uhlen (2004). Using this tool, a Hanning filter was applied to the data to remove edge effects at the beginning and end of the movie. Then a Fourier transformation was done using 2^9 bins to separate the F/F_0 data from its time component and view the relative power spectral density for each frequency in every cell.

Construction of Multi-Welled Dishes

Sylgard 184 silicone elastomer, base & curing agent (Dow Corning Corporation, Midland MI) was to used to attach cut rings of 10mL Stripette (4101; Corning Incorporated, Corning NY) to FluoroDish (FD-35-100, World Precision Instruments, Inc., Sarasota FL). Two days of cure time were allowed before use of these multi-welled chambers.

Constructs

- pCIG4-tomato - gift from Dr. Tom Maynard (University of North Carolina - Chapel Hill)
- pCIG4-hKCC2-IRES-tomato
- pMES-KCC2 - hKCC2-IRES-EGFP gift from Dr David Mount (Harvard Insitute of Medicine, Harvard University) and Dr. Karl Kandler (University of Pittsburgh)

- pMES control – gift from Dr. Catherine E. Krull (University of Missouri – Columbia MO)
- shKCC2 – Short hairpin RNAi targeting vector was designed using Ambion's Insert Design Tool (http://www.ambion.com/) against sequence spanning amino acids 2874-2894 of mouse KCC2 (5'-AGCGTGTGACAATGAGGAGAA-3'). The shKCC2 was cloned into pSilencer 2.0-U6 (Applied Biosystems - Ambion, Austin TX) for expression.
- pCIG2-K_{ir}2.1 – modified by Marie Rougie in the lab from plasmid provided by Dr. Yu-Qiang Ding (Chinese Academy of Sciences - Shanghai, China)
- Non-specific shRNA vector – Built by Randal Hand using non-specific shRNA sequence provided by Applied Biosystems

***Ex Vivo* Electroporation**

Dorsal electroporations were used to label progenitors of pyramidal cells with before dissociations. Intact decapitated E14.5 wild-type heads were punctured through the skull at the junction between the 2 cortical hemispheres and the developing midbrain. Trough this hole a small glass capillary pippette (electrode puller and glass capillary) filled with pCIG4-Tomato (greater than 1ug/uL endotoxin free plasmid DNA; MEGA EF Kit; Clontech, Mountain View CA) and Fast Green FCF (0.5% at 1:20; Sigma-Aldrich, St. Louis MO), could inject into the lateral ventricals by positioning the tip between the eyes and 1 mm off midline. A Picospritzer III (General Valve) was used for the injection using several 10psi 5ms pulses to fill both ventricles. Following the injection 4x 35V 100ms pulse / 100ms pause currents were applied to each hemisphere with an ECM 830 electroporator (BCX) using Genepaddles (Model 542, BTX) with the negative electrode paddle positioned underneath the head and the positive one parallel to the ventricle. Brains were then either dissociated or sliced as normal.

Slicing for *ex vivo* organotypic cortical slice culture

Brains were immediately removed, with pia intact, from skull into 4^{o}C HBSS complete (HBSSc; Polleux and Ghosh, 2002). Twenty-five milliliters of 3% low melting agar in HBSSc was heated by microwaving until boiling while inverting several times between each boil. A 3mm layer of agar was allowed to chill on bottom of tear away dish (Cat#18646C; Polysciences; Warrington PA) until solid. The remaining agar was poured into the cast, on ice, and stirred with a digital thermometer until it read 50^{o}C. It was then removed from the ice and placed on the bench top and continually stirred while cooling. At 42^{o}C dissected brains were removed from the HBSSc with a spatula (Cat#10090-13; Fine Science Tools; Foster City CA) and blotted with Kimwipes (Cat#34120; Kimberly-Clark Professional; Roswell GA) to remove excess media. Upon addition to the agar brains were batted around to remove any excess media. After remaining brains were added they were positioned so that the rostral caudal axis was parallel to the bottom of the dish. The cast was placed on ice until the agar was cold to the touch. Mounted brains were then cut coronally to 300 micron sections and either mounted onto inserts (Cat# 353102; Becton Dickinson Labware; Franklin Lakes NJ) for culture or confocal inserts (PICM ORG; Millipore; Cork, Ireland) for culture and time-lapse. Slice media was added under the insert as described (Polleux and Ghosh, 2002).

MGE Slice Electroporations

Before mounting slices were electroporated directly into the MGE to label migrating interneurons. A 1mm section of agar was cut and placed over the positive electrode. A coronal section containing the MGE was then placed on the agar. One pulse of DNA (greater than 1μg/μL endotoxin free plasmid DNA; MEGA EF Kit; Clontech, Mountain View CA) and Fast Green FCF (0.5% at 1:20; Sigma-Aldrich, St. Louis MO) was picospritzed into the ventricular zone and sub-ventricular zone of the MGE. To the negative electrode media was applied with a pippette and used to connect the circuit by touching the media to the top of the slice. When only the MGE/striatum is between the paddles a 5x 60V 5ms pulse / 500 ms pause was applied (Cobos et al., 2007). Slices could then be cultured as normal.

Explanting to Dissociated Cortical Cultures

E14.5 dissociations were conducted as described previously (Polleux and Ghosh, 2002). Explants from E14.5 EGFP or electroporated MGEs (same as slice electroporation protocol) were

then cut into 6-8 pieces and explanted to the dish after the dissociation had time settle for 30 minutes and had serum free media applied. Multi-well chambers were plated at a density equal to that of the normal dishes by diluting to 500,000 cell per mL and applying 300μL of dissociate. One to three explants were applied to each dish.

Confocal Microscopy

Confocal microscopy on fixed tissue was done as described previously (Hand et al., 2005). Time-lapse microscopy was done as described previously (Hand et al., 2005) with an imaging frequency of a picture taken every 10 minutes for migration studies. These movies are played back at a rate of 7 frames per second (sped up 4200x real time). Calcium imaging movies were and every 4 seconds for calcium imaging sessions (see calcium imaging section for details).

Quantification of Migration Dynamics

Positions of interneuron cell bodies were recorded frame by frame using ImageJ (NIH, Bethesda MD). The movement of these cells over time was extracted using Microsoft Excel custom functions and macros. Average speed was calculated as the total time of movie divided by the total distance traveled. Moving speed was calculated as the total time the cell was moving divided by the total distance traveled. Percent time moving was quantified as the total time spent moving divided by the total time of the movie. Even after applying stack registry (Turboreg and Stackreg, Thevenaz et al., 1998) to align the images, some vibrations were still present. After visually comparing distances measures to actual movements observed, it was determined that movements less than 1.1 μm were noise. Therefore movements below the threshold of 1.1 μm were considered to be not moving for all movies.

Quantification of KCC2 immunofluorescence was measured with ImageJ (NIH). For data matched to time-lapse information, post-hoc KCC2 immunostained interneurons were sampled with a consistent sampling radius in the 3 most intense portions of the cell. These were typically located, though not limited to, the base of the leading process. The average of these three values was used for binning and plotting the corresponding cell's time-lapse information. For up-regulation info, including confirmation of the short hairpin's knockdown potential, only the most intense sampling radius was used for quantifications.

Statistical analysis

Figure 1

Mann-Whitney test (E) E15: n=388 cells, p=0.0002; P1: n=970; P7: n=366, p<0.0001 (F) E15: n=119, p=0.0004; P1: n=88; P7: n=24 (G) E15: n=119, p<0.0001; P1: n=88; P7: n=24, p<0.0011

Figure 2

Mann-Whitney test (L) Low KCC2: n=125; High KCC2: n=81 (M) GABA Low KCC2: n=125; GABA High KCC2: n=81, p=0.0004; GABA+BMI Low KCC2: n=44, p=0.0271; GABA+BMI High KCC2: n=39, p=0308

Figure 3

Mann-Whitney test (L) control media: n=114; control muscimol: n=117, p=0.0375; control BMI: n=101, p=0.0019; shKCC2 media: n=125; shKCC2 muscimol: n=136; shKCC2 BMI: n=64, p<0.0001; shKCC2+KCC2* media: n=111, p<0.0001; shKCC2+KCC2* muscimol: n=116, p<0.0001; shKCC2+KCC2* BMI: n=48, p<0.0001; shKCC2+K_{ir}2.1 media: n=57, p<0.0001(compared to shKCC2 media).

Figure 4

Mann-Whitney test (E) moving: n=51;sedentary: n=51, p<0.0001.

Figure 5

Mann-Whitney test (D) control: n=4067; KCC2*: n=3143, p<0.0001.

Chi-square test (H) control: n=298; shKCC2: n=131, p<0.0001; shKCC2+KCC2*: n=138, p<0.0001 (compared to shKCC2), p=0.0003 (compared to control).

Figure 6
Mann-Whitney test (J) shKCC2: n=16; KCC2*: n=14, p=0.0084; shKCC2+BMI: n=11, p=0.0512; high frequency shKCC2: p<0.0001.
Chi-square test (M) E15: n=388; E15+BAPTA-AM: n=204, p<0.0001.

Figure 7
Mann-Whitney test (C) media: n=125; omega-conotoxin: n=52, p<0.0001; nifedipine: n=60, p<0.0001 (F) media: n=111; muscimol: n=116, p<0.0001; muscimol APV NBQX: n=144, p<0.0001(compared to muscimol alone); shKCC2 muscimol APV NBQX: n=53, p<0.0001 (compared to KCC2 muscimol APV NBQX).

Supplementary figure 1
Chi-square test (D) 2div/2div: n=494, p<0.0001; 7div/7div: n=436; 2dvi/7div: n=406, p<0.0001.
Mann-Whitney test (E) 2div/2div: n=203, p<0.0001; 7div/7div: n=141; 2dvi/7div: n=101, p<0.0001.

Supplementary figure 2
Mann-Whitney test post-media (n=147) addition vs. post-GABA (n=206) addition p=0.0183.

Supplementary figure 3
(AA) Mann-Whitney test 4div: interneurons (n=52) vs. pyramidal neurons (n=59), p<0.0001; 8div: interneurons (n=56) vs. pyramidal neurons (n=50), p<0.0001.

Supplementary figure 7
Chi-square test compared all conditions to activated caspase-3(+) cells (n=54) with threshold for positive cell being 2x that of control average fluorescence. Non-specific shRNA: n=50, p<0.0001; shKCC2: n=50, p<0.0001; shKCC2+KCC2*: n=50, p<0.0001.

Supplementary figure 8
Mann-Whitney test comparing to shKCC2+KCC2*-NTD (D) shKCC2 media: n=125; shKCC2+KCC2*-NTD media: n=48; shKCC2+KCC2* media: n=111, p=0.0058; shKCC2 muscimol: n=136; shKCC2+KCC2*-NTD muscimol: n=53; shKCC2+KCC2* muscimol: n=116, p=0.0018; shKCC2 BMI: n=64; shKCC2+KCC2*-NTD BMI: n=51; shKCC2+KCC2* BMI: n=48, p<0.0001.
Mann-Whitney test comparing shKCC2+KCC2*-NTD BMI to media BMI (Figure 3): p=0.0008.

Supplementary figure 10
Mann-Whitney test (C) media: n=298; bayK8644: n=187, p<0.0001.

Supplementary figure 11
Mann-Whitney test (C) media: n=125; shKCC2 muscimol: n=136;APV NBQX: n= 53, p<0.0001 (compared to media); muscimol APV NBQX: n=119, p=0.0375 (compared to APV NBQX).

* p<0.05; ** p<0.01 ; *** p<0.001.
Box plots show 10th, 25th, 50th, 75th, and 90th percentile values of given population.
Mann-Whitney stats calculated by VassarStats (http://faculty.vassar.edu/lowry/utest.html)
Chi squared calculated using a JavaScript by Professor Hossein Arsham (http://home.ubalt.edu/ntsbarsh/Business-stat/otherapplets/Catego.htm)

REFERENCES

Cobos, I., Borello, U., and Rubenstein, J.L. (2007). Dlx transcription factors promote migration through repression of axon and dendrite growth. Neuron *54*, 873-888.

Hand, R., Bortone, D., Mattar, P., Nguyen, L., Heng, J.I., Guerrier, S., Boutt, E., Peters, E., Barnes, A.P., Parras, C.*, et al.* (2005). Phosphorylation of Neurogenin2 specifies the migration properties and the dendritic morphology of pyramidal neurons in the neocortex. Neuron *48*, 45-62.

Polleux, F., and Ghosh, A. (2002). The slice overlay assay: a versatile tool to study the influence of extracellular signals on neuronal development. Sci STKE *2002*, PL9.

Thevenaz, P., Ruttimann, U.E., and Unser, M. (1998). A pyramid approach to subpixel registration based on intensity. IEEE Trans Image Process *7*, 27-41.

Uhlen, P. (2004). Spectral analysis of calcium oscillations. Sci STKE *2004*, pl15.

Neuron, Volume 62

Supplementary Figures and Supplementary Experimental Procedures and Statistics

KCC2 expression promotes the termination of cortical interneuron migration in a voltage-sensitive calcium-dependent manner

Bortone D. and Polleux F.

Supplementary Figures

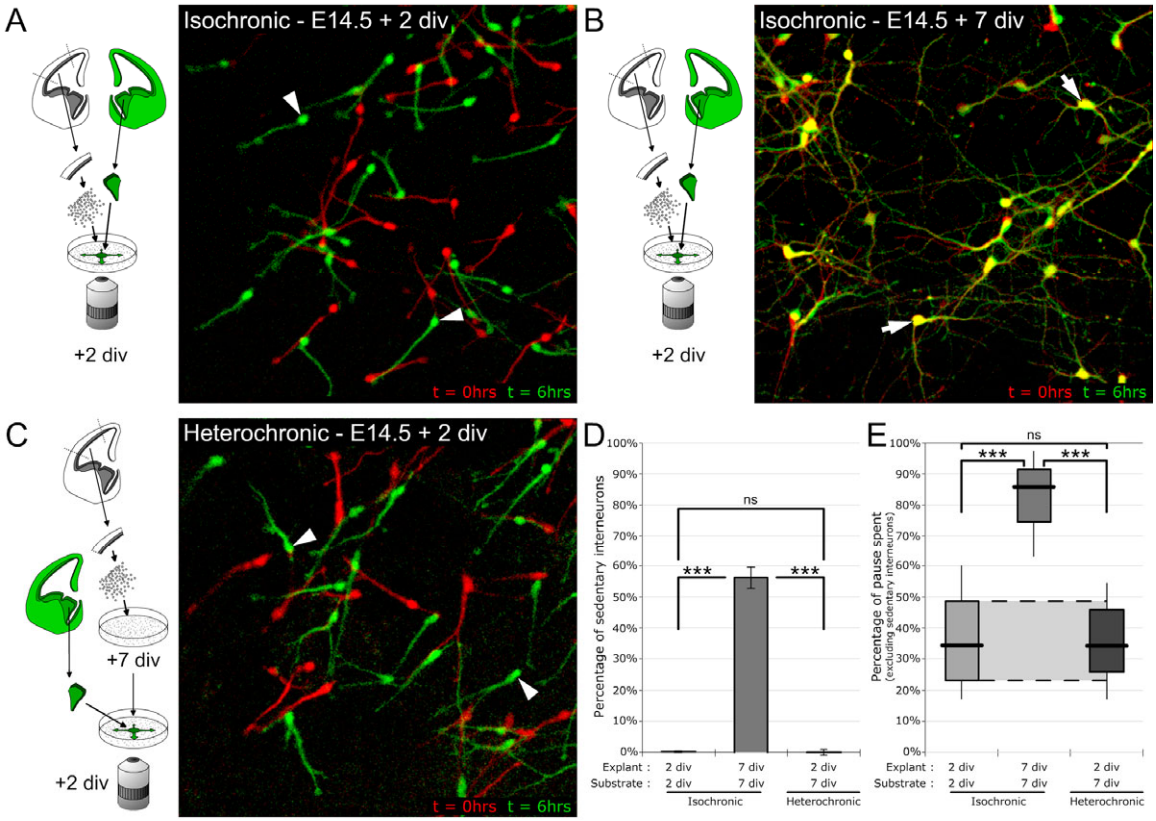

Supplementary Figure 1. Termination of migration has a cell autonomous component
E14.5 wild-type cortical cells were dissociated, plated and co-cultured with EGFP-expressing MGE explants. Frame corresponding to the start of imaging (t=0) is pseudo-colored in red. Image taken six hours later is pseudo-colored in green. Yellow cell bodies indicate interneurons did not migrate between beginning and end of imaging session. Arrowheads indicate migrating interneurons while arrows point to sedentary interneurons. Note isochronic cultures of interneurons phenocopy increase in pause times from 2div (**A**) to 7div (**B**) as observed *in situ*. In heterochronic cultures (**C**), the dissociated E14.5 wild-type substrate was aged 7-9 days before placing E14.5 EGFP-MGE explants. (**D,E**) Quantification shows no significant difference in percentage of sedentary interneurons (E) or pause time (D) on an aged substrate indicating interneurons require a cell autonomous maturation to slow and terminate migration. Since including the pause times of the steadily increasing proportion of sedentary interneurons would have doubtlessly caused our measurements to increase with age, these non-moving cells have been excluded for panel E.

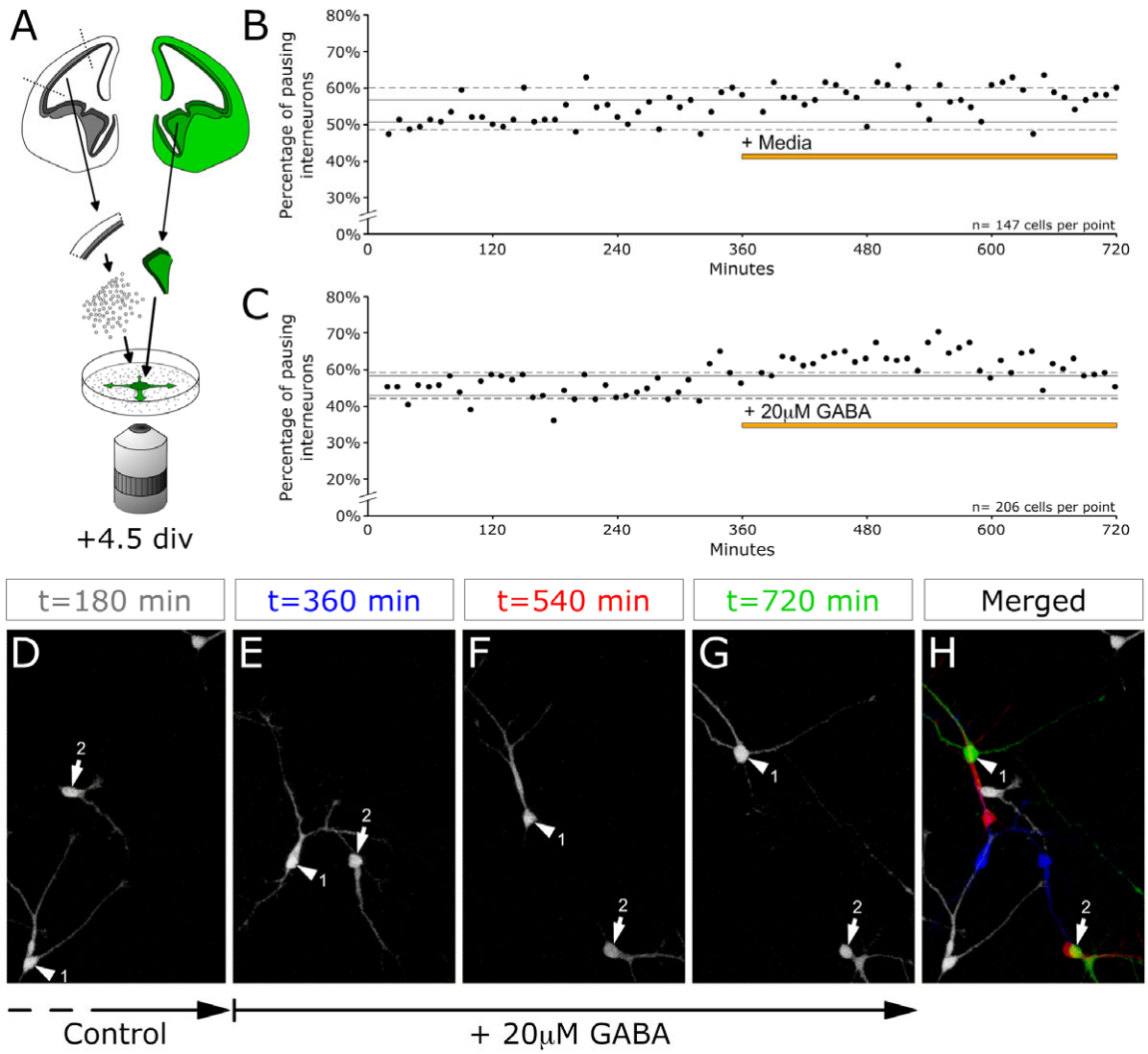

Supplementary figure 2. MGE-derived interneurons have heterogeneous response to GABA application.

(**A**) Illustration of experimental design. Wild-type cortices were dissociated to provide a substrate for explants of EGFP-MGE. After 4.5div interneurons were time-lapsed for a control period of 6 hours. The same interneurons were then time-lapsed for another 6 hours to note individual changes in pausing following drug application (20microM GABA or media). (**B-C**) Percentage of pausing interneurons is shown for each frame for control media (B) and GABA addition (C). Solid lines indicate 50th percentile range of first 6 hours of imaging, while dashed lines indicate 90th an 10th percentile range. Control experiment (B) shows a slight but steady increase in pausing during course of 12 hours time-lapse with no response to media application. GABA-treated interneurons (C) show an increase in pausing in response to GABA application ($p=0.0183$ compared to post-media addition). (**D-G**) Montage of GABA addition time-lapse is shown before and after drug application at 360 minutes. Cell 1 (arrowhead) shows no response to GABA application while cell 2 (arrow) stops migrating. (**H**) Merged image shows time points before GABA addition in white and blue (180 and 360 minutes respectively) and those after GABA addition in red and green (540 and 720 minutes respectively). Yellow 'colocalization' indicates little movement in cell 2 after GABA application.

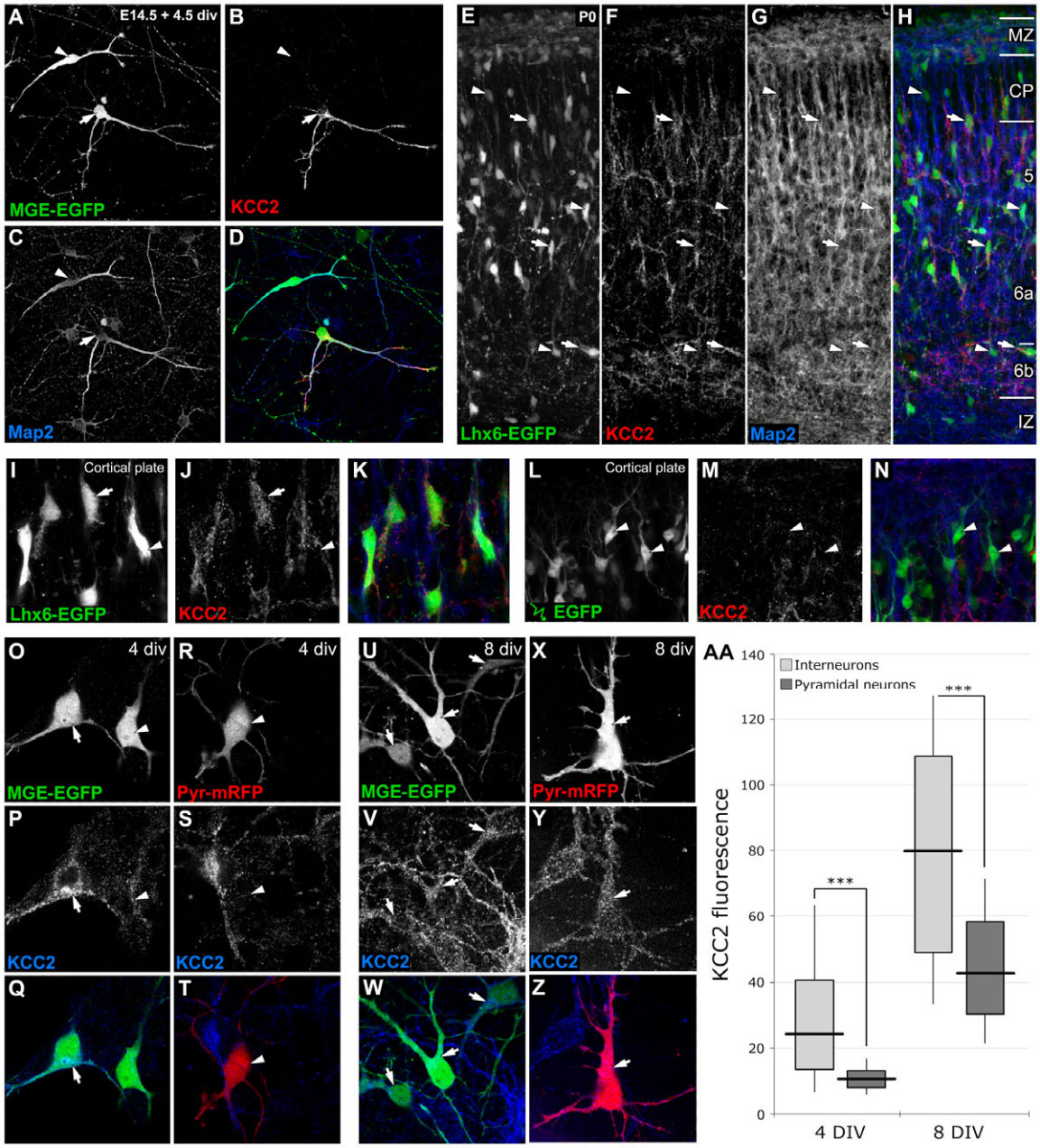

Supplementary figure 3. KCC2 expression is highly variable among cortical interneurons. **(A-D)** Explanted E14.5 EGFP-MGE interneurons show drastically different KCC2 expression after 4.5div in culture. Throughout the figure, arrowheads identify cells expressing low levels of KCC2, while arrows indicate cells expressing high levels of KCC2. **(E-K)** Immunostained sections from a P0 Lhx6-EGFP mouse reveal heterogeneous KCC2 expression in cortical interneurons *in vivo*. **(L-M)** E14.5 dorsal telencephalic progenitors were electroporated with EGFP and slices containing radially migrating pyramidal neurons in the cortical plate (CP) stained for KCC2 after 4.5div. No KCC2 expression is detected. **(O-Z)** Isochronic co-cultures of MGE-EGFP-derived interneurons with mRFP-electroporated dorsal telencephalic progenitors reveals that interneurons up-regulate KCC2 earlier than pyramidal cells *in vitro*. (**AA**) Quantification of KCC2 fluorescence in cortical pyramidal cells was significantly lower than interneurons at 4 and 8div ($p<0.0001$ for both). This box plots reveals also that the variability of KCC2 expression among interneurons was more significant than in pyramidal neurons at early ages.

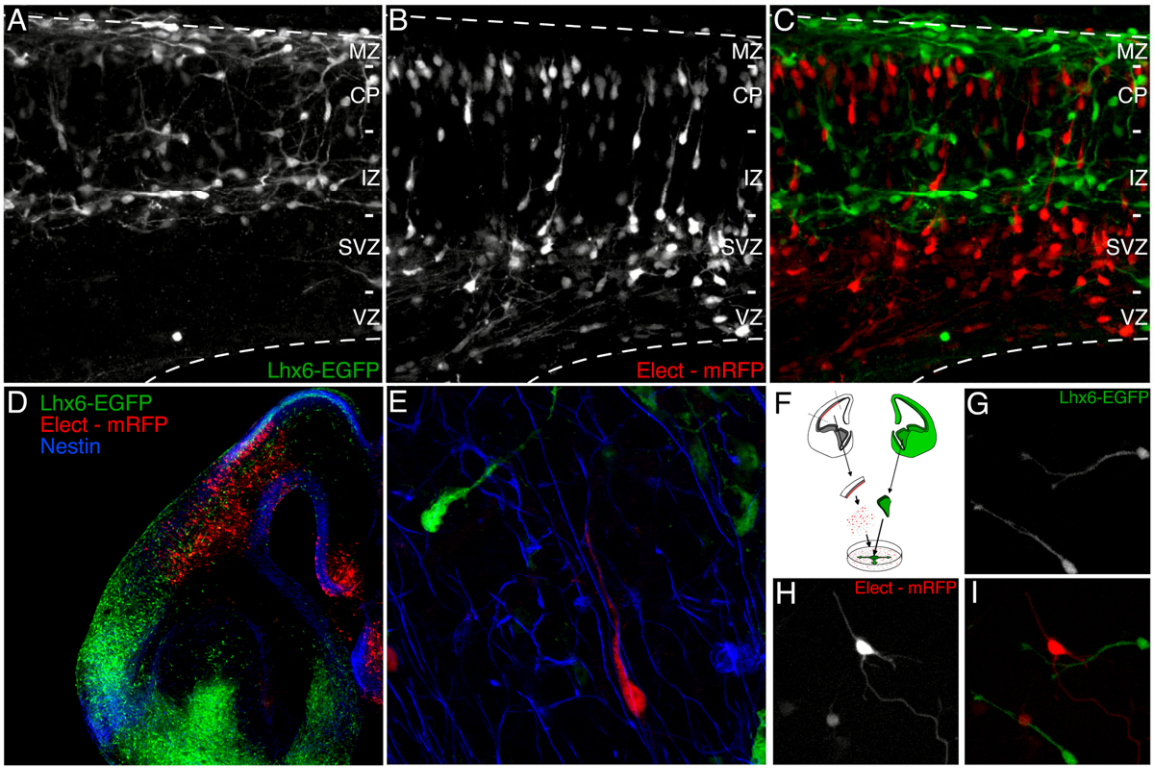

Supplementary figure 4. Dorsal telencephalic electroporation specifically labels radially migrating pyramidal neurons and not tangentially migrating interneurons.
(**A-E**) E14 Lhx6-EGFP embryos underwent dorsal electroporation with monomeric red fluorescent protein (mRFP) and cultured 4 days revealing no co-transfection which indicates this is an effective method to specifically label pyramidal cells. At higher magnification (E) radially migrating neurons (red) but not tangentially migrating interneurons (green) are found closely fasciculated with radial glial fibers labeled with Nestin (blue). (**F-I**) Dissociating dorsally electroporated wild-type pyramidal cells and applying an EGFP-MGE explant enables concurrent culturing and imaging of labeled interneurons and pyramidal cells in 2D.

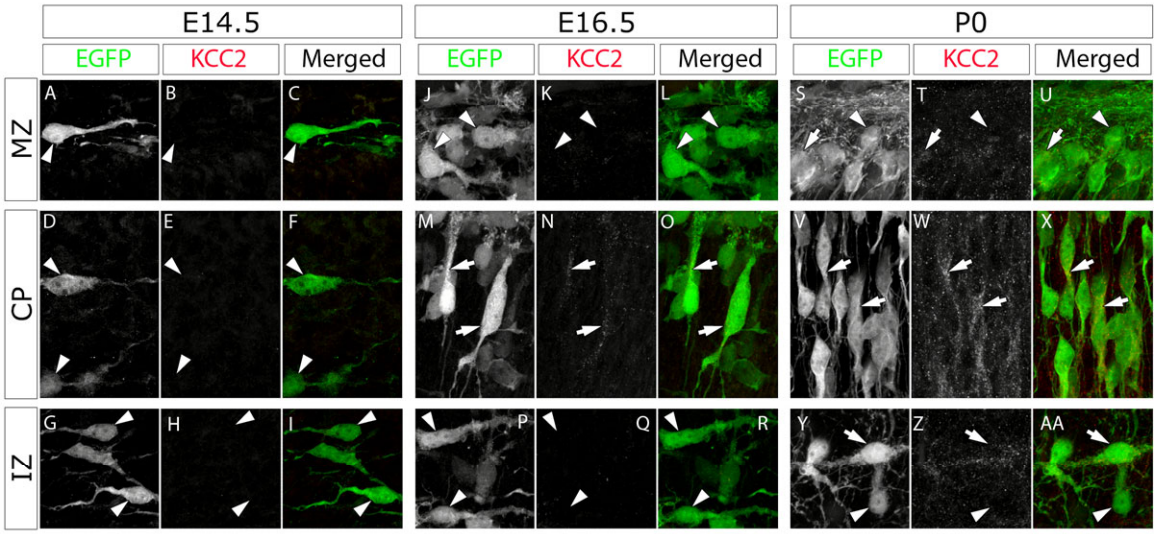

Supplementary figure 5. Migrating cortical interneurons up-regulate KCC2 after reaching the cortex.
Lhx6-EGFP embryos were perfused at E14.5 (A-I), E16.5 (J-R) or P0 (S-AA) and immunostained for EGFP and KCC2. Note that when migrating interneurons reach the cortex at E14.5 and E16.5 they express very little, if any, KCC2 and start up-regulating KCC2 only at P0 i.e. several days after they reach the cortical plate.
Abbreviations: CP - cortical plate; IZ - intermediate zone; MZ - marginal zone; E14.5 - Embryonic day 14.5.

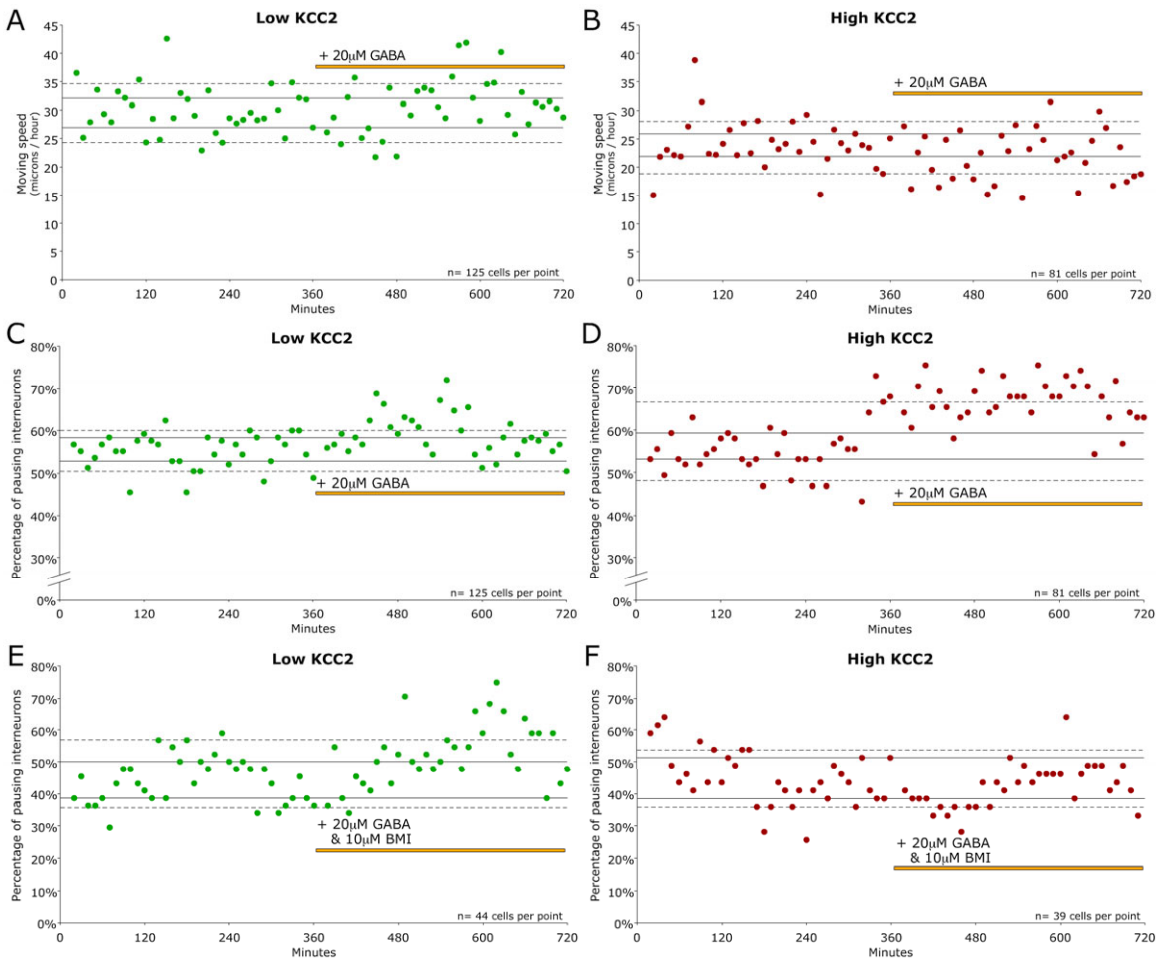

Supplementary figure 6. Frame-by-frame responses to GABA addition

(A-F) Data shown in Figure 4K-M is shown here as frame-by-frame average values of interneurons binned into low and high KCC2 sub-populations. Yellow lines indicate the time of addition of 20microM GABA (A-D) or 20microM GABA plus 10microM BMI (E,F). Solid black lines indicate 25th and 75th percentiles before drug addition. Dotted black lines indicate 10th and 90th percentiles before drug addition. Note the increase in frequency of pausing after GABA addition for high KCC2 expressing interneurons (D), but not upon co-application of GABA and $GABA_A$ antagonist BMI (F). Also note that the frequency of pausing increases in low KCC2-expressing interneurons when GABA is co-applied with BMI.

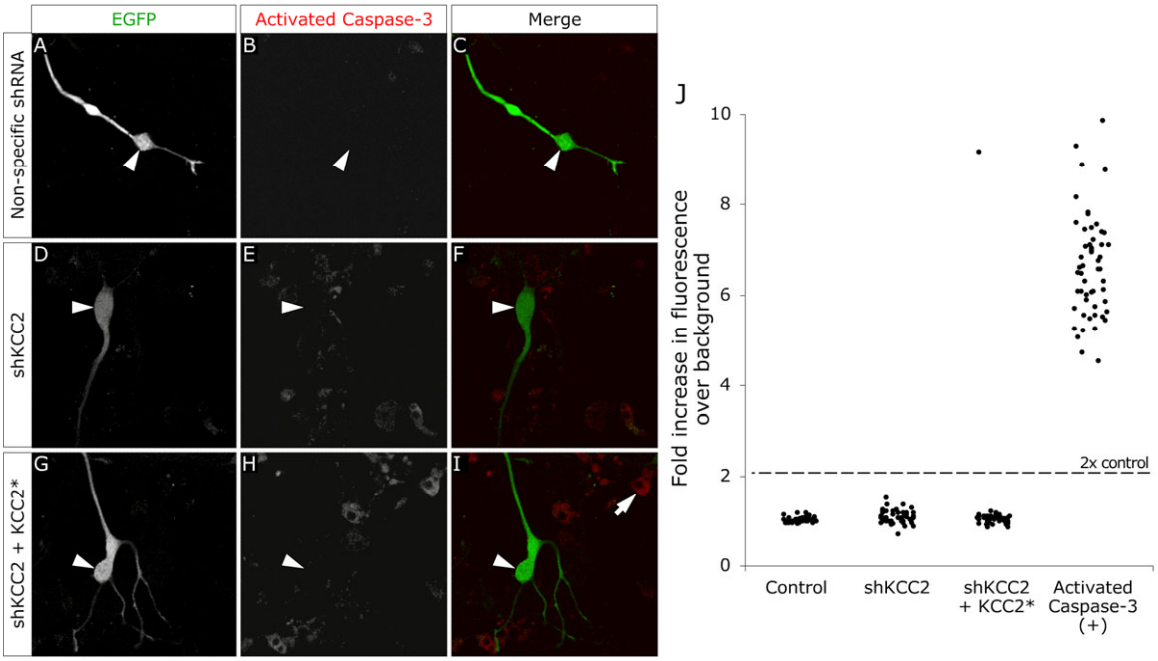

Supplementary figure 7. Manipulating KCC2 expression in migrating interneurons does not induce apoptosis.

(**A-I**) E14.5 MGE explants electroporated with either non-specific shRNA, shKCC2 or shKCC2 rescued with KCC2* were cultured on wild-type cortical dissociations for 4.5div, fixed and immunostained for activated caspase-3. (I) Arrow indicates activated caspase-3 expression in an apoptotic neuron from the substrate wild-type cortical culture. (**J**) Quantifications show the measured fluorescence of KCC2 with respect to background fluorescence in individual interneurons expressing the indicated plasmids. No significant difference in activated caspase-3 expression was found between the 3 conditions (B,E,H arrowheads) using 2 times the average control value as a threshold.

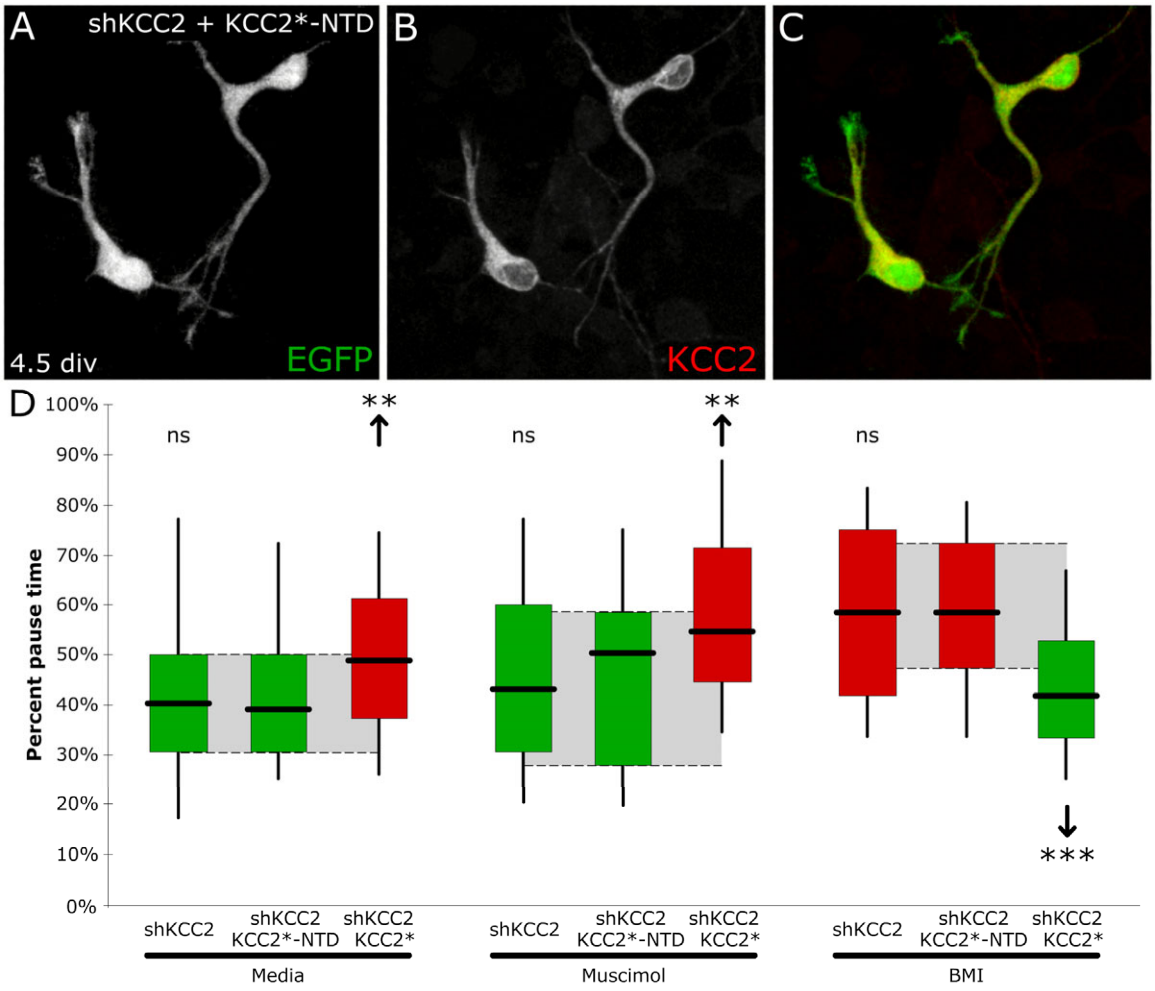

Supplementary figure 8. Effects associated with KCC2 are due to its transport activity
(**A-C**) E14.5 MGE explants were electroporated with constructs expressing shKCC2 and EGFP transport-dead N-terminal deleted human KCC2 (NTD-KCC2*) at 4.5div. Immunostaining for KCC2 (B) shows NTD-KCC2* does not affect expression or localization of the protein. **(D)** Box plots are color-coded to represent whether treatment would result in more depolarized (green) or hyperpolarized (red) cells with respect to non-electroporated cells. Light-grey shading shows middle 50th percent range of appropriate control population. NTD-KCC2* fails to rescue KCC2 knockdown in contrast with full-length human KCC2 (KCC2*). The shKCC2 and full-length KCC2* data is the same as shown in Figure 3.

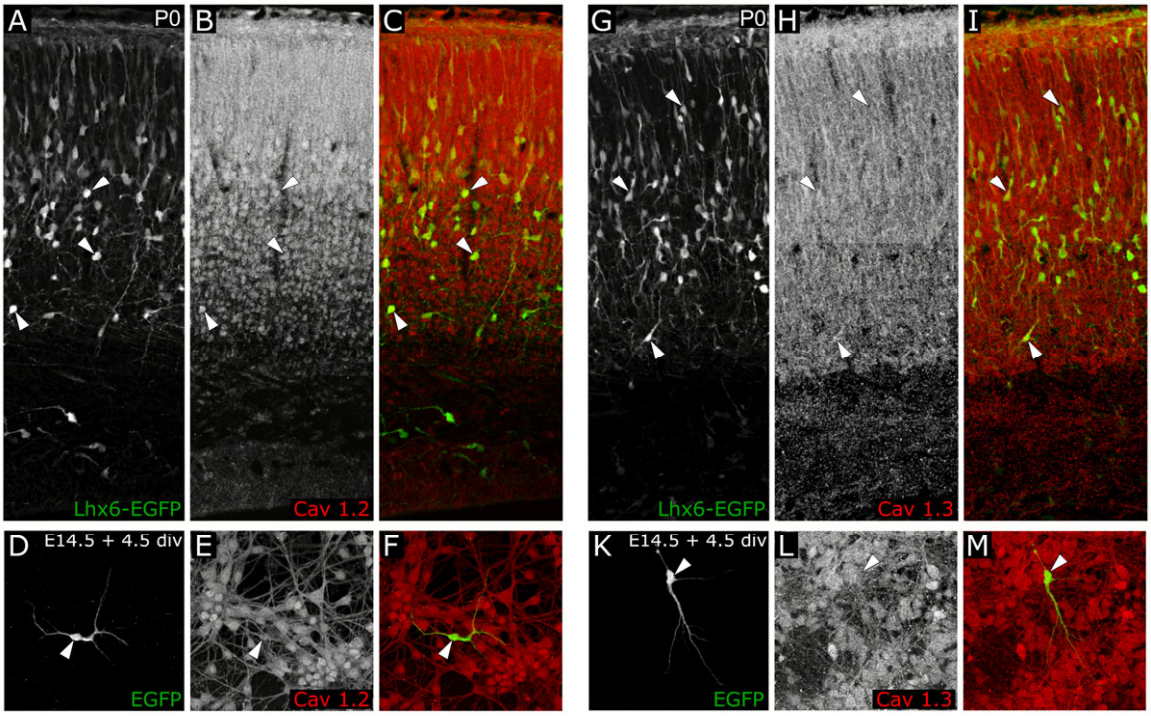

Supplementary figure 9. L-type calcium channel subunits $Ca_V1.2$ and $Ca_V1.3$ are expressed in developing cortical interneurons

(**A-C, G-I**) Sections of P0 Lhx6-EGFP mice brains were sectioned and immunostained for subunits 1.2 and 1.3 of L-type voltage sensitive calcium channels. (**D-F, K-M**) The expression of these subunits is maintained after culturing E14.5 MGE explants for 4.5div. Arrowheads indicate co-labeled cells.

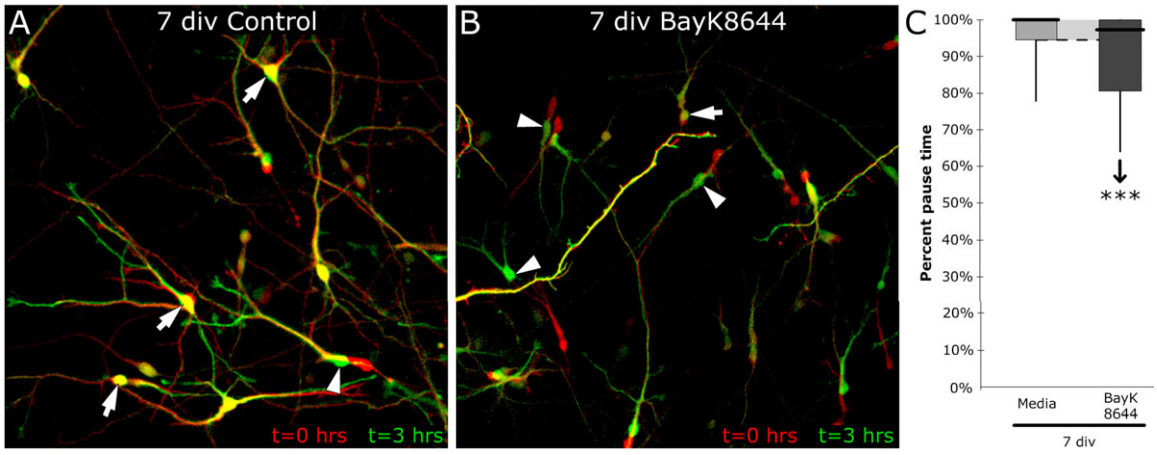

Supplementary figure 10. L-type calcium channel agonist bayK8644 prolongs migration of cortical interneurons

E14.5 explants were electroporated with control constructs, plated on wild-type dissociations, incubated with the L-type VSCC agonist bayK8644 from 4-7div and time-lapsed. Box plots show percent pause times of the cortical interneuron population. Light-grey shading shows the 25th-75th percentiles range of control values. Increasing open-channel frequency of L-type calcium channels delays the termination of migration for the majority of cortical interneurons ($p<0.0001$). Data shown in A and C were previously shown in figure 5. See Suppl. Movies 9 and 21 for corresponding time-lapse.

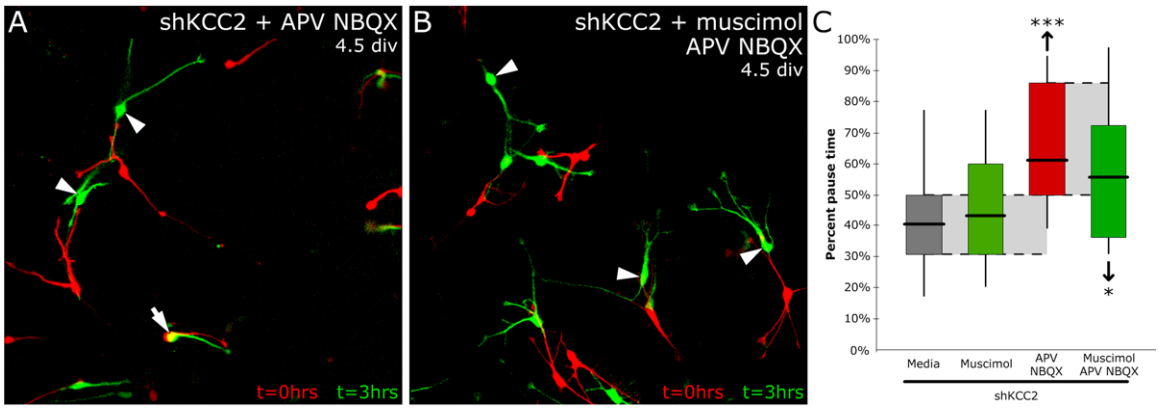

Supplementary figure 11. Muscimol-induced depolarization reduce cortical interneuron pausing frequency in the absence of glutamatergic signaling.
E14.5 MGEs were electroporated with shKCC2 and cultured for 4.5div before time-lapsing in the presence of either (**A**) 100μM APV and 10μM NBQX to block NMDA/AMPA receptors-mediated depolarization or (**B**) APV, NBQX and 10μM muscimol in order to block NMDA/AMPA receptors-mediated depolarization and activate $GABA_A$ receptor-mediated depolarization (shKCC2 cells). (**C**) Box plots are color-coded to represent whether treatment would result in more depolarized (**green**) or hyperpolarized (**red**) cell with respect to control cells. Light-grey shading shows middle 50th percent range of appropriate control population. While antagonizing glutamate signaling significantly decreases motility (i.e. increases pause times ($p<0.0001$)) compared to control, depolarizing shKCC2 interneurons with muscimol significantly rescues this effect ($p=0.0375$). Data shown in B and C were previously shown in figures 7 and 3, respectively. See Suppl. Movies 19 and 22 for corresponding time-lapse.

ww

Supplementary Material and Methods

Tissue preparation and sectioning

Time-pregnant mice are euthanized by rapid cervical dislocation before embryo collection. To prepare avertin 40x stock solution, 1g of 2,2,2-tribromoethanol (99%) (840-2; Sigma-Aldrich, St. Louis MO) was dissolved with 1mL of Tert-amyl alcohol (99%) (246-3; Sigma-Aldrich, St. Louis MO) in a glass container and stored at 4^{o}C protected from light for no more than 6 months before use. Working solution was made adding 40x stock solution to 37^{o} C PBS dropwise. Intraperitioneal injections of Avertin were made of 250-300uL per 10 grams of mouse body weight to achieve deep anesthesia. After the pups failed to respond to a toe prick the mice were perfused with 4% PFA in PBS made from 16% Paraformaldehyde solution (Cat. # 15710, Electron Microscopy Sciences, Hatfield PA). Brains were then dissected and fixed overnight in 4% PFA before rinsing 3x 30 minutes with PBS, orbital shaking at room temperature, sectioning at 80 microns with a vibratome (VT1000S; Leica; Wetzlar, Germany) and immunostained.

Calcium imaging/quantification

A stock solution of calcium indicator was made by adding 10microL DMSO (D2650; Sigma-Aldrich, St. Louis MO) to 50 μg of Oregon Green 488 BAPTA-1, AM (OGB-1; O6807; Invitrogen - Molecular Probes, Eugene OR). After vortexing for 1 min 5x 2microL aliquots were frozen at –80^{o}C. Warm 9.12 microL Pluronic F-127 in 20% DMSO (P3000MP; Invitrogen - Molecular Probes, Eugene OR) was then added to one aliquot of stock solution. After vortexing for 1 min, a 5μM working solution was made by adding 5microL of pluronic - stock solution to 715microL HBSS and vortexing for another minute.

Interneurons electroporated with pCIG4-Tomato (gift from Dr. Tom Maynard, University of North Carolina - Chapel Hill) or pCIG4-Tomato-IRES-hKCC2 were loaded with working solution at 4div by removing media from dissociation (saving it at 37^{o}C) and washing 3x in 37^{o}C HBSS. Working solution was applied to the dish and incubated for 30min at room temperature, while protected from light. Cells were then washed once with HBSS, once with 37^{o}C serum free media, and then the old conditioned media was added back to the dish.

Imaging sessions were done by sequentially scanning the red (plasmid) and green (OGB-1) channels with an open pinhole to allow faster scanning (once every 4 seconds). Data were extracted from these movies by creating a macro for ImageJ (NIH, Bethesda MD). This macro divides the green by the red channel to correct for changes in cell thickness as the interneuron migrates. The macro also masks out all data not corresponding to the cell bodies of interneurons as they migrate. The average intensity values of these cell bodies were measured and used to calculate a Fluorescence/Fluorescence at t=0 (F/F_0) for every frame.

The spectral analysis was done using the protocol and SpectralAnalysis tool designed for MatLab (The Mathworks, Natick MA) by Per Uhlen (2004). Using this tool, a Hanning filter was applied to the data to remove edge effects at the beginning and end of the movie. Then a Fourier transformation was done using 2^9 bins to separate the F/F_0 data from its time component and view the relative power spectral density for each frequency in every cell.

Construction of Multi-Welled Dishes

Sylgard 184 silicone elastomer, base & curing agent (Dow Corning Corporation, Midland MI) was to used to attach cut rings of 10mL Stripette (4101; Corning Incorporated, Corning NY) to FluoroDish (FD-35-100, World Precision Instruments, Inc., Sarasota FL). Two days of cure time were allowed before use of these multi-welled chambers.

Constructs

- pCIG4-tomato - gift from Dr. Tom Maynard (University of North Carolina - Chapel Hill)
- pCIG4-hKCC2-IRES-tomato
- pMES-KCC2 - hKCC2-IRES-EGFP gift from Dr David Mount (Harvard Insitute of Medicine, Harvard University) and Dr. Karl Kandler (University of Pittsburgh)

- pMES control – gift from Dr. Catherine E. Krull (University of Missouri – Columbia MO)
- shKCC2 – Short hairpin RNAi targeting vector was designed using Ambion's Insert Design Tool (http://www.ambion.com/) against sequence spanning amino acids 2874-2894 of mouse KCC2 (5'-AGCGTGTGACAATGAGGAGAA-3'). The shKCC2 was cloned into pSilencer 2.0-U6 (Applied Biosystems - Ambion, Austin TX) for expression.
- pCIG2-K_{ir}2.1 – modified by Marie Rougie in the lab from plasmid provided by Dr. Yu-Qiang Ding (Chinese Academy of Sciences - Shanghai, China)
- Non-specific shRNA vector – Built by Randal Hand using non-specific shRNA sequence provided by Applied Biosystems

***Ex Vivo* Electroporation**

Dorsal electroporations were used to label progenitors of pyramidal cells with before dissociations. Intact decapitated E14.5 wild-type heads were punctured through the skull at the junction between the 2 cortical hemispheres and the developing midbrain. Trough this hole a small glass capillary pippette (electrode puller and glass capillary) filled with pCIG4-Tomato (greater than 1ug/uL endotoxin free plasmid DNA; MEGA EF Kit; Clontech, Mountain View CA) and Fast Green FCF (0.5% at 1:20; Sigma-Aldrich, St. Louis MO), could inject into the lateral ventricals by positioning the tip between the eyes and 1 mm off midline. A Picospritzer III (General Valve) was used for the injection using several 10psi 5ms pulses to fill both ventricles. Following the injection 4x 35V 100ms pulse / 100ms pause currents were applied to each hemisphere with an ECM 830 electroporator (BCX) using Genepaddles (Model 542, BTX) with the negative electrode paddle positioned underneath the head and the positive one parallel to the ventricle. Brains were then either dissociated or sliced as normal.

Slicing for *ex vivo* organotypic cortical slice culture

Brains were immediately removed, with pia intact, from skull into 4^{o}C HBSS complete (HBSSc; Polleux and Ghosh, 2002). Twenty-five milliliters of 3% low melting agar in HBSSc was heated by microwaving until boiling while inverting several times between each boil. A 3mm layer of agar was allowed to chill on bottom of tear away dish (Cat#18646C; Polysciences; Warrington PA) until solid. The remaining agar was poured into the cast, on ice, and stirred with a digital thermometer until it read 50^{o}C. It was then removed from the ice and placed on the bench top and continually stirred while cooling. At 42^{o}C dissected brains were removed from the HBSSc with a spatula (Cat#10090-13; Fine Science Tools; Foster City CA) and blotted with Kimwipes (Cat#34120; Kimberly-Clark Professional; Roswell GA) to remove excess media. Upon addition to the agar brains were batted around to remove any excess media. After remaining brains were added they were positioned so that the rostral caudal axis was parallel to the bottom of the dish. The cast was placed on ice until the agar was cold to the touch. Mounted brains were then cut coronally to 300 micron sections and either mounted onto inserts (Cat# 353102; Becton Dickinson Labware; Franklin Lakes NJ) for culture or confocal inserts (PICM ORG; Millipore; Cork, Ireland) for culture and time-lapse. Slice media was added under the insert as described (Polleux and Ghosh, 2002).

MGE Slice Electroporations

Before mounting slices were electroporated directly into the MGE to label migrating interneurons. A 1mm section of agar was cut and placed over the positive electrode. A coronal section containing the MGE was then placed on the agar. One pulse of DNA (greater than 1μg/μL endotoxin free plasmid DNA; MEGA EF Kit; Clontech, Mountain View CA) and Fast Green FCF (0.5% at 1:20; Sigma-Aldrich, St. Louis MO) was picospritzed into the ventricular zone and sub-ventricular zone of the MGE. To the negative electrode media was applied with a pippette and used to connect the circuit by touching the media to the top of the slice. When only the MGE/striatum is between the paddles a 5x 60V 5ms pulse / 500 ms pause was applied (Cobos et al., 2007). Slices could then be cultured as normal.

Explanting to Dissociated Cortical Cultures

E14.5 dissociations were conducted as described previously (Polleux and Ghosh, 2002). Explants from E14.5 EGFP or electroporated MGEs (same as slice electroporation protocol) were

then cut into 6-8 pieces and explanted to the dish after the dissociation had time settle for 30 minutes and had serum free media applied. Multi-well chambers were plated at a density equal to that of the normal dishes by diluting to 500,000 cell per mL and applying 300μL of dissociate. One to three explants were applied to each dish.

Confocal Microscopy

Confocal microscopy on fixed tissue was done as described previously (Hand et al., 2005). Time-lapse microscopy was done as described previously (Hand et al., 2005) with an imaging frequency of a picture taken every 10 minutes for migration studies. These movies are played back at a rate of 7 frames per second (sped up 4200x real time). Calcium imaging movies were and every 4 seconds for calcium imaging sessions (see calcium imaging section for details).

Quantification of Migration Dynamics

Positions of interneuron cell bodies were recorded frame by frame using ImageJ (NIH, Bethesda MD). The movement of these cells over time was extracted using Microsoft Excel custom functions and macros. Average speed was calculated as the total time of movie divided by the total distance traveled. Moving speed was calculated as the total time the cell was moving divided by the total distance traveled. Percent time moving was quantified as the total time spent moving divided by the total time of the movie. Even after applying stack registry (Turboreg and Stackreg, Thevenaz et al., 1998) to align the images, some vibrations were still present. After visually comparing distances measures to actual movements observed, it was determined that movements less than 1.1 μm were noise. Therefore movements below the threshold of 1.1 μm were considered to be not moving for all movies.

Quantification of KCC2 immunofluorescence was measured with ImageJ (NIH). For data matched to time-lapse information, post-hoc KCC2 immunostained interneurons were sampled with a consistent sampling radius in the 3 most intense portions of the cell. These were typically located, though not limited to, the base of the leading process. The average of these three values was used for binning and plotting the corresponding cell's time-lapse information. For up-regulation info, including confirmation of the short hairpin's knockdown potential, only the most intense sampling radius was used for quantifications.

Statistical analysis

Figure 1

Mann-Whitney test (E) E15: n=388 cells, p=0.0002; P1: n=970; P7: n=366, p<0.0001 (F) E15: n=119, p=0.0004; P1: n=88; P7: n=24 (G) E15: n=119, p<0.0001; P1: n=88; P7: n=24, p<0.0011

Figure 2

Mann-Whitney test (L) Low KCC2: n=125; High KCC2: n=81 (M) GABA Low KCC2: n=125; GABA High KCC2: n=81, p=0.0004; GABA+BMI Low KCC2: n=44, p=0.0271; GABA+BMI High KCC2: n=39, p=0308

Figure 3

Mann-Whitney test (L) control media: n=114; control muscimol: n=117, p=0.0375; control BMI: n=101, p=0.0019; shKCC2 media: n=125; shKCC2 muscimol: n=136; shKCC2 BMI: n=64, p<0.0001; shKCC2+KCC2* media: n=111, p<0.0001; shKCC2+KCC2* muscimol: n=116, p<0.0001; shKCC2+KCC2* BMI: n=48, p<0.0001; shKCC2+K_{ir}2.1 media: n=57, p<0.0001(compared to shKCC2 media).

Figure 4

Mann-Whitney test (E) moving: n=51;sedentary: n=51, p<0.0001.

Figure 5

Mann-Whitney test (D) control: n=4067; KCC2*: n=3143, p<0.0001.

Chi-square test (H) control: n=298; shKCC2: n=131, p<0.0001; shKCC2+KCC2*: n=138, p<0.0001 (compared to shKCC2), p=0.0003 (compared to control).

Figure 6
Mann-Whitney test (J) shKCC2: n=16; KCC2*: n=14, p=0.0084; shKCC2+BMI: n=11, p=0.0512; high frequency shKCC2: p<0.0001.
Chi-square test (M) E15: n=388; E15+BAPTA-AM: n=204, p<0.0001.

Figure 7
Mann-Whitney test (C) media: n=125; omega-conotoxin: n=52, p<0.0001; nifedipine: n=60, p<0.0001 (F) media: n=111; muscimol: n=116, p<0.0001; muscimol APV NBQX: n=144, p<0.0001(compared to muscimol alone); shKCC2 muscimol APV NBQX: n=53, p<0.0001 (compared to KCC2 muscimol APV NBQX).

Supplementary figure 1
Chi-square test (D) 2div/2div: n=494, p<0.0001; 7div/7div: n=436; 2dvi/7div: n=406, p<0.0001.
Mann-Whitney test (E) 2div/2div: n=203, p<0.0001; 7div/7div: n=141; 2dvi/7div: n=101, p<0.0001.

Supplementary figure 2
Mann-Whitney test post-media (n=147) addition vs. post-GABA (n=206) addition p=0.0183.

Supplementary figure 3
(AA) Mann-Whitney test 4div: interneurons (n=52) vs. pyramidal neurons (n=59), p<0.0001; 8div: interneurons (n=56) vs. pyramidal neurons (n=50), p<0.0001.

Supplementary figure 7
Chi-square test compared all conditions to activated caspase-3(+) cells (n=54) with threshold for positive cell being 2x that of control average fluorescence. Non-specific shRNA: n=50, p<0.0001; shKCC2: n=50, p<0.0001; shKCC2+KCC2*: n=50, p<0.0001.

Supplementary figure 8
Mann-Whitney test comparing to shKCC2+KCC2*-NTD (D) shKCC2 media: n=125; shKCC2+KCC2*-NTD media: n=48; shKCC2+KCC2* media: n=111, p=0.0058; shKCC2 muscimol: n=136; shKCC2+KCC2*-NTD muscimol: n=53; shKCC2+KCC2* muscimol: n=116, p=0.0018; shKCC2 BMI: n=64; shKCC2+KCC2*-NTD BMI: n=51; shKCC2+KCC2* BMI: n=48, p<0.0001.
Mann-Whitney test comparing shKCC2+KCC2*-NTD BMI to media BMI (Figure 3): p=0.0008.

Supplementary figure 10
Mann-Whitney test (C) media: n=298; bayK8644: n=187, p<0.0001.

Supplementary figure 11
Mann-Whitney test (C) media: n=125; shKCC2 muscimol: n=136;APV NBQX: n= 53, p<0.0001 (compared to media); muscimol APV NBQX: n=119, p=0.0375 (compared to APV NBQX).

* p<0.05; ** p<0.01 ; *** p<0.001.
Box plots show 10th, 25th, 50th, 75th, and 90th percentile values of given population.
Mann-Whitney stats calculated by VassarStats (http://faculty.vassar.edu/lowry/utest.html)
Chi squared calculated using a JavaScript by Professor Hossein Arsham (http://home.ubalt.edu/ntsbarsh/Business-stat/otherapplets/Catego.htm)

REFERENCES

Cobos, I., Borello, U., and Rubenstein, J.L. (2007). Dlx transcription factors promote migration through repression of axon and dendrite growth. Neuron *54*, 873-888.

Hand, R., Bortone, D., Mattar, P., Nguyen, L., Heng, J.I., Guerrier, S., Boutt, E., Peters, E., Barnes, A.P., Parras, C.*, et al.* (2005). Phosphorylation of Neurogenin2 specifies the migration properties and the dendritic morphology of pyramidal neurons in the neocortex. Neuron *48*, 45-62.

Polleux, F., and Ghosh, A. (2002). The slice overlay assay: a versatile tool to study the influence of extracellular signals on neuronal development. Sci STKE *2002*, PL9.

Thevenaz, P., Ruttimann, U.E., and Unser, M. (1998). A pyramid approach to subpixel registration based on intensity. IEEE Trans Image Process *7*, 27-41.

Uhlen, P. (2004). Spectral analysis of calcium oscillations. Sci STKE *2004*, pl15.